# ADIPOGENIC INDUCTION UNDER MACROMOLECULAR CROWDING WITH FICOLL UNLOCKS THE INTRINSIC POTENTIAL IN ADULT HUMAN BONE MARROW MESENCHYMAL STEM CELLS TOWARDS A BROWN ADIPOCYTE PHENOTYPE

**LEE HUI CHING MICHELLE**

*B.Sc. (Hons.), NUS*

**A THESIS SUBMITTED**

**FOR THE DEGREE OF DOCTOR OF PHILOSOPHY**

**NUS GRADUATE SCHOOL FOR INTEGRATIVE SCIENCES AND ENGINEERING**

**NATIONAL UNIVERSITY OF SINGAPORE**

**2014**

## DECLARATION

I hereby declare that this thesis is my original work and it has been written by me in its entirety. I have duly acknowledged all the sources of information which have been used in the thesis. This thesis has also not been submitted for any degree in any university previously.

Lee Hui Ching Michelle

28 Oct 2014

**ACKNOWLEDGEMENTS**

*Associate Professor Michael Raghunath*, thank you for everything. You have given me many opportunities to grow, to challenge myself and to enjoy the science amidst the work. Thank you for your patience, guidance, friendship, respect for my beliefs, and for the many conversations we have had. I am blessed to have been able to work on a project with a tangible goal in mind, and I hope I will be able to continue in this endeavor of pursuing translational science for the benefit of mankind.

*Dr. Allan Sheppard*, thank you for your guidance in my project, friendship, and the engaging conversations we have had in science and of life. I have learnt a lot from you and I hope that we will have more opportunities for discussion and collaboration.

*Associate Professor Scott Andrew Summers*, thank you for being on my thesis advisory committee and for giving me expert advice in my project. Thank you also for supporting me with the key resources I needed to advance my project forward. You are someone I look up to.

*Dr. Ying Li and Dr. Rafi Rashid*, thank you for helping me with key experiments and for your friendship and guidance.

*Dr. Sue-Anne Toh and Muhammad Shabeer*, thank you for the gift of the progenitor cells from the abdominal subcutaneous SVF and for teaching me how to culture these cells.

*Dr. Cedric Badowski*, thank you for patiently acquiring all the beautiful images on the laser scanning confocal microscope. It has been a pleasure learning from you.

*John Lim*, thank you for giving me tips on how to analyse my images using Image J.

*My BAT teammates Xiu Min, Rókus, Anna, Jean-Yves and Jarrod*, thank you for being my think-tank, for your support and friendship. It has been wonderful working with you talented people and I am proud to have you as my teammates.

*TML members past and present*, thank you for your support, kindness, happy memories and friendship all these years. I am thankful to have you as my lab mates.

*My mom, brother, Cindy and Dwi*, you guys are the light of my life. Thank you for being there for me and for believing in me when the going got tough.

*My Lord and my God*, thank You for everything. I put my best foot forward for You.

## TABLE OF CONTENTS

**SUMMARY**

Brown adipose tissue, comprising classical brown and beige adipocytes, holds therapeutic and diagnostic promise for the treatment of diabetes and metabolic syndrome. Key to realizing this potential is the ability to generate functional human brown adipocytes from a readily available and sustainable cell source. Here, I demonstrate the generation of a functional brown phenotype from adult human bone marrow-derived mesenchymal stem cells (bmMSCs) under macromolecular crowding (MMC), a biophysical principle applied to cell culture in order to mimic a more crowded *in vivo* environment by sterically excluding volume and speeding up the rate of extracellular matrix formation. Adipogenic differentiation of bmMSCs yielded substantial *UCP1* expression only with the addition of Ficoll to generate MMC during the induction phase, indicating that adult human bmMSCs possess the intrinsic potential to undergo brown adipogenesis. The bmMSC-derived adipocytes generated under MMC were functionally capable of activating the thermogenic programme, which included the upregulation of thermogenic genes, lipolysis, mitochondrial membrane depolarisation, uncoupled respiration and increased oxygen consumption. Ficoll-induced MMC increased the deposition of collagen IV and heparan sulphate proteoglycans, indicative of a richer pro-adipogenic matrix, which through cell-matrix reciprocity would drive adipogenesis of bmMSCs into a more mature phenotype. Additionally, bmMSC-derived white adipocytes could be 'browned' under MMC, suggesting that bmMSC-derived adipocytes or their precursor cells possess the plasticity to interconvert between white and brown. Moreover, there is preliminary data showing that the addition of Ficoll during adipogenic induction of progenitor cells isolated from the stromal vascular fraction also enhanced brown

adipogenesis, adding another potential sustainable cell source to the list. This study highlights the importance of the lineage-directing capacity of the microenvironment, which is enhanced under MMC. Interestingly Ficoll, may also enhance brown adipogenesis in bmMSC-derived adipocytes in an MMC-independent manner. Regardless, the relative ease of differentiating bmMSCs into the brown adipocyte phenotype (800-fold induction of *UCP1* mRNA over white when stimulated) without the need for gene transfer or induced pluripotency unlocks the metabolic and therapeutic potential lying dormant in human bone marrow. I hereby report for the first time that adult human bmMSCs are a functional human brown adipocyte progenitor cell source comparable with other human brown adipocyte differentiation models, and present a sustainable cell source for therapeutic and diagnostic applications.

## LIST OF TABLES

## LIST OF FIGURES

## LIST OF SYMBOLS AND ACRONYMS

| | |
|---|---|
| **18F-FDG** | 18F-fluorodeoxyglucose |
| **Acot2** | acyl-CoA thioesterase 2 |
| **ADRB3** | adrenoceptor beta 3 |
| **Agt** | angiotensinogen |
| **ATF2** | activating-transcription factor 2 |
| **ATP** | adenosine triphosphate |
| **BAT** | brown adipose tissue |
| **bmMSCs** | bone marrow mesenchymal stem cells |
| **BMP7** | bone morphogenetic protein 7 |
| **C/EBPβ** | CCAAT-enhancer binding protein β |
| **cAMP** | cyclic adenosine monophosphate |
| **Car4** | carbonic anhydrase 4 |
| **CIDEA** | cell death-inducing DNA fragmentation factor, alpha subunit-like effector a |
| **Cited1** | Cbp/p300-interacting transactivator with Glu/Asp-rich carboxy-terminal domain 1 |
| **CREB** | cAMP response element binding protein |
| **DAPI** | 4',6-diamidino-2-phenylindole |
| **DIO2** | deiodinase, iodothyronine, type II |
| **DMSO** | dimethyl sulfoxide |
| **Ear2** | eosinophil-associated, ribonuclease A family, member 2 |
| **Ebf3** | early B cell factor 3 |
| **ECM** | extracellular matrix |
| **EGF** | epidermal growth factor |
| **ELOVL3** | elongation of very long chain fatty acid elongase 3 |
| **Epstl1** | epithelial stromal interaction 1 |
| **Eva1** | epithelial V-Like antigen 1 |
| **EVE** | excluded volume effect |
| **FBP4** | fatty acid binding protein 4 |
| **FBS** | foetal bovine serum |
| **Fbxo31** | F-box protein 31 |
| **Fc400** | Ficoll400 |
| **Fc70** | Ficoll70 |
| **FCCP** | carbonyl cyanide-ptrifluoromethoxyphenylhydrazone |
| **FDA** | U.S. Food and Drug Administration |
| **FFAs** | free fatty acids |
| **FGF1** | fibroblast growth factor 1 |
| **FGF2** | fibroblast growth factor 2 |
| **Fgf21** | fibroblast growth factor 21 |
| **FITC** | fluorescein isothiocyanate |
| **FSC** | forward scatter |
| **FVO** | fraction volume occupancy |
| **GLU4** | glucose transporter type 4 |
| **HBSS** | Hank's balanced salt solution |
| **hESCs** | human embryonic stem cells |
| **HGDMEM** | high glucose Dulbecco's Modified Eagle's Medium |
| **hMADS** | human multipotent adipose-derived stem cells |

| | |
|---|---|
| **Hox9a** | homeobox gene 9 |
| **HOXC8** | homeobox C8 |
| **Hoxc9** | homeobox C9 |
| **HSL** | hormone sensitive lipase |
| **Hspb7** | heat shock protein family, member 7 |
| **HSPG** | heparin sulphate proteoglycans |
| **ib** | brown induction cocktail |
| **IBMX** | 3-isobutyl-1methylxanthine |
| **iPS** | induced pluripotent stem cells |
| **ITGA1** | integrin alpha 1 |
| **ITGA2** | integrin alpha 2 |
| **ITGB1** | integrin beta 1 |
| **iw** | white induction cocktail |
| **JC-1** | 5,5',6,6'-tetrachloro-1,1',3,3'-tetraethylbenzimidazolylcarbocyanine iodide |
| **Klhl13** | kelch-like family member 13 |
| **LEP** | leptin |
| **LGDMEM** | low glucose Dulbecco's Modified Eagle's Medium |
| **Lhx8** | LIM homeobox protein 8 |
| **MCP1** | monocyte chemoattractant protein 1 |
| **mito. G** | mitotracker Green |
| **MMC** | macromolecular crowding |
| **Myf5** | myogenic factor 5 |
| **Mylpf** | myosin regulatory light chain |
| **OCR** | oxygen consumption rate |
| **Oplah** | 5-oxoprolinase (ATP-hydrolysing) |
| **P/S** | penicillin and streptomycin |
| **Pax7** | paired box 7 |
| **PBS** | phosphate buffered saline |
| **PDGFRα** | platelet-derived growth factor receptor α |
| **Pdk4** | pyruvate dehydrogenase kinase, isozyme 4 |
| **PET/CT** | positron-emission tomography in combination with computed tomography |
| **PGC1α** | PPARγ co-activator 1α |
| **PKA** | protein kinase A |
| **PPARγ** | peroxisome proliferator-activated receptor gamma |
| **PRDM16** | PRD1-BF1-RIZ1 homologous domain containing 16 |
| **qPCR** | quantitative PCR |
| **Rosi** | rosiglitazone |
| **RPLP0** | ribosomal phosphoprotein P0 |
| **RT** | room temperature |
| **SDS** | sodium dodecyl sulphate |
| **SDS-PAGE** | sodium dodecyl sulphate polyacrylamide gel electrophoresis |
| **SHOX2** | short stature homeobox 2 |
| **Slc27a1** | solute carrier family 27 (fatty acid transporter), member 1 |
| **Slc29a1** | solute carrier family 29 (nucleoside transporters), member 1 |

| | |
|---|---|
| **SSC** | side scatter |
| **SVF** | stromal vascular fraction |
| **T3** | triiodothyronine |
| **T4** | thyroxine |
| **TBP** | TATA-box binding protein |
| **TBST** | Tris buffered saline with Tween20 |
| **Tbx1** | T-box 1 |
| **Tcf21** | transcription factor 21 |
| **Tmem26** | transmembrane protein 26 |
| **TNFα** | tumour necrosis factor α |
| **TRITC** | tetramethylrhodamine isothiocyanate |
| **TRP** | transient receptor potential (channel) |
| **TRPV4** | transient receptor potential vanilloid-4 |
| **TRPM8** | transient receptor potential melastin 8 |
| **UCP1** | uncoupling protein 1 |
| **VLDL** | very low density lipoproteins |
| **WAT** | white adipose tissue |
| **Wdnm1** | WDNM1-like protein |
| **Zic1** | zinc finger protein of the cerebellum 1 |
| **Δψm** | mitochondrial membrane potential |

# CHAPTER 1: INTRODUCTION

## *1.1 Global burden of obesity*

The ability to store excess energy efficiently has been evolutionarily advantageous to the survival of mankind as those who did were able to utilize these energy reserves to sustain themselves between meals when food was scarce. The human body has evolved to store excess energy in the form of fat (triglycerides) (Cinti, 2011), which has the highest energy-to-mass ratio as compared to other endogenous energy-bearing molecules such as carbohydrates (Da Poian et al., 2010); the cells specialized to store fat are the white adipocytes (Cinti, 2011). However, what was once a beneficial adaptation to cope with food scarcity has become a major health liability. Today presents an unnatural situation where food is abundant and easily accessible. Coupled with an increasingly sedentary lifestyle, the energy balance of an individual becomes upset, with energy intake far exceeding energy expenditure, leading to the condition of obesity (Bellisari, 2008). Obesity is defined as one's Body Mass Index (BMI) $\geq 30$ $kg/m^2$ (WHO, 2014) and of abnormal or excessive fat accumulation over a prolonged period which leads to multiple organ-specific pathological consequences (Lean, 2010). According to the World Health Organisation, obesity rates have doubled since 1980, causing obesity to reach epidemic proportions. Obesity affects more than 10% of the world's adult population. Obesity and being overweight (BMI $\geq 25$ $kg/m^2$) are leading causes for global deaths. They are implicated in major disease burdens, such as 44% of diabetes, 23% of ischaemic heart disease and 7-41% of certain cancers. Obesity is a major risk factor for cardiovascular disease, metabolic syndrome and diabetes, osteoarthritis and cancer (endometrial, breast and colon) (WHO, 2014). Obesity is high in developed countries such as the United States of America and

Australia (WHO, 2008), but is also on the rise in low-income countries as well (WHO, 2014). In Singapore, the sharp rise in obesity prevalence from 6.9% in 2004 to 10.8% in 2010 is a cause for worry (MOH, 2010).

### *1.2 Obesity and disease*

The contribution of obesity in the etiology of disease is due to the dysfunction of white adipocytes in the progression of obesity. White adipose tissue (WAT) is not just a passive organ for storing and releasing fat; it is also an active endocrine organ, secreting adipokines such as leptin and adiponectin which regulate metabolism and satiety, as well as other peptides such as monocyte chemoattractant protein 1 (MCP1) and tumour necrosis factor α (TNFα) which have systemic effects on other organs. At the early stages of high calorific intake, the white adipocytes initially enlarge in size and actively store the excess triglycerides to maintain normal lipolytic rates during fasting periods. However, as adiposity increases, the white adipocytes are unable to cope with the prolonged high calorific load and enter into a pro-inflammatory state by secreting MCP1 and TNFα. This attracts the infiltration of macrophages and results in a chronic inflammation in WAT. The cytokines released during the inflammatory process alter white adipocyte metabolism greatly by decreasing triglyceride synthesis and insulin sensitivity to uptake glucose, and increasing the rate of lipolysis, resulting in increased levels of circulating free fatty acids (FFAs). Insulin sensitivity to uptake glucose decreases in muscle due to the overload of FFAs and the build-up of ectopic lipid droplets, as well as through the action of the secreted cytokines from WAT. This sets the foundation of the development of insulin resistance, metabolic syndrome and finally diabetes mellitus (Guilherme et al., 2008). Also the influx of FFAs and cytokines into the liver alters its metabolism greatly, leading to the increased

production of very low density lipoproteins (VLDL) and apolipoprotein B which increases the risk of atherosclerosis and cardiovascular disease. Hypertension also develops due to the increased blood volume in response to an increased body mass and blood viscosity. Stroke risk increases with hypertension and cardiovascular disease (Haslam and James, 2005).

Despite an increased risk, some obese people do not progress to developing diabetes and other related diseases, suggesting other factors play a role in determining the severity of co-morbidity between obesity and disease. White adipose distribution, measured indirectly by waist-to-hip ratio, is a major risk indicator. Abdominal obesity is associated with an increased risk of diabetes and cardiovascular disease while subcutaneous obesity is not. This could be due to an unusually high influx of portal FFAs and cytokines from the omental adipocytes to the liver (Haslam and James, 2005). Another reason could be that abdominal or visceral fat may possess a metabolic profile distinct from subcutaneous fat (Billon and Dani, 2012). Genetics also play a role in body fat distribution (Nelson et al., 2000) and the predisposition to obesity (Bell et al., 2005). Epigenetic imprinting of metabolic pathways during foetal life due to generations of malnutrition *in utero*, coupled to the recent abundance of food have been implicated to cause certain populations (India for example) to be more susceptible to developing insulin resistance and diabetes (Yajnik, 2000).

### *1.3 Current treatment options for obesity*

Interventions aimed to treat obesity need to either reduce energy intake, increase energy expenditure, or both. Aside from exercise, practically all current interventions are aimed to reduce the energy intake side of the equation. Behavioural changes to adopt a more active physical lifestyle and healthier eating habits are hard to sustain for the long-term except for the very disciplined and committed individuals. Pharmacological interventions have met limited success due to undesirable side effects or inefficacy at curbing obesity in the long-term (Kim et al., 2014; Tseng et al., 2010). As of September 2013, there are only 3 drugs approved by the FDA for use as adjunctive therapy for chronic weight management: orlistat (Alli, GlaxoSmithKline; Xenical, Roche), phentermine/ topimerate extended release formulation (Qsymia, Vivus), and lorcaserin (Belviq, Arena Pharmaceuticals). These either act at the satiety centres in the brain (Qysmia and Belviq) or reduce systemic fat absorption from the intestine by inhibiting gastrointestinal lipases (Alli / Xenical) (Kim et al., 2014). Bariatric procedures have been proven more effective than lifestyle and medical interventions in reducing obesity but they are not without risks such as perioperative mortality and post-surgical complications (Arterburn and Courcoulas, 2014). Failure of these interventions to curb the rising trend of obesity by reducing energy intake is not surprising. The human body is designed to guard against starvation. When there is a decrease in food intake, the body's homeostatic mechanisms kick in to conserve energy by decreasing its basal metabolic rate, thus making it even harder for further weight loss. Targeting energy expenditure presents a more attractive option, as increasing energy output may be able to reset the homeostatic threshold for body weight of an obese individual to a lower, healthier range (Tseng et al., 2010).

### *1.4 Brown adipose tissue and its unique function of non-shivering thermogenesis*

In addition to WAT, mammals possess another type of fat, known as brown adipose tissue (BAT). Although both have the ability to store lipids, the function of BAT is entirely different from that of WAT. The main function of BAT is the expenditure of energy to produce heat in response to environmental temperature or diet, a process known as non-shivering thermogenesis. It serves the purpose of protection against cold exposure as well as regulation of energy balance (Yoneshiro et al., 2011). The protein responsible for conferring BAT its thermogenic function is the uncoupling protein 1 (UCP1), a 32kDa transmembrane inner mitochondrial membrane protein specific to brown adipocytes. When activated, UCP1 uncouples ATP synthesis from the electrochemical proton gradient in the electron transport chain, thereby producing heat (Fig. 1.1). When activated, UCP1 provides a channel for protons to rush out from the inter-membrane space down its electrochemical gradient to the mitochondrial matrix without being coupled to ATP generation. Heat is generated by the dissipation of the inter-membrane proton-motive force, and indirectly by the increased activity of the electron transport chain to maintain the electrochemical gradient (Tseng et al., 2010).

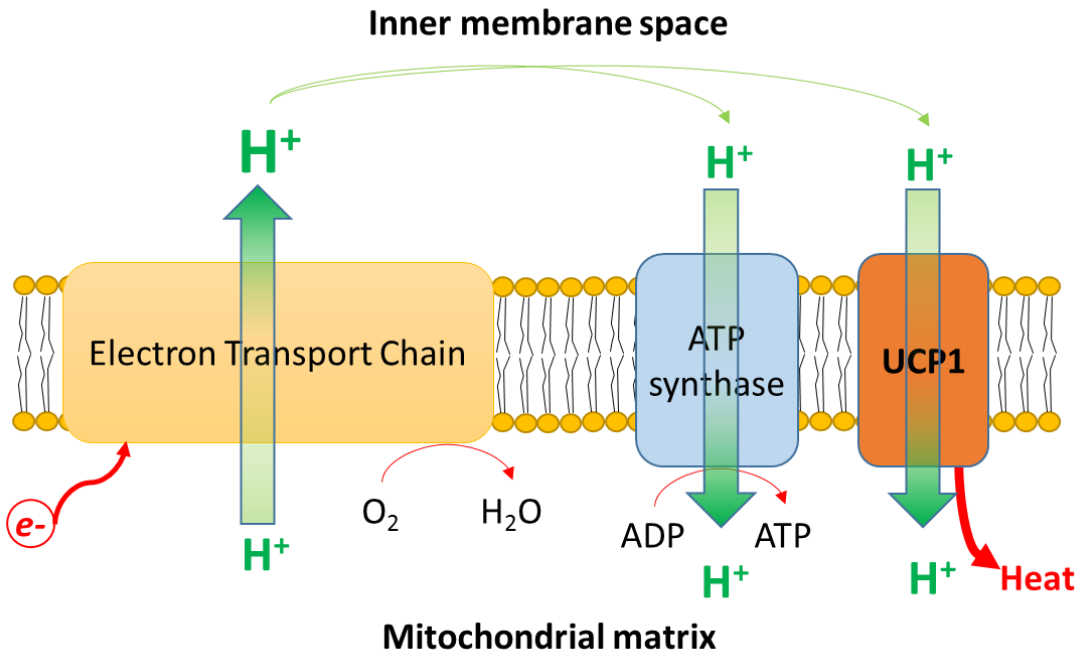


**Figure 1.1. Uncoupling function of UCP1.** Activated UCP1 residing in the inner mitochondrial membrane uncouples the proton gradient built up by the electron transport chain from ATP production, generating heat in the process. (Figure adapted from (Tseng et al., 2010).

In mice, thermogenesis in brown adipocytes is activated by the sympathetic nervous system in response to cold exposure. Noradrenaline acts principally through the β-adrenergic receptors, which leads to an increase in intracellular cyclic adenosine monophosphate (cAMP) levels. This in turn activates protein kinase A (PKA) and through multiple signalling transduction cascades drives thermogenesis. PKA stimulates gluconeogenesis and lipolysis, providing metabolic fuel for the mitochondria via the tricarboxylic acid cycle and β-oxidation respectively (Bonet et al., 2013; Tseng et al., 2010). Moreover, the free fatty acids (FFAs) produced upon lipolysis activate UCP1 by directly binding to UCP1 and removing the inhibitory effect of purine nucleotides (e.g. guanidine diphosphate) on UCP1 (Cannon and Nedergaard, 2004). Activation of PKA and its resulting downstream pathways lead to the phosphorylation of various transcription factors such as activating-transcription factor 2 (ATF2) and cAMP response element binding protein (CREB), which directly

induce UCP1 transcription. PKA also promotes the transcription of thermogenic genes such as deiodinase, iodothyronine, type II (DIO2) and PPARγ co-activator 1α (PGC1α). DIO2 converts thyroxine (T4) to its active form triiodothyronine (T3), which then activates UCP1 transcription through the thyroid hormone receptor. PGC1α is a co-factor which binds to other transcription factors to induce UCP1 transcription. In addition, it also promotes mitochondrial biogenesis to further increase the cell's thermogenic capacity (Bonet et al., 2013). Besides noradrenaline, β-agonists like isoproterenol (Wang et al., 2008a), and pharmacologic agents which act on downstream targets to increase cAMP such as forskolin (Seale et al., 2008) and dibutyryl cAMP (Tseng et al., 2008) are used to induce the thermogenic programme in brown adipocytes, summarized in figure 1.2. Besides UCP1, other functional markers typically associated with brown adipocytes are listed in table 1.1.

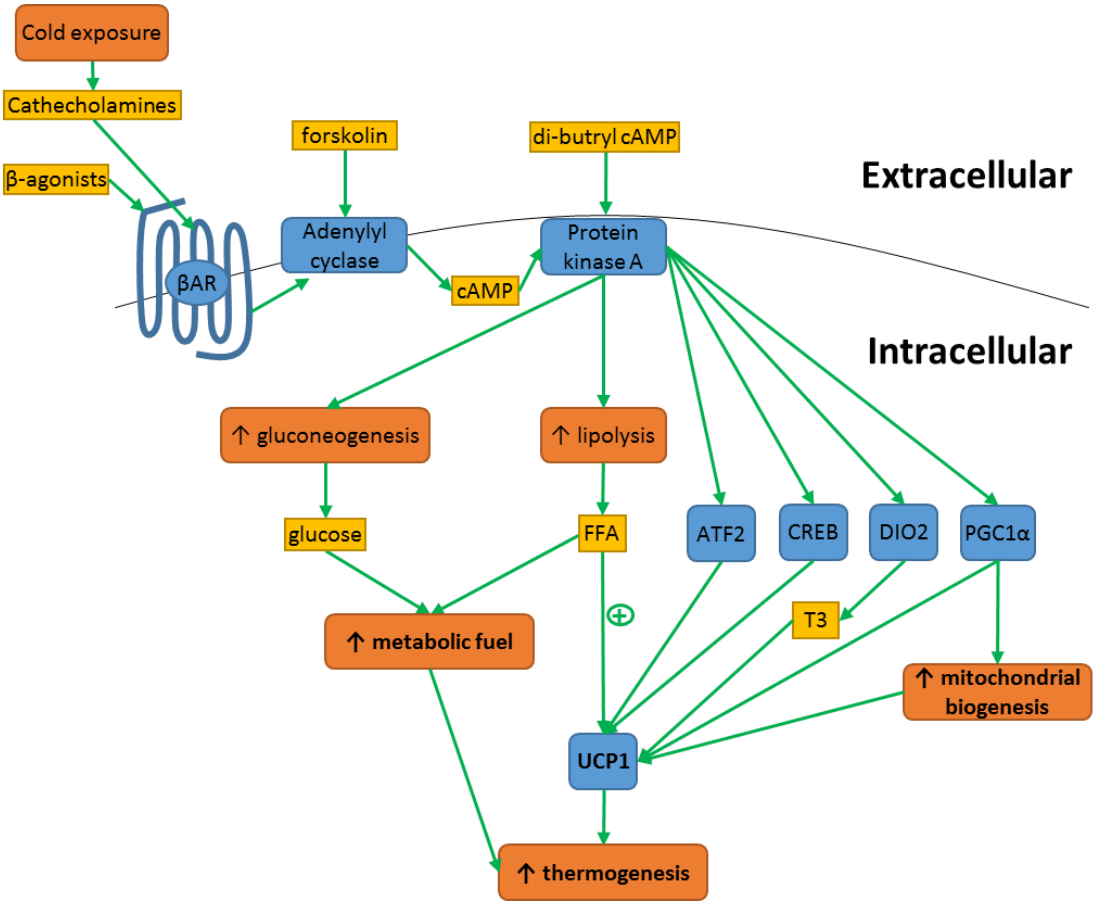


**Figure 1.2. Activation of thermogenesis in brown adipocytes.** Cold exposure, or pharmacological agents stimulate the β-adrenergic pathway which results in the activation of protein kinase A (PKA). PKA then initiates a cascade of events which lead to increase in metabolic fuel, mitochondrial biogenesis, UCP1 transcription and activity and ultimately an increase in thermogenesis. cAMP = cyclic AMP, FFA = free fatty acids, ATF2 = activating-transcription factor 2, CREB = cAMP response element binding protein, DIO2 = deiodinase, iodothyronine, type II, PGC1α = PPARγ co-activator 1α, T3 = triiodothyronine, UCP1 = uncoupling protein 1.
(Figure adapted from (Bonet et al., 2013; Tseng et al., 2010))

**Table 1.1. Brown-selective markers.**

| Factor | Name | Function | Reference |
|---|---|---|---|
| UCP1 | Uncoupling protein 1 | Protein responsible for uncoupled respiration in brown fat mitochondria. | (Cannon and Nedergaard, 2004) |
| CIDEA | cell death-inducing DNA fragmentation factor | Negatively regulates thermogenic function in brown fat, possibly by inhibiting UCP1. | (Lin and Li, 2004) |
| PRDM16 | PRD1-BF1-RIZ1 homologous domain containing 16 | Transcription regulator controlling the stem cell fate between brown fat and skeletal muscle. | (Kajimura et al., 2009; Seale et al., 2008) |
| ELOVL3 | Elongation of very long chain fatty acid elongase 3 | Involved in brown fat hyperplasia upon cold exposure or β-adrenergic stimulation, possibly due to the synthesis of saturated very long chain fatty acids in brown fat. | (Tvrdik et al., 1997; Westerberg et al., 2006) |
| PGC1α | PPARγ co-activator 1α | Increase mitochondrial biogenesis and UCP1 transcription during cold exposure or β-adrenergic stimulation. | (Bonet et al., 2013; Uldry et al., 2006) |
| DIO2 | deiodinase, iodothyronine, type II | Converts T4 to T3 during cold exposure or β-adrenergic stimulation, which then activates UCP1 transcription. | (Bonet et al., 2013) |

### *1.5 Types of brown adipose tissue*

Emerging evidence suggests that brown adipocytes from different anatomical locations originate from different developmental lineages (Billon and Dani, 2012; Rosenwald and Wolfrum, 2014). At least two populations of brown adipocytes exist – the classical brown adipocytes and the beige adipocytes. Rodents possess a substantial amount of BAT in the interscapular region (Harms and Seale, 2013). The brown adipocytes from this depot are termed classical brown adipocytes which originated from cells that expressed myogenic factor 5 positive ($myf5^{+}$) (Seale et al., 2008) and paired box 7 ($Pax7^{+}$) (Lepper and Fan, 2010). They are developmentally distinct from white adipocytes, but share a common progenitor with skeletal muscle. *In vivo* fate-mapping studies in mice embryos have shown that the myogenin-expressing central dermomyotome gave rise not only to the dermis and skeletal

muscle, but also to interscapular BAT, suggesting that skeletal muscle and interscapular BAT share a common developmental pathway (Atit et al., 2006). In support of this notion, cultured brown adipocyte progenitors expressed a myogenic transcriptional signature, which included myogenin and myf5 (Timmons et al., 2007). *In vivo* lineage tracing studies in mice by (Seale et al., 2008) further confirmed that myf5$^{+}$ expressing cells gave rise to BAT from the interscapular and peri-renal depots and skeletal muscle, but not to WAT. The existence of a common transcriptional programme for both BAT and skeletal muscle precursors was verified by discovering that PRD1-BF1-RIZ1 homologous domain containing 16 (PRDM16) functioned as a molecular switch to the BAT cell fate instead of skeletal muscle (Seale et al., 2008) through forming a transcriptional complex with CCAAT-enhancer binding protein β (C/EBPβ) (Kajimura et al., 2009). Through lineage tracing studies using endothelial marker (vascular endothelial) VE-cadherin, progenitors of classical brown adipocytes, like their white adipocyte counterparts, are found as perivascular cells in the capillaries of the respective depots (Gupta et al., 2012; Tran et al., 2012).

Beige adipocytes are UCP1-expressing adipocytes that appear ectopically in WAT depots in response to cold-induced β-adrenergic stimulation (Guerra et al., 1998) or chronic PPARγ (peroxisome proliferator-activated receptor gamma) agonist treatment (Petrovic et al., 2010; Vernochet et al., 2009). They are also known as "brown-in-white" / "brite" / "inducible-brown" adipocytes. The recruitment of beige adipocytes in a white adipose depot is known as "browning" (Bartelt and Heeren, 2014). Lineage tracing studies showed that beige adipocytes found in epididymal (Seale et al., 2008) and inguinal (Sanchez-Gurmaches et al., 2012) WAT in mice were myf5-, indicating that they do not share the same myogenic origin as classical brown adipocytes. Interestingly, (Sanchez-Gurmaches et al., 2012) discovered a

subpopulation of white adipocytes that were derived from myf5+ progenitors, challenging the notion that only myf5+ precursors gave rise to muscle and classical brown adipocytes. The beige cells induced by chronic PPARγ agonist treatment using thiazolidinediones during differentiation of white adipocytes in mice are developmentally closer to white adipocytes than the classical brown population (Petrovic et al., 2010), although this phenotypic conversion represses a series of "visceral white fat" genes (Vernochet et al., 2009). The recruitment of beige adipocytes in WAT depots may occur either by *de novo* generation of precursor cells, or interconversion of white adipocytes into beige, a process known as transdifferentiation (Bartelt and Heeren, 2014). In mice epididymal WAT, both white adipocytes and brown adipocytes that appeared from prolonged β-adrenergic stimulation arose from the proliferation and differentiation of a population of bipotential progenitor cells that expressed platelet-derived growth factor receptor α (PDGFRα) (Lee et al., 2012). Progenitor cells from inguinal WAT were isolated, cloned and shown to be able to differentiate into beige cells with a molecular signature distinct from white and classical brown adipocytes (Wu et al., 2012). The notion of beige adipocytes appearing in WAT depots by transdifferentiation of white adipocytes has been suspected (Barbatelli et al., 2010; Cinti, 2009). But only recently through *in vivo* lineage tracing studies, it was shown that the beige adipocytes which appeared in mice inguinal WAT upon cold-stimulation were able to transdifferentiate into white adipocytes upon 5 weeks of warm adaptation, and convert back into beige adipocytes on additional cold stimulation (Rosenwald et al., 2013). Figure 1.3 summarises the discussion on the developmental lineage of classical brown and beige adipocytes.

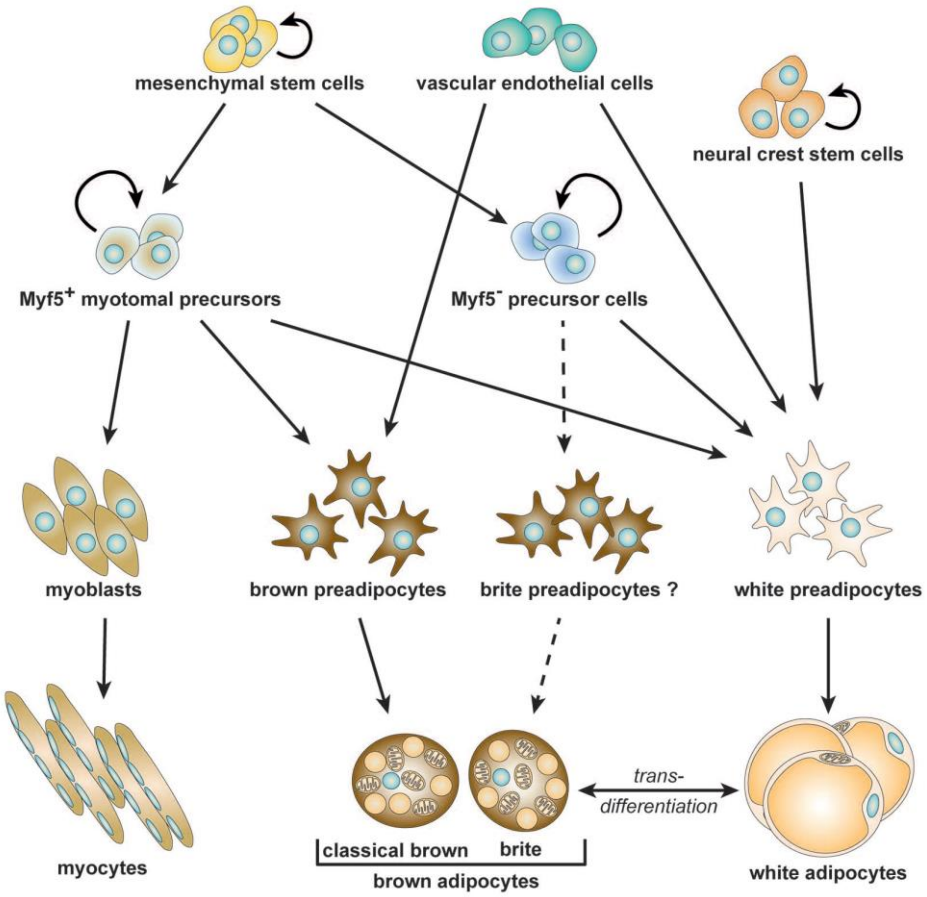


**Figure 1.3. Developmental lineages of adipocytes.** Figure reprinted from (Rosenwald and Wolfrum, 2014). [Permission is not required for reuse in a thesis/dissertation.]

Besides differences in anatomical location and developmental origin, attempts have been made to establish a molecular signature to differentiate classical brown, beige and white adipocytes in mice. (Sharp et al., 2012) compared gene expression levels between differentiated cells from interscapular BAT (classical brown), inguinal WAT that has been exposed to rosiglitazone (beige) and inguinal WAT without rosiglitazone treatment (white). (Walden et al., 2012) carried out a more extensive analysis on multiple adipose depots in mice and categorised them into classical brown (interscapular, cervical, axillary, mediastinal BAT), beige (cardiac, inguinal, retroperitoneal WAT) and white (mesenteric, epididymal WAT) based on high, intermediumte and low levels of *UCP1* expression, respectively. The approach of comparing different adipose depots has its limitations on distinguishing white from

beige adipocytes as inducible beige adipocytes exist even in the "white" epididymal adipose depot (Seale et al., 2008), suggesting that the depots that have been classically termed as "white" contain a heterogenous population of both white and beige adipocytes. To obtain a homogenous population of beige adipocytes, (Wu et al., 2012) isolated progenitor cells from the stromal vascular fraction of mice inguinal adipose tissue and established different clonal populations. The cells were differentiated and treated with forskolin, and the mRNA was used for a gene array analysis. A subset of the clonal populations showed a significant increase in *UCP1* expression after a 4h forskolin stimulus, and displayed a molecular signature unique to the low *UCP1*-expressing clonal populations and interscapular BAT (classical brown control). However, this study did not report a white-selective marker panel. Table 1.2 summarizes the marker panels reported in mice from these three studies.

**Table 1.2. Marker panel comparison of white, beige and classical brown adipocytes in mice.**

| Adipocyte markers | (Sharp et al., 2012) | (Walden et al., 2012) | (Wu et al., 2012) |
|---|---|---|---|
| **White-selective** | *Agt*<br>*Resistin*<br>*Wdnm1*<br>*Serpina3a* | *Tcf21* | *Nil* |
| **Beige-selective** | *Fgf21*<br>*Car4*<br>*Cited1*<br>*Hox9a* | *Hoxc9* | *Klhl13*<br>*Cd40*<br>*Ear2*<br>*Tmem26*<br>*Cd137*<br>*Sp100*<br>*Tbx1*<br>*Slc27a1* |
| **Classical brown-selective** | ***Zic1***<br>***Lhx8***<br>*Epstl1* | ***Zic1***<br>***Lhx8***<br>*Mylpf* | *Eva1*<br>*Fbxo31*<br>*Pdk4*<br>*Acot2*<br>*Ebf3*<br>*Hspb7*<br>*Slc29a1*<br>*Oplah* |

Markers common to at least 2 studies are in bold. *Agt* = angiotensinogen, *Wdnm1* = WDNM1-like protein, *Fgf21* = fibroblast growth factor 21, *Car4* = carbonic anhydrase 4, *Cited1* = Cbp/p300-interacting transactivator with Glu/Asp-rich carboxy-terminal domain 1, *Hox9a* = homeo box gene 9, *Zic1* = zinc finger protein of the cerebellum 1, *Lhx8* = LIM homeobox protein 8, *Epstl1* = epithelial stromal interaction 1, *Tcf21* = transcription factor 21, *Hoxc9* = homeobox C9, *Mylpf* = myosin regulatory light chain, *Klhl13* = kelch-like family member 13, *Ear2* = eosinophil-associated, ribonuclease A family, member 2, *Tmem26* = transmembrane protein 26, *Tbx1* = T-box 1, *Slc27a1* = solute carrier family 27 (fatty acid transporter), member 1, *Eva1* = Epithelial V-Like Antigen 1, *Fbxo31* = F-box protein 31, *Pdk4* = pyruvate dehydrogenase kinase, isozyme 4, *Acot2* = acyl-CoA thioesterase 2, *Ebf3* = early B cell factor 3, *Hspb7* = heat shock protein family, member 7, *Slc29a1* = solute carrier family 29 (nucleoside transporters), member 1, *Oplah* = 5-oxoprolinase (ATP-hydrolysing).

In addition, ectopic brown adipocytes and their progenitors have been identified in non-adipose tissue depots such as skeletal muscle (Almind et al., 2007; Schulz et al., 2011) as well.

### *1.6 Brown adipose tissue in adult humans*

BAT in humans, for a long time was assumed to exist in infants, primarily in the interscapular region (Fig. 1.4), and regressed in adulthood. Thus the importance and function of BAT was considered biologically irrelevant in adult humans. With the advent of positron-emission tomography in combination with computed tomography (PET/CT) to search for metabolically active tumours using 18F-fluorodeoxyglucose (18F-FDG) uptake, radiologists noted small, but distinct, non-tumour collections of adipose tissue (termed as "USA-fat") with high uptake of this tracer (Cohade et al., 2003). In 2007, a review by (Nedergaard et al., 2007) put forth the hypothesis from evidence accumulated from 18F-FDG PET/CT uptake studies, that BAT was present in adult humans in the neck and supraclavicular regions, as well as the mediastinum, paravertebral and suprarenal regions (Fig. 1.4). The presence of adult BAT inferred from these studies was suspected as early as 2002 (Hany et al., 2002), but only in 2009 did five independent groups manage to show conclusively the presence of BAT in adult humans (Cypess et al., 2009; Saito et al., 2009; van Marken Lichtenbelt et al., 2009; Virtanen et al., 2009; Zingaretti et al., 2009). Using 18F-FDG PET/CT uptake technique to locate these metabolically active depots under cold exposure (Fig. 1.4), fat biopsies were taken and tested positive for UCP1. The adipocytes also displayed a multi-locular appearance, typical of murine BAT histology.

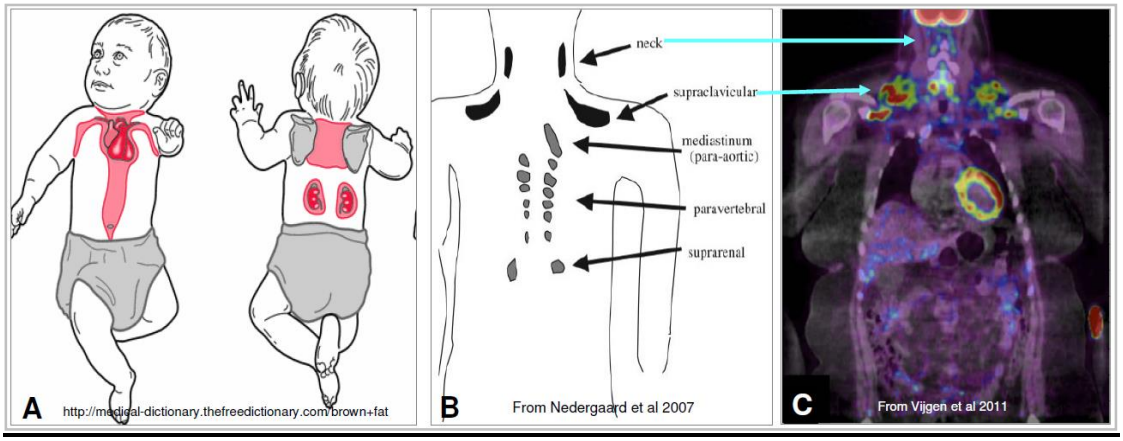


**Figure 1.4. Distribution of BAT in newborns, infants in comparison to that in adults.** (A) BAT in infants is located in the interscapular region, perirenal, mediastinal, in the neck region above and below the clavicles. (B) Schematic of BAT in cold-challenged adults via FDG-PET highlighting areas of high glucose uptake, a method originally used to detect tumors. (C) example of FDG-PET uptake in a morbidly obese female patient after cold challenge. Superimposition of CT and glucose PET. The supraclavicular and neck BAT patches are evident (Vijgen et al., 2011). [Figures B and C are reprinted from (Nedergaard et al., 2007) and (Vijgen et al., 2011). [Permission is not required for reuse in a thesis/dissertation.]

In light of the recent studies in mice, various research groups have used the set of gene markers distinguishing between the white, beige and classical brown populations in mice on human samples in order to identify the type of BAT found in humans. Substantial amounts of classical brown adipocytes clustered in the interscapular region, but only during infancy (Lidell et al., 2013). The supraclavicular BAT region found in adults appeared to be composed mainly of beige adipocytes (Sharp et al., 2012; Wu et al., 2012), or a mixture of both beige and classical brown adipocytes (Cypess et al., 2013; Jespersen et al., 2013). Table 1.3 summarizes the gene marker panel analysis reported from these five studies. There are some discrepancies between mice and human studies, e.g. homeobox C9 (HOXC9), a murine beige marker had the highest expression in the superficial WAT in neck region, as well as abdominal subcutaneous WAT, compared to the beige tissue counterparts (Cypess et al., 2013; Jespersen et al., 2013). There are also variations between human studies, e.g. there was no difference in expression of epithelial V-

Like antigen 1 (*EVA1*), a murine classical brown marker, between WAT and beige depots in (Sharp et al., 2012; Wu et al., 2012), but *EVA1* had the highest expression in the superficial WAT neck region compared to deeper neck BAT (Cypess et al., 2013). Overall, there seems to be a consensus between the studies on some of the markers in humans that distinguish a) classical brown: zinc finger protein of the cerebellum 1 (*ZIC1*) and LIM homeobox protein 8 (*LHX8*), b) beige markers: transmembrane protein 26 (*TMEM26*), *CD137* and T-box 1 (*TBX1*), and c) white: *HOXC9* (Table 1.3).

**Table 1.3. Marker panel comparison of white, beige and classical brown adipocytes in humans.**

| **Adipocyte markers** | **(Sharp et al., 2012)** | **(Wu et al., 2012)** | **(Lidell et al., 2013)** | **(Cypess et al., 2013)** | **(Jespersen et al., 2013)** |
|---|---|---|---|---|---|
| **White-selective** | Nil | Nil | Nil | *LEP*<br>***HOXC9***<br>*EVA1*<br>*EBF3*<br>*FBXO31* | *HOXC8*<br>***HOXC9*** |
| **Beige-selective** | ***TMEM26***<br>***CD137***<br>*HOXC8*<br>*HOXC9*<br>*FGF21*<br>*CITED1* | ***TMEM26***<br>***CD137***<br>***TBX1*** | ***TBX1*** | ***TMEM26***<br>***CD137***<br>*SHOX2* | ***TMEM26***<br>***TBX1*** |
| **Classical brown-selective** | ***ZIC1***<br>***LHX8***<br>*EPSTL1* | *EVA1*<br>*FBXO31*<br>*EBF3* | ***ZIC1*** | ***ZIC1***<br>***LHX8***<br>*UCP1* | ***ZIC1***<br>***LHX8***<br>*miR-206* |
| **Samples used in study** | Supraclavi-cular BAT*<br>WAT location not mentioned | Supraclavi-cular BAT<br>Supraclavicular WAT | Interscapular infant BAT<br>Supraclavicular BAT* | Fat depots from deep, intermediate and superficial regions in the neck | Supraclav-icular BAT<br>Abdominal subcutaneous WAT |
| **Comments** | No difference between groups in the classical brown marker panel | No difference between groups in the classical brown marker panel | 'Murine classical brown marker' EVA1 – no difference between groups<br>Beige markers TMEM26, SHOX2 and HOXC9 – no difference between groups | 'Murine classical brown markers' EVA1, FBXO31 and EBF3 were highest in superficial white fat | 'Murine beige markers' CITED1 and CD137 – no difference between groups |

Markers common to at least 2 studies are in bold. *Other BAT depots were used in the study but only supraclavicular BAT results are reflected in this table. *TMEM26* = transmembrane protein 26, *HOXC8* = homeobox C8, *HOXC9* = homeobox C9, *FGF21* = fibroblast growth factor 21, *CITED1* = Cbp/p300-interacting transactivator with Glu/Asp-rich carboxy-terminal domain 1, *ZIC1* = zinc finger protein of the cerebellum 1, *LHX8* = LIM homeobox protein 8, *EPSTL1* = epithelial stromal interaction 1, *TBX1* = T-box 1, *EVA1* = epithelial V-Like antigen 1, *FBXO31* = F-box protein 31, *EBF3* = early B cell factor 3, *LEP* = leptin, *SHOX2* = short stature homeobox 2, *miR-206* = mircroRNA 206.

### *1.7 Brown adipose tissue as a target for obesity therapy*

It has been observed in mice that BAT and possibly the extent of browning of WAT play a significant role in resisting diet-induced obesity. Initially, studies in mice with

various models of genetically ablated BAT presented conflicting findings on increasing the susceptibility to obesity, with (Lowell et al., 1993) showing the development of obesity and insulin resistance in UCP1-ablated mice which also developed hyperphagia, while others showed that UCP1-ablated mice failed to develop an obese phenotype (Enerback et al., 1997; Liu et al., 2003). In 2009, Feldman and colleagues reconciled the conflicting views in literature by showing that UCP1-ablated mice only developed obesity when living at thermoneutrality (~30$^{o}$C), which explains the earlier observations as typical housing conditions for mice were at ~18-22$^{o}$C, and served as a chronic thermal stress to the mice which in turn possibly influenced the outcome of those studies (Feldmann et al., 2009). When activated by the sympathetic nervous system, interscapular BAT becomes a fuel-guzzling organ in order to sustain thermogenesis in mice (Bartelt et al., 2011). As BAT lipolyses fat stores to FFAs to activate UCP1 and sustain mitochondrial activity through β-oxidation, it also takes up triglycerides from the systemic circulation. Furthermore, it also acts as a glucose sink, taking up blood glucose to further sustain thermogenesis (Nedergaard et al., 2011).

An early finding suggesting a possible link between the browning of WAT in resisting obesity in mice was reported in (Kopecky et al., 1995). Overexpression of UCP1 specific to adipocytes was performed using an aP2 gene promoter and particularly increased UCP1 expression in WAT. Obesity was reduced significantly in genetically obese $A^{vy}/+$ mice expressing this transgene. Inbred mice from different genetic backgrounds had a differential capability of upregulating UCP1 in WAT but not in interscapular BAT, and there was a correlation between UCP1-expression in WAT and weight loss in response to β3-adrenergic stimulation (Guerra et al., 1998). Besides β-adrenergic stimuli and PPARγ agonists, other agents that cause browning

in WAT have been reported (Bonet et al., 2013). However, more research needs to be carried out to ascertain the true metabolic contribution of beige adipocytes in WAT during adaptive thermogenesis to assess its role in preventing diet-induced obesity (Bartelt and Heeren, 2014).

In conjunction with previous estimates that in humans as little as 50g of maximally stimulated BAT could account for 20% of daily energy expenditure (Rothwell and Stock, 1983), an enormous therapeutic potential is currently ascribed to brown adipocytes or methods for browning WAT for tackling obesity and pertinent co-morbidities such as type 2 diabetes, and metabolic syndrome (Cypess and Kahn, 2010). Yoneshiro et al. (2011) reported that in humans, after a 2h cold exposure, energy expenditure increased by about 28% in a group with detectable BAT and this correlated with increased BAT activity estimated by FDG-uptake into the neck and paravertebral regions, compared to a 3% increase in energy expenditure in the BAT-negative group (Yoneshiro et al., 2011). In another study, upon cold exposure, there was an increased uptake of glucose and non-esterified fatty acids into supraclavicular BAT but not in adjoining skeletal muscles and subcutaneous adipose tissue, as well as increased BAT oxidative metabolism, and this was associated with an increased total energy expenditure probably to sustain thermogenesis in BAT (Ouellet et al., 2012). Moreover, the amount and activity of BAT are negatively correlated with BMI, age and diabetic status (Orava et al., 2013; Ouellet et al., 2011; van Marken Lichtenbelt et al., 2009), suggesting a causal link between decreased BAT activity and weight gain. As the amount of BAT in humans is typically quite low, the idea of increasing the amount of beige adipocytes through browning of existing WAT depots is also a very attractive option (Bartelt and Heeren, 2014). Therefore, a great demand for a

sustainable source of human classical brown / beige adipocytes for clinically relevant studies has arisen.

### *1.8 The therapeutic and biotechnological gap – the need for progenitor cells*

There are 2 main approaches to utilise the thermogenic capacity of BAT as a treatment option for obesity – the *ex vivo* approach where functional BAT is generated in vitro from progenitor cells and then transplanted back into the patient as a cell therapy; and the *in vivo* approach where pharmacological agents or nutraceutical compounds are administered to the patient to increase differentiation and thermogenic activation of BAT (Tseng et al., 2010). As mentioned in section 1.3, current pharmacological interventions for use in chronic weight management have met limited success due to limited efficacy or safety concerns. Much of the anti-obesity drug research targets have focused on regulating the neurological networks that control satiety. However, with the recent discovery of functional BAT in adult humans, there has been great interest in identifying pharmacological and nutraceutical compounds that target BAT differentiation and thermogenesis to increase energy expenditure as a strategy to counteract obesity. New pathways involving BAT differentiation and thermogenic activation are being unraveled, increasing the number of potential targets for pharmacological intervention (Villarroya and Vidal-Puig, 2013). Dietary compounds such as capsinoids have been shown to increase energy expenditure in humans by activating BAT (Yoneshiro et al., 2012). Thus a human cell-based screening platform would be useful to identify promising pharmacological and nutraceutical targets (Dulloo, 2011). For the cell system to be used in the screening platform, primary human progenitor cells that can differentiate into functional brown adipocytes would provide a response more representative of the *in*

*vivo* condition as compared to immortalized or genetically modified cell lines (Ebert and Svendsen, 2010; Zang et al., 2012). In fact, some of the leading scientists in the brown fat field are involved in industry ventures to develop this screening platform capability, or for cell therapy (Table 1.4).

**Table 1.4. Scientists involved in biotechnology companies that are developing BAT screening platforms or for cell therapy.**

| Company | Website | Scientists involved | Key publications |
|---|---|---|---|
| Biorestorative Therapies | http://www.biorestorative.com/content/thermostem%C2%AE-program | Francisco Silva | (Silva et al., 2014) |
| Ember Therapeutics | http://www.embertx.com/approach.php | Bruce M Spiegelman<br>C Ronald Kahn | (Seale et al., 2008)<br>(Tseng et al., 2008) |

However, given the anatomical location and amount of BAT in humans (see figure 1.4), the isolation of sufficient and sustainable numbers of human primary brown and beige adipocytes is problematic. Currently brown adipocyte differentiation protocols for human progenitor cells require the isolation of precursor cells from tissue locations difficult to attain (e.g. FDG/PET-positive BAT depots in humans), or require substantial reprogramming of starting material, or require precursor cells obtained from non-adult sources. Generating brown adipocytes through gene manipulation presents a major hurdle in translating the technology from bench to bedside. Attempts to obtain progenitor cells that can differentiate into brown adipocyte-like cells have been done from very young subjects or aborted foetuses, which do not represent a readily available, cost-effective, autologous, or ethically sound solution. Moreover, progenitor cells obtained from young subjects or foetal sources are not representative of BAT in adults as the type of BAT in infants and adults is different (Lidell et al., 2013). Therefore it is essential that a method for

generating human BAT from a readily available adult cell source be found in order to advance the field. The current human cell models of brown adipogenesis are reviewed in (Beranger et al., 2013), and summarised in table 1.5.

**Table 1.5. Comparison of current *in vitro* human cellular models of brown adipogenesis.**

| Cell model | Functional efficiency (*UCP1* mRNA upregulation) | Pros and Cons | Reference |
|---|---|---|---|
| Progenitor cells from the SVF or preadipocytes of supraclavicular fat | 20-40 fold higher than subcut. WAT.<br><br>60-fold higher than preadipocytes from subcut. abdominal WAT. | **Pros**<br>• Isolation of progenitor cells from an identified PET/FDG-positive human BAT depot<br>• Robust expression of UCP1 and response to cAMP stimuli<br>**Cons**<br>• Invasive harvest, hard to obtain | (Lee et al., 2011b)<br><br>(Jespersen et al., 2013) |
| Progenitor cells from the SVF of neck fat | 5-fold upregulation in response to di-butyryl cAMP. | | (Cypess et al., 2013) |
| Progenitor cells from mediastinal fat | Upregulation of *UCP1* compared to non-induced cells. No fold change was reported. | **Pros**<br>• Isolation of progenitor cells from a possible human BAT depot<br>**Cons**<br>• Invasive harvest, hard to obtain | (Silva et al., 2014) |
| Preadipocytes from omental, subcutaneous perirenal fat | Upregulation of *UCP1* in thiazolidinedione-differerentiated adipocytes compared to vehicle controls. No fold change was reported. | **Pros**<br>• Available cell source<br>**Cons**<br>• Browning effect not robust<br>• No functional metabolic tests available | (Digby et al., 1998) |
| hMADS *Adipose-derived stem cells isolated from biopsies of subcutaneous fat taken from the pubic region of infants and young children* | 13-39 fold higher compared to treatment with rosiglitazone for only 3-9 days during differentiation (no *UCP1* expression but comparable expression of WAT genes). | **Pros**<br>• Robust expression of UCP1 and thermogenesis<br>• Platform for white-to-brown conversion available<br>**Cons**<br>• Cell source not readily available<br>• Non-adult source | (Elabd et al., 2009) (Pisani et al., 2011) |
| Foetal bmMSCs *MSCs were adipogenically induced and the authors found they could differentiate into either brown or white fat* | 60-fold higher compared to another bone marrow sample. | **Pros**<br>• High expression of UCP1<br>**Cons**<br>• Cell source not readily available<br>• Unpredictable – one donor source contained brown adipocytes whereas the other contained white adipocytes<br>• Ethical issues<br>• Non-adult source | (Morganstein et al., 2010) |
| Foetal muscle progenitor CD34+ cells | *UCP1* mRNA levels a forth of mouse BAT. 8-fold upregulation in response to cAMP stimulation. | **Pros**<br>• Novel cell source<br>**Cons**<br>• Cell source not readily available<br>• Ethical issues<br>• Non-adult source | (Crisan et al., 2008) |

| **Cell model** | **Functional efficiency** (*UCP1* mRNA upregulation) | **Pros and Cons** | **Reference** |
|---|---|---|---|
| PAZ6<br>*Isolated from the SVF of infant BAT and immortalised using T and t SV40 antigens* | *UCP1* mRNA was detected and increased upon NE stimulation. No fold change was reported. | **Pros**<br>• Cell line, easily obtainable<br>**Cons**<br>• No functional metabolic tests available<br>• Genetically manipulated | (Zilberfarb et al., 1997) (Kazantzis et al., 2012) |
| iPS cells transduced with various genes | 20-fold upregulation compared to transduced "WAT". | **Pros**<br>• Robust expression of UCP1 and thermogenesis<br>**Cons**<br>• Tedious, genetically manipulated | (Ahfeldt et al., 2012) |
| iPS / hESCs cells differentiated without gene transduction | 20-fold upregulation compared to bmMSC-derived adipocytes. | **Pros**<br>• Robust expression of UCP1 and thermogenesis<br>**Cons**<br>• Complicated protocol | (Nishio et al., 2012) |
| bmMSCs overexpressing PGC1α | 4-fold upregulation compared with non-transduced bmMSCs. | **Pros**<br>• Available cell source<br>**Cons**<br>• Genetically manipulated<br>• Differentiation length was too short to attain a mature adipocyte phenotype | (Huang et al., 2011) |
| Preadipocytes from subcutaneous WAT overexpressing PGC1α | 10-fold upregulation compared to control WAT. | **Pros**<br>• Available cell source<br>**Cons**<br>• Genetically manipulated | (Tiraby et al., 2003) |

SVF = stromal vascular fraction, hMADS = human multipotent adipose-derived stem cells, bmMSCs = bone marrow mesenchymal stem cells, iPS = induced pluripotent stem cells, hESCs = human embryonic stem cells.

### *1.9 Macromolecular crowding, a novel cell culture platform that enhances adipogenic differentiation of adult human bone marrow mesenchymal stem cells via an enriched microenvironment*

It is recognized that *in vitro* monolayer culture conditions differ greatly from the *in vivo* tissue microenvironments from which the cells are derived (Abbott, 2003; Mazzoleni et al., 2009). A major limitation of 2D monolayer cultures is that they fail to capture the complexity of the *in vivo* microenvironment that is rich in extracellular matrix (ECM) and sequestered growth factors (Discher et al., 2009). For stem cell differentiation, it is important for *in vitro* culture conditions to emulate the native microenvironment as differentiation to a specific lineage is governed by specific cues within each unique local microenvironment (Moore and Lemischka, 2006). The extracellular microenvironment has a high solute content of macromolecules which occupy volume and exclude like-sized molecules through steric repulsion (Ellis, 2001). Macromolecules such as proteins, carbohydrates, lipids and nucleic acids found in biological systems typically have a size range of 50-500kDa (Chen et al., 2011). *In vitro* cell culture systems commonly employ 5-20% foetal bovine serum in culture media resulting in a macromolecular solute content of 4-16mg/ml (Chen et al., 2011), which is much lower than that observed in interstitial fluids (30-40 mg/ml) (Bates et al., 1993) or blood plasma (80 mg/ml) (Wadsworth and Oliveiro, 1953). Biological reactions performed in dilute *in vitro* conditions proceed at much slower rates than in *in vivo* conditions which have a much higher macromolecular solute content (Minton, 2001), Volume exclusion due to the high macromolecular solute content lowers the configurational entropy, leading to an elevated basal free energy of reactant macromolecules which results in increased reaction rates (Chen et al., 2011; Ellis, 2001). Hence it is no surprise that the sparse microenvironment formation *in*

*vitro* culture systems fails to replicate the *in vivo* conditions. It is based on this observation of the lack of "crowdedness" in *in vitro* cell culture systems that I introduce macromolecular crowding (MMC) to address this issue. MMC is defined by exerting an excluded-volume effect (EVE) due to the addition of one or more types of inert macromolecules of size 50-500kDa with low viscosity in solution into the system in order to increase the rate of various extracellular biological reactions, such as the deposition and remodeling of the extracellular matrix (Chen et al., 2011). The amount of EVE is dependent on the fraction volume occupancy (FVO) of the macromolecules. The calculation of the FVO, expressed as the percentage volume that the macromolecules occupy at a given concentration ***x*** **g/ml** assumes that the soluble macromolecules are mutually impenetrable and form spheres of a certain hydrodynamic radius (Chen et al., 2011):

**Volume of one molecule =** $\frac{4}{3}\pi r^3$
where *r* is the hydrodynamic radius of the molecule in $m^3$
**Total number of molecules in *x* g =** $\frac{x}{M} \times N_A$
where M is the molar mass of the molecule in g/mol and $N_A$ is the Avogadro constant = 6.023 x $10^{23}$ molecules/mol
**FVO (v/v) =** $\frac{4}{3}\pi r^3 \times \frac{xN_A}{M} \div 10^{-6} \times 100\%$

It was previously reported that using MMC in cell culture increased ECM deposition in various cell types, enabling them to build their respective microenvironments *in vitro* with greater speed and efficiency (Chen et al., 2011; Chen et al., 2009; Zeiger et al., 2012).

Adult human bone marrow mesenchymal stem cells (bmMSCs) are multipotent stem cells of mesodermal origin with the ability to differentiate into bone, cartilage and fat (Mackay et al., 2006; Pittenger et al., 1999). Given their relative ease of isolation and expansion to sustainable numbers, bmMSCs would be an ideal cell source if they could be induced to differentiate to brown adipocytes also of

mesodermal origin. Currently, adult bmMSCs have been shown to differentiate into white but not into brown adipocytes (Mackay et al., 2006) using the classic adipogenic cocktail (insulin, dexamethasone, indomethacin and 3-isobutyl-1methylxanthine (IBMX)) as established by (Pittenger et al., 1999). I have recently described an improved WAT differentiation model that encompasses adipogenesis from adult human bmMSCs to higher degree of maturation using MMC with polysucrose polymers (Ficoll). The enhanced adipogenesis was caused by dynamic cell-matrix reciprocity between the differentiating bmMSCs and the increased deposition and remodelling of the ECM which tunes the microenvironment to augment adipogenic differentiation (Ang et al., 2014). As MMC is able to enhance white adipogenic differentiation of bmMSCs, I questioned the possibility of MMC enhancing brown adipogenesis of bmMSCs when a brown adipogenic cocktail is used.

### *1.10 Hypotheses*

So far literature has assumed that adult human bmMSCs differentiate into white adipocytes based on the absence of UCP1, and in Ang et al. (2014) we further assumed that WAT differentiation was augmented when the cells were adipogenically induced under MMC using Ficoll. This project is based on stepping back and asking the fundamental question: "What kind of adipocytes are we obtaining in our cultures when bmMSCs are differentiated under crowded conditions?" I initially hypothesized that white adipogenesis would be enhanced in bmMSC-derived adipocytes grown under MMC using the classic adipogenic cocktail. However, when I performed qPCR on my samples with a home-made *UCP1* primer I realized that *UCP1* was upregulated in adipocytes generated under MMC. It was indeed a serendipitous

finding. This led me to speculate that adult human bmMSCs may have the intrinsic potential to differentiate into brown adipocytes under the right conditions without genetic manipulation, a phenomenon not described before. As adult bone marrow mesenchymal stem cells (bmMSCs) are multipotent of mesodermal origin, and are able to differentiate into white adipocytes, I hypothesized that bmMSCs possess the intrinsic potential to differentiate into brown adipocytes, also of mesodermal origin. This potential would be augmented by macromolecular crowding (MMC). The specific hypotheses are:

1. Adult human bmMSCs possess the intrinsic potential to differentiate into functional brown adipocytes.
2. The potential of bmMSCs to differentiate into functional brown adipocytes is greatly augmented with the addition of Ficoll during adipogenic induction.
3. Ficoll augments brown adipogenesis in adult human bmMSCs through the generation of macromolecular crowding (MMC) in the cultures which enhances the microenvironment formation of the bmMSC-derived adipocytes towards a mature adipocyte phenotype.

The proposed work here suggests that adult human bmMSCs could be another important and highly interesting source of brown adipocyte progenitors by demonstrating that through the use of MMC in our cell culture systems, adult human bmMSCs can differentiate into functional brown adipocytes.

# CHAPTER 2: MATERIALS AND METHODS

## *2.1 Calculation for emulating bone marrow crowdedness and choice of macromolecular crowder*

Calculations for bone marrow crowdedness and choice of crowder were performed as described previously (Chen et al., 2011). As no data is available for the calculation of bone marrow crowdedness, concentration of albumin with hydrodynamic radius = 4nm, in blood serum was used to estimate the fractional volume occupancy (FVO) of bone marrow (Chen et al., 2011). Referring to the equation in *Introduction section 1.9*:

$$\text{Concentration of albumin in blood} = 80\text{mg/ml}$$
$$\text{Hydrodynamic radius of albumin} = 4\text{nm}$$
$$\text{MW of albumin} = 69\,000\text{ Da}$$
$$\text{Volume of one albumin molecule} = \frac{4}{3}\pi r^3 = 268.1 \times 10^{-27}\text{m}^3$$
$$\text{Total number of albumin molecules in 80mg} = \frac{0.08}{\text{M}} \times N_A$$
$$= \frac{0.08}{69000} \times 6.023 \times 10^{23}\text{molecules}$$
$$\boldsymbol{FVO}\ (\boldsymbol{v/v}) = (268.1 \times 10^{-27}) \times \left(\frac{0.08}{69000} \times 6.023 \times 10^{23}\right) \div 10^{-6} \times 100\%$$
$$= \mathbf{18.7}\%$$

The choice of using Ficoll$^{TM}$70 and Ficoll$^{TM}$400 (PM70 17-0310-50 and PM400 17-0300-50, GE Healthcare, Bio-sciences AB, Uppsala, Sweden) at the prescribed ratio of 37.5mg/ml and 25mg/ml respectively had been determined experimentally by past colleagues to be optimal for bmMSC culture (Chen et al., 2011). Ficoll70 was chosen as it has been commonly used as a crowder because of its relatively low viscosity in solution (Ellis, 2001; Rashid et al., 2014b). A mixture of Ficoll70 and Ficoll400 was used as mixed macromolecular crowding proved to be more effective than crowding by a single crowding agent (Chen et al., 2011; Du et al., 2006). When the FVO of the

Ficoll cocktail was calculated, it amounted to ~17%, close to the FVO of bone marrow, thus providing a possible explanation for the effectiveness of the current concentration of these macromolecular crowders used in bmMSC culture (Chen et al., 2011). The FVO calculations for the Ficoll cocktail are shown below as described in Chen et al., (2011):

**Table 2.1. Properties of Ficoll 70 and Ficoll 400.**

| **Crowder** | Fc70 | Fc400 |
|---|---|---|
| **Concentration (mg/ml)** | 37.5 | 25 |
| **Hydrodynamic radius** | 4 | 8 |

$$\text{Volume of one Fc400 molecule} = 2145 \times 10^{-27}\text{m}^3$$

$$\text{Total number of Fc70 molecules in 37.5mg} = \frac{0.0375}{70000} \times 6.023 \times 10^{23}\text{molecules}$$

$$\text{Total number of Fc400 molecules in 25mg} = \frac{0.025}{400000} \times 6.023 \times 10^{23}\text{molecules}$$

$$\boldsymbol{FVO}\ (\boldsymbol{v/v}) = \left[(268.1 \times 10^{-27}) \times \left(\frac{0.0375}{70000} \times 6.023 \times 10^{23}\right) + (2145 \times 10^{-27}) \times \left(\frac{0.025}{400000} \times 6.023 \times 10^{23}\right)\right] \div 10^{-6} \times 100\% = \mathbf{16.7}\%$$

### *2.2 Adult human bone marrow mesenchymal stem cell culture*

Adult human bone-marrow derived mesenchymal stem cells (bmMSCs) were obtained commercially (Lonza/Cambrex Bioscience, PT-2501, Walkersville, MD, USA) at passage 2 and cultured in low glucose Dulbecco's modified Eagle's medium (LGDMEM) supplemented with GlutaMAX™, 10% foetal bovine serum (FBS), 100units/ml penicillin and 100μg/ml streptomycin (1% P/S) (10567, 10270 and 15140, Gibco/Life Technologies, Carlsbad, CA, USA). Cells were maintained at 37˚C in a humidified atmosphere of 5% $CO_2$, with medium change every 3-4 days. To prevent spontaneous differentiation, cells were maintained at subconfluent levels prior to being detached using TrypLE™ Express (12604, Gibco/Life Technologies,

Carlsbad, CA, USA), passaged at 1:3 – 4 and cultured to generate subsequent passages. Directed differentiation was carried out with cells at passage 5 or 7-8.

### *2.3 Adipogenic induction of bone marrow mesenchymal stem cells*

Unless stated otherwise, bmMSCs were seeded at an initial density of 10.5k cells/cm$^2$ in well plates. Adipogenic differentiation was stimulated when the cells reached confluence as described (McBeath et al., 2004; Pittenger et al., 1999) (with modifications) via three or six cycles of 4 days of induction, followed by 3 days of maintenance. Non-induced control bmMSCs were maintained with basal medium alone on the same schedule. The basal medium used in the differentiation process consisted of high glucose Dulbecco's modified Eagle's medium (HGDMEM) supplemented with GlutaMAX$^{TM}$, 10% foetal bovine serum (FBS), 100units/ml penicillin and 100µg/ml streptomycin (1% P/S) (10569, 10270 and 15140, Gibco/Life Technologies, Carlsbad, CA, USA). For white adipocyte differentiation, the induction medium was supplemented with 0.5mM 3-isobutyl-1methylxanthine (IBMX), 0.2mM indomethacin, 1µM dexamethasone and 10µg/ml insulin (I5879, I7378, D4902 and I6634/91077C, Sigma-Aldrich, St-Louis, MO, USA). Basal medium alone was used during the maintenance phase. For brown adipocyte differentiation, cells were pre-treated with 125ng/ml (8.0nM) bone morphogenetic protein 7 (BMP7) (354-BP, R&D Systems, Minneapolis, MN, USA) in LGDMEM (with FBS and 1% P/S) 3 days prior to induction. The brown adipogenic induction medium was supplemented with 0.5mM IBMX, 0.2mM indomethacin, 1µM dexamethasone, 10µg/ml insulin, 1nM triiodothyronine (T3, T5516, Sigma-Aldrich, St-Louis, MO, USA) and 1µM rosiglitazone (ALX-350-125, Enzo Life Sciences Inc., Farmingdale, NY, USA). Basal medium alone was used during the maintenance phase. For conditions treated

with macromolecular crowding (+MMC), the medium was supplemented with a cocktail of macromolecules; Ficoll$^{TM}$70 at 37.5mg/ml and Ficoll$^{TM}$400 at 25mg/ml (PM70 17-0310-50 and PM400 17-0300-50, GE Healthcare, Bio-sciences AB, Uppsala, Sweden), throughout the differentiation process. The cocktail of macromolecules was dissolved in the medium at room temperature (RT) with gentle agitation, and then sterile filtered with a 0.2µm syringe filter (16532, Satorius Stedim Biotech GmbH, Goettingen, Germany) prior to use. Figure 2.1 shows the 3-week induction timeline. For stimulation with forskolin (F6886 Sigma-Aldrich, St-Louis, MO, USA), 10µM was used. Unstimulated cultures were incubated with either only basal medium (without MMC) or with the addition of an equal amount of dimethyl sulfoxide (DMSO) as a vehicle.

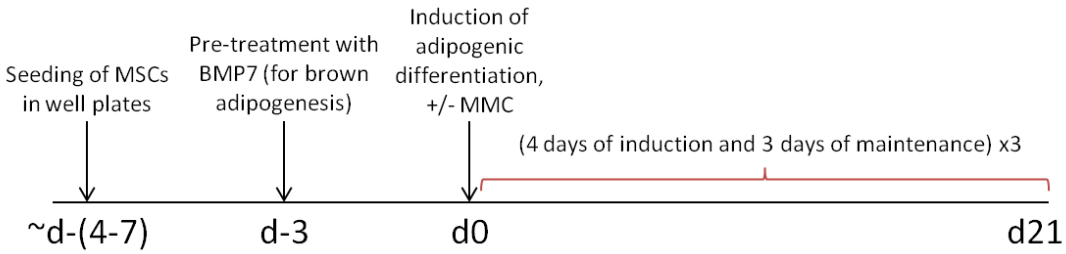


**Figure 2.1. 3-week induction timeline of adipogenic differentiation of bmMSCs.** hbmMSCs were seeded in well plates and adipogenic differentiation was induced at confluence. 3 days before induction, cells to be treated with a brown induction protocol were treated with BMP7 prior to adipogenic differentiation. Adipogenic differentiation was performed on the cells via 3 cycles of a 4-day treatment with induction media followed by a 3-day treatment with maintenance media. The Ficoll cocktail used to generate macromolecular crowding (MMC) were added throughout the adipogenic differentiation period for the MMC conditions.

### *2.4 Culture and adipogenic induction of progenitors isolated from the stromal vascular fraction (SVF) of abdominal subcutaneous fat*

The progenitor cells, isolated from the SVF of abdominal subcutaneous adipose tissue, were a kind gift from Dr. Sue-Anne Toh at passage 4. The cells were cultured in high glucose Dulbecco's modified Eagle's medium (HGDMEM) supplemented with GlutaMAX$^{TM}$, 10% foetal bovine serum (FBS), 100units/ml penicillin and 100µg/ml streptomycin (1% P/S) (10569, 10270 and 15140, Gibco/Life Technologies, Carlsbad, CA, USA). Cells were maintained at 37˚C in a humidified atmosphere of 5% $CO_2$, with medium change every 3-4 days. To prevent spontaneous differentiation, cells were maintained at subconfluent levels prior to being detached using TrypLE™ Express (12604, Gibco/Life Technologies, Carlsbad, CA, USA). Directed differentiation was carried out with the cells at passage 5. Adipogenic differentiation of these cells followed the protocols used for bmMSCs.

### *2.5 Nile Red area quantification*

Cells were seeded in a 24-well plate format (662160, Cellstar, Greiner, Bio-one GmbH, Frickenhausen, Germany). Monolayers were washed in PBS, fixed in 4% methanol-free formaldehyde (28908, Pierce Biotechnology Inc., Rockford, IL, USA) for 30min at RT, then co-stained for 30min with 5µg/ml Nile Red (N3013, Sigma-Aldrich, St-Louis, MO, USA), for cytoplasmic lipid droplets and 0.5µg/ml of 4',6-diamidino-2-phenylindole (DAPI) (D3571, Molecular Probes®, Life Technologies, Carlsbad, CA, USA) for nuclear DNA as described previously (Greenspan et al., 1985). Images were captured with an IX71 inverted fluorescence microscope (Olympus, Center Valley, PA, USA). Adherent cytometry was performed according to previously described protocol (Ang et al., 2014; Chen et al., 2009). Nine image

sites per well were acquired using a 2X objective with a coolSNAP HQ camera attached to a Nikon TE2000 microscope (Nikon Instruments, Melville, NY, USA), stored and analysed using the Metamorph Imaging System Software 6.3v3 (Molecular Devices, Sunnyvale, CA, USA). An image field of 4.48 x 3.34mm per site was defined for each 24-well plate with a final image of 13.43 x 10.03mm; covering 134.70 $mm^2$ per well. Nile Red was viewed under a rhodamine filter [Ex 545nm/Em610nm] while DAPI fluorescence was assessed with a DAPI filter [Ex350nm/Em460nm]. The Cell Count module was used for cell enumeration while the Integrated Morphometry Analysis module was used to evaluate the area of fluorescent Nile Red staining. A specified threshold defined by fluorescent intensity below a defined pixel value was subtracted to eliminate background area. In addition, triangle masks were applied to remove autofluorescence of corners. Extent of adipogenic differentiation was quantified by area of Nile Red fluorescence from thresholded events normalized to nuclei count. End data corresponded to total area of lipid droplets present per well normalised to cell number $\mu m^2$/nuclei) and the average of biological triplicate was taken.

### *2.6 Flow cytometry of Nile Red-positive cells*

Cells were seeded in a 6-well plate format (657160, Cellstar, Greiner, Bio-one GmbH, Frickenhausen, Germany). Monolayers were washed twice in PBS, trypsinised and pelleted by centrifugation for 5min at 200g. ~100k cells per sample were fixed with 1% methanol-free formaldehyde (28908, Pierce Biotechnology Inc., Rockford, IL, USA) for at least an hour at 4$^o$C, then stained with Nile Red (10μg/ml in PBS) for 30min in the dark at RT (adapted from (Abdallah et al., 2004)). Samples were washed and resuspended in phophate buffered saline (PBS), filtered using a

60µm nylon mesh to remove debris (03-60/42, Lab Pak Sefar Nitex, Sefar AG, Heiden, Switzerland) and analysed using a Beckman Coulter CyAn$^{TM}$ ADP Analyzer (Beckman Coulter, Inc., Fullerton, CA, USA). Nile Red fluorescence was measured on the FL2 emission channel through a 585 ± 21nm band pass filter, following excitation with an argon ion laser source at 488nm. Using a forward scatter (FSC)/side scatter (SSC) representation of events, a gating region was defined to exclude cellular debris from the analysis. Using an overlay histogram (event count/FL2) with non-induced MSCs stained with Nile Red as background control, a bar region was established on the gated population to count cells with high FL2 values (adipocytes). Data analysis was performed using Summit 4.3 software (Beckman Coulter, Inc., Fullerton, CA, USA). Each sample represented 4-5k gated events. Results were expressed as percentage of cells appearing in the bar region. Experiment was performed in duplicate.

### *2.7 Quantitative polymerase chain reaction (qPCR)*

Total RNA was extracted from monolayers in a 12-well plate format (665180, Cellstar, Greiner, Bio-one GmbH, Frickenhausen, Germany) using Trizol (15596, Gibco/Life Technologies, Carlsbard, CA) and chloroform (C2432, Sigma-Aldrich, St-Louis, MO, USA) followed by the RNeasy® Mini Kit 250 (74106, Qiagen, Hilden, Germany) according to the manufacturer's protocol. Concentration of isolated RNA was determined by measuring the absorbance ratio at 260/280nm using Nanodrop (ND-1000, Thermo Fisher Scientific Inc., Waltham, MA, USA). cDNA were synthesized from isolated mRNA using the Maxima™ First strand cDNA synthesis kit (K1642, Fermentas, Thermo Fisher Scientific Inc., Rockford, IL, USA). Real time qPCR was performed and monitored on a real-time PCR instrument (MxPro 3000P

QPCR, Stratagene, Agilent Technologies Inc., Santa Clara, CA, USA) using Maxima™ SYBR Green/ROX qPCR Master Mix (K0222, Fermentas, Thermo Fisher Scientific Inc, Rockford, IL, USA). Data analysis was carried out with the MxPro software v4.01 (Stratagene, Agilent Technologies Inc., Santa Clara, CA, USA). For each cDNA sample, the Ct value was defined as the cycle number at which the fluorescence intensity reached the amplification based-threshold fixed by the instrument-software. Relative gene expression levels were determined using the ΔΔ-Ct method. Unless stated otherwise, the results were normalised to the geometric mean of human ribosomal phosphoprotein P0 (*RPLP0*) and TATA-box binding protein (*TBP*). Primer sequences used are shown in Table 2.2.

**Table 2.2. List of primers used in qPCR analysis.**

| Gene | Accession no. | Reference | Forward primer | Reverse Primer |
|---|---|---|---|---|
| *RPLP0* | NM_001002.3 | (Jansen et al., 2009) | CACCATTGAAATCCTGAGTGATGT | TGACCAGCCCAAAGGAGAAG |
| *TBP* | NM_003194.4 | (Elabd et al., 2008) | CACGAACCACGGCACTGATT | TTTTCTTGCTGCCAGTCTGGAC |
| *FABP4* | NM_001442.2 | | TGTGCAGAAATGGGATGGAAA | CAACGTCCCTTGGCTTATGCT |
| *GLUT4* | NM_001042.2 | (Lee et al., 2011a) | TCAACAATGTCCTGGCGGTG | TTCTGGATGATGTAGAGGTAGCGG |
| *HSL* | NM_005357.2 | (Mairal et al., 2006) | CTCAGTGTGCTCTCCAAGTG | CACCCAGGCGGAAGTCTC |
| *LEP* | NM_000230.2 | (Degawa-Yamauchi et al., 2005) | TTTGGCCCTATCTTTTCTATGTCC | TGGAGGAGACTGACTGCGTG |
| *UCP1* | NM_021833.4 | (Virtanen et al., 2009) | CTGGAATAGCGGCGTGCTT | AATAACACTGGACGTCGGGC |
| *PRDM16* | NM_022114.3 | | GAGGAGGACGATGAGGACAG | CGGCTCCAAAGCTAACAGAC |
| *PGC1α* | NM_013261.3 | | GCCAAACCAACAACTTTATCTCTTC | CACACTTAAGGTGCGTTCAATAGTC |
| *DIO2* | NM_013989.4 | | CCTCCTCGATGCCTACAAAC | GCTGGCAAAGTCAAGAAGGT |
| *ELOVL3* | NM_152310.2 | (Nishio et al., 2012) | CACTGGTACCACCACAGCAC | ATCCTGCCTCCAGATGTACG |
| *TBX1* | NM_080646.1 | (Wu et al., 2012) | ACGACAACGGCCACATTATTC | CCTCGGCATATTTCTCGCTATCT |
| *CD137* | NM_001561.5 | | AGCTGTTACAACATAGTAGCCAC | TCCTGCAATGATCTTGTCCTCT |
| *TMEM26* | NM_178505.6 | | ATGGAGGGACTGGT | CTTCACCTCGGTCAC |

| Gene | Accession no. | Reference | Forward primer | Reverse Primer |
|---|---|---|---|---|
| | | | CTTCCTT | TCGC |
| *ZIC1* | NM_003412.3 | (Lidell et al., 2013) | GCATCCCAGTTCGCTGCGCAAA | GGAGACACGATGGTGGGAGGCG |
| *HOXC9* | NM_006897.1 | | GCAGCAAGCACAAAGAGGAGAAG | GCGTCTGGTACTTGGTGTAGGG |
| *LHX8* | NM_001001933.1 | (Cypess et al., 2013) | ACAACCCAGATGCACAGACA | TGTGGCGTGCTCTACAATTC |
| *ITGB1* | NM_002211.3 | (Mayanagi et al., 2008) | GAGGAGGATTACTTCGGACTTCAG | GCTGGTGTTGTGCTAATGTAAGG |
| *ITGA1* | NM_181501.1 | | GGTGCTTATTGGTTCTCCGTTAG | TTCTCCTTTACTTCTGTGACATTGG |
| *ITGA2* | NM_002203.3 | (Zhang et al., 2012) | AGGACGGACTTTGCATTTCTGAT | CCACCTGGCATGTTACTTCTGT |
| *FGF1* | NM_000800.4 | (Sato et al., 2009) | CATTACCACGCCTTGACC | AGCCAGTTTCCCTTTCTTTC |
| *FGF2* | NM_002006.4 | | AGCGACCCTCACATCAAG | ATCTTCCATCTTCCTTCATAGC |
| *FGF21* | NM_019113.2 | (Dushay et al., 2010) | ACTCCAGTCCTCTCCTGCAA | GCACAGGAACCTGGATGTCT |

*RPLP0* = ribosomal phosphoprotein P0, *TBP* = TATA-box binding protein, *FABP4* = fatty acid binding protein 4, *GLUT4* = glucose transporter type 4, *HSL* = hormone sensitive lipase, *LEP* = leptin, *UCP1* = uncoupling protein 1, *PRDM16* = PRD1-BF1-RIZ1 homologous domain containing 16, *PGC1α* = PPARγ co-activator 1α, *DIO2* = deiodinase, iodothyronine, type II, *ELOVL3* = elongation of very long chain fatty acid elongase 3, *TBX1* = T-box 1, *TMEM26* = transmembrane protein 26, *ZIC1* = zinc finger protein of the cerebellum 1, *HOXC9* = homeobox C9, *LHX8* = LIM homeobox protein 8, *ITGB1* = integrin beta 1, *ITGA1* = integrin alpha 1, *ITGA2* = integrin alpha 2, *FGF1* = fibroblast growth factor 1, *FGF2* = fibroblast growth factor 2, *FGF21*= fibroblast growth factor 21.

### *2.8 Western blotting*

Protocol was adapted from (Tan et al., 2013). Cells were seeded in a 6-well plate format (657160, Cellstar, Greiner, Bio-one GmbH, Frickenhausen, Germany). Protein was extracted as whole cell lysates from cell monolayers with Laemmli buffer (31.25mM Tris-HCl pH 6.8, 1% SDS, 0.005% bromophenol blue and 9.5% glycerol) and protease inhibitor cocktail (Roche, Basel, Switzerland). Sample protein extracts were separated using SDS-PAGE under reducing conditions and then transferred onto a nitrocellulose membrane (Bio-Rad, Hercules, CA, USA). For immune-detection, the membrane was first blocked with 5% non-fat milk in Tris buffered saline with Tween20 (TBST) for 1h at RT, then incubated with the primary antibody in 1% non-

fat milk in TBST for 1.5h at RT. Primary antibodies used were anti-rabbit UCP1 (1:100, ab10983 Abcam, Cambridge, UK) and anti-mouse β-actin (1:1000 A228 Sigma-Aldrich, St-Louis, MO, USA) as a loading control. Bound primary antibody was detected with Dako HRP goat-anti mouse antibody (P0447) or Dako HRP goat-anti rabbit antibody (P0447 and P0448, Dako, Glostrup, Denmark) at 1:1000 in 1% non-fat milk in TBST for 1h at RT. Chemiluminescence was captured with a VersaDoc Imaging System (5000MP, Bio-Rad, Hercules, CA, USA) and analysed with Quantity One Image analysis software (Bio-Rad, Hercules, CA, USA). After detecting UCP1, the blot was stripped (stripping buffer – 7.5g glycine, 0.5g SDS, 5ml Tween20 in 500ml dd$H_2O$ at pH2.2) (formulation was obtained from Abcam protocols, Abcam, Cambridge, UK) and blocked before detecting for β-actin.

### *2.9 Immunocytochemistry of UCP1*

Cells were grown on glass coverslips. Monolayers were fixed with 4% methanol-free formaldehyde (28908, Pierce Biotechnology Inc., Rockford, IL, USA). The samples were then permeabilised with 0.1% Triton-X for 10min at RT then blocked with 3% bovine serum albumin (BSA) (A9647, Sigma-Aldrich, St-Louis, MO, USA) and 0.1% Tween20 in PBS for 1h at RT. Immunofluorescence was carried out using primary antibody rabbit anti-human UCP1 1:1000 (U6382, Sigma-Aldrich, St-Louis, MO, USA), incubation for 16 hours at 4°C in a humidified chamber. Secondary antibody used was AlexaFluor® 594 goat anti-rabbit (A11072, Molecular Probes®, Life Techonologies, Carlsbad, CA, USA) at 1:400 dilution, incubation of 1 hour at RT. Cell nuclei were counterstained with 0.5µg/ml DAPI (D1306, Molecular Probes®, Life Techonologies, Carlsbad, CA, USA). Images were captured using a confocal microscope.

### *2.10 Determination of membrane potential by JC-1*

Cells were seeded in 8-well Nunc labtek chamber slides (155411, Thermo Fisher Scientific Inc., Waltham, MA, USA). Cells were washed in PBS and incubated with 5µM 5,5′,6,6′-tetrachloro-1,1′,3,3′-tetraethylbenzimi-dazolocarbo-cyanine iodide (JC-1) (T3168, Molecular Probes®, Life Technologies, Carlsbad, CA, USA) for 15min at 37ºC. Cells were then washed in PBS and stimulated with 10µM forskolin or DMSO for 4h before images were taken using confocal microscopy.

### *2.11 Measuring mitochondrial oxygen consumption*

Cells were seeded at a higher density of 10k/well (33k cells/$cm^2$) in the XF24 cell culture plates (100850-001, XK24 Fluxpacks, Seahorse Bioscience, Chicopee, MA, USA). Cells were washed once in HBSS and incubated in 500µl of XF assay medium (Seahorse Bioscience, Chicopee, MA, USA) for about 20min at 37ºC in the absence of $CO_2$ before loading into the Seahorse XF24 analyser (Seahorse Bioscience, Chicopee, MA, USA) to measure the oxygen consumption rate (OCR). 10µM Forskolin (or DMSO as vehicle control) was added to stimulate the cells for 100min. Oligomycin (2µM), carbonyl cyanide-ptrifluoromethoxyphenylhydrazone (FCCP) (0.6µM), and Rotenone (2µM) plus Antimycin A (2µM) from the XF Cell Mito Stress Test Kit (101706-100, Seahorse Bioscience, Chicopee, MA, USA) were then added sequentially to dissect the different components contributing to total oxygen consumption in each well: mitochondrial respiration = OCR just before the addition of oligomycin; uncoupled respiration = the minimum OCR after the addition of oligomycin before FCCP; respiratory capacity = the highest OCR after the addition of FCCP. The minimum OCR after the addition of rotenone and antimycin A were subtracted from these values to account for non-mitochondrial respiration. After

measurement, cells were lysed using 0.1mg/ml Proteinase K (P2308, Sigma-Aldrich, St-Louis, MO, USA) (enzyme was dissolved in 10mM Tris-HCl pH 8.5-9.0 with 40% glycerol to a concentration of 1mg/ml, then diluted to a working concentration of 0.1mg/ml in lysis buffer consisting of 10mM Tris-HCl (pH 8.5), 1mM EDTA, 0.1% (v/v) Triton X-100) and dsDNA content was measured using Quant-iT™ PicoGreen® dsDNA Kit (MP7581, Molecular Probes®, Life Techonologies, Carlsbad, CA, USA). Raw OCR data were normalized by the amount dsDNA in each well before analysis.

### *2.12 Immunocytochemistry of extracellular matrix deposition*

Images were captured with an IX71 inverted fluorescence microscope (Olympus, Center Valley, PA, USA). Adherent cytometry was performed according to previously described protocol (Ang et al., 2014; Chen et al., 2009). Nine image sites per well were acquired using a 2X objective with a coolSNAP HQ camera attached to a Nikon TE2000 microscope (Nikon Instruments, Melville, NY, USA), stored and analysed using the Metamorph Imaging System Software 6.3v3 (Molecular Devices, Sunnyvale, CA, USA). An image field of 4.48 x 3.34mm per site was defined for each 24-well plate with a final image of 13.43 x 10.03mm; covering 134.70 $mm^2$ per well. Fluorescent ECM proteins were viewed under a fluorescein isothiocyanate (FITC) filter [Ex470nm/Em525nm] and a Texas Red filter [Ex572nm/Em630nm] while DAPI fluorescence was assessed with a DAPI filter [Ex350nm/Em460nm]. The Cell Count module was used for cell enumeration while the Integrated Morphometry Analysis module was used to evaluate the area of fluorescent staining. A specified threshold defined by fluorescent intensity below a defined pixel value is subtracted to eliminate background area. In addition, triangle masks were applied to remove autofluorescence of corners. Extent of ECM deposition was quantified by area of

fluorescence from thresholded events normalized to nuclei count. End data corresponded to total area of ECM deposition present per well normalised to cell number $\mu m^2$/nuclei). The end data per well was substracted off its corresponding secondary antibody conjugate control before the average of biological triplicate is taken.

For confocal microscopy studies, Cells were seeded in 35mm dishes with glass bottom coverslips (3911-035, Iwaki, Scitech Division, Asahi Techno Glass, Tokyo, Japan). Monolayers were fixed with 4% methanol-free formaldehyde (28908, Pierce Biotechnology Inc., Rockford, IL, USA) for 10min at RT, then blocked with 3% bovine serum albumin (BSA) (A9647, Sigma-Aldrich, St-Louis, MO, USA) in PBS for an hour. Immunofluorescence was carried out using primary antibodies rabbit anti-human collagen IV 1:500 (6586 Abcam, Cambridge, UK), incubation for 16 hours at 4°C. Secondary antibody used is AlexaFluor® 594 goat anti-rabbit (A11072, Molecular Probes®, Life Techonologies, Carlsbad, CA, USA) at 1:400 dilution, incubation of 1 hour at RT. Cell nuclei and neutral lipids were counterstained with 0.5µg/ml DAPI (D1306, Molecular Probes®, Life Techonologies, Carlsbad, CA, USA) and 0.1µg/ml BOPIDY® (4,4-difluoro-1,3,5,7,8-pentamethyl-4-bora-3a,4a-diaza-s-indacene, D3922, Molecular Probes®, Life Techonologies, Carlsbad, CA, USA). Image acquisition was performed by using a Confocal Laser Scanning Microscope (LSM510, Zeiss, Germany) with an EC Plan-Neofluar 40x/1.30 Oil objective. Images of the collagen IV staining were processed using the Image J software (National Institutes of Health, Bethesda, MD, USA) to remove background noise and calculate the average pixel intensity per confocal plane, which was then plotted against the Z-distance (µm) for each image stack. Assuming a normal distribution, the parabolic section of the resulting curve was then fitted to a

Gaussian function (Equation 1) using, as floating parameters: the area under the curve (A), the peak position (μ) and the standard deviation (σ) (Fig. 2.2). Following the density of probability model, the limit of the collagen IV signal along the Z-axis was determined as (μ+3σ), with a 99% confidence level, and the corresponding Z-distance was used to estimate the thickness of collagen IV. The area under the curve up to the limit was obtained using OriginPro 9.1 (OriginLab Corporation, Northhampton, MA, USA) to estimate the density of collagen IV.

$$y = \frac{A}{\sigma\sqrt{2\pi}} e^{-0.5\times(\frac{x-\mu}{\sigma})^2} \qquad \text{(eq.1)}$$

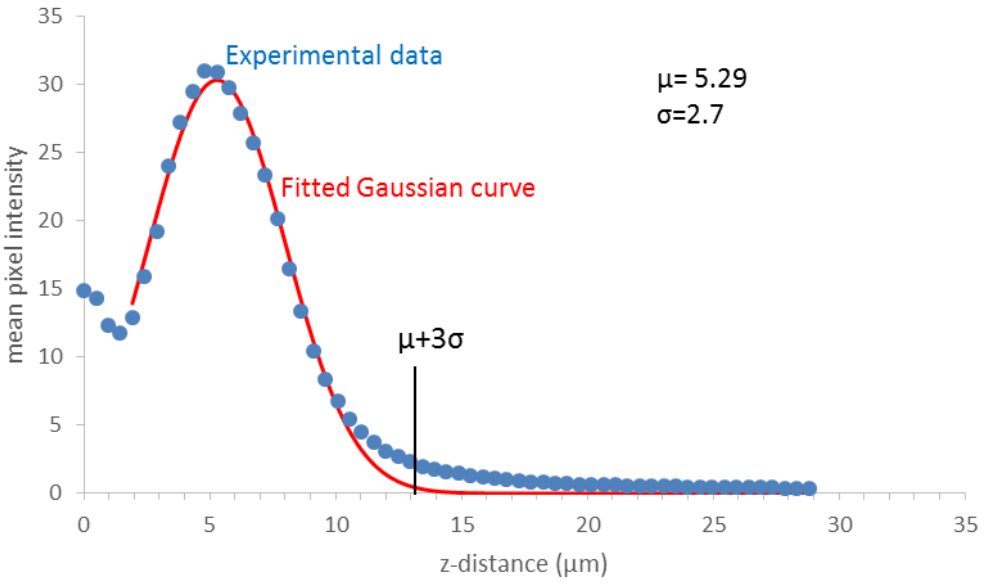


**Figure 2.2. An example of collagen IV matrix characterization using a normal distribution.** The mean pixel intensity per confocal plane was measured using the Image J software and plotted against the vertical Z-distance. A Gaussian curve was fitted to the parabolic section of the experimental data, yielding the peak position and the standard deviation. The limit of the signal was determined at (μ+3σ), with a 99% confidence level. (Image provided by Jean-Yves Dewavrin, NUS)

### *2.13 Elution of FGFs from the extracellular matrix*

Cells were seeded in a 24-well plate format (662160, Cellstar, Greiner, Bio-one GmbH, Frickenhausen, Germany). Cell layers were washed with PBS and low binding affinity fibroblast growth factors (FGFs) were eluted with 2M NaCl (in 20mM HEPES, pH 7.4) as previously described for eluting low binding affinity FGF2 bound to HSPG (Moscatelli, 1992). ELISA was performed on the eluates for the detection of fibroblast growth factor 1 (FGF1) and fibroblast growth factor 2 (FGF2) (DFA00B and DBF50, R&D Systems, Minneapolis, MN, USA).

### *2.14 Ficoll uptake studies*

Cells were seeded in 8-well Nunc labtek chamber slides (155411, Thermo Fisher Scientific Inc., Waltham, MA, USA) at a higher density of 15k/well (19k cells/$cm^2$). Cells were washed in Hank's balanced salt solution (HBSS) and incubated in HGDMEM (10% FBS and 1% P/S) without MMC overnight. Cells were then washed in HBSS and incubated with 1µM of Ficoll70 or Ficoll400-labelled tetramethylrhodamine isothiocyanate (TRITC) (TF70 and TF400, TdB Consultancy, Uppsala, Sweden) or just TRITC (87918, Sigma-Aldrich, St-Louis, MO, USA) for 1 hour at 37ºC. Cells were washed in HBSS and incubated with 200nM Mitotracker Green (M7514, Molecular Probes®, Life Techonologies, Carlsbad, CA, USA) for 15min at 37ºC. Cells were then washed in HBSS, and underwent confocal imaging using phenol-free HGDMEM (21063, Gibco/Life Technologies, Carlsbad, CA, USA).

### *2.15 Statistical analysis*

Unless otherwise stated, all assays were performed in triplicate and results reported as mean ± standard error. Student's t-test was used for comparison between two groups. For multiple pairwise comparisons, one-way ANOVA statistical analysis was performed followed by Tukey-Kramer Multiple Comparisons Test using Graphpad InStat software (GraphPad Software, Inc., La Jolla, CA, USA). n.s. not significant, *$p<0.05$, **$p<0.01$, ***$p<0.001$.

# CHAPTER 3: RESULTS

## *3.1 Macromolecular crowding using Ficoll enhances adipogenic differentiation towards a brown adipocyte phenotype in adult human bone marrow mesenchymal stem cells*

Adult human bone marrow mesenchymal stem cells (bmMSCs) were subjected to a 3-week adipogenic induction using a white (iw) or a brown (ib) induction protocol (refer to *Materials and methods section 2.3*), and Ficoll, a sucrose co-polymer, was used to generate the condition of macromolecular crowding (MMC) throughout the differentiation process as described recently (Ang et al., 2014). The iw protocol consisted of 3-isobutyl-1methylxanthine (IBMX), indomethacin, dexamethasone and insulin as described (Mackay et al., 2006; Pittenger et al., 1999). The ib protocol included the addition of factors known to promote brown adipocyte differentiation, namely T3 (Klaus et al., 1995), Rosiglitazone (Vernochet et al., 2009) and BMP7 (Tseng et al., 2008). To analyse MMC effects on brown adipogenic differentiation, mRNA expression of *UCP1* and other brown-selective genes *PRDM16* and *CIDEA* (refer to *Introduction section, table 1.1*) were quantified in bmMSC-derived adipocytes at the end of the 3-week induction. The ib protocol alone failed to significantly upregulate *UCP1* expression (Fig. 3.1, ib no mmc group). In contrast, under MMC (ib mmc) *UCP1* expression was significantly upregulated by over 20-fold compared to the iw protocol, and 5-fold compared to ib protocol alone. As expected, no *UCP1* mRNA upregulation occurred in the iw protocol (compared to non-induced controls, data not shown), but surprisingly, *UCP1* was upregulated 10-fold using the iw protocol under MMC (iw mmc) (Fig. 3.1). Interestingly, despite the upregulation of *UCP1*, the expression levels of *PRDM16* were not significantly

different between groups (Fig. 3.1). *CIDEA* expression was low (raw Ct values > 32.7 out of 35 cycles, data not shown) for all groups and hence was considered absent from the cultures.

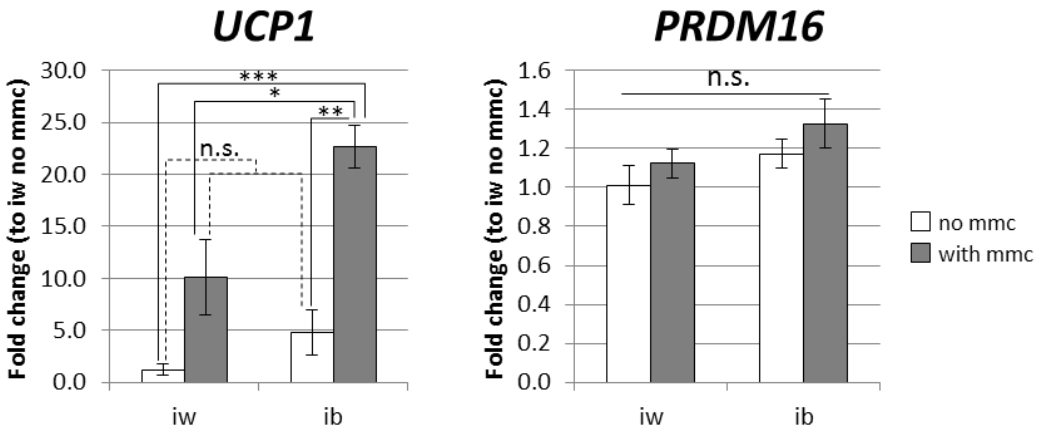


| Condition | Ct value |
|---|---|
| iw | 34.2 ± 0.6 |
| ib | 32.3 ± 0.6 |
| iw mmc | 31.0 ± 0.7 |
| ib mmc | 29.5 ± 0.1 |

| Condition | Ct value |
|---|---|
| iw | 29.0 ± 0.2 |
| ib | 28.9 ± 0.3 |
| iw mmc | 28.8 ± 0.0 |
| ib mmc | 28.5 ± 0.1 |

**Figure 3.1. Macromolecular crowding using Ficoll enhances adipogenic differentiation towards a brown-like phenotype in adult human bone marrow mesenchymal stem cells.** bmMSCs were chemically induced with a white (iw) or brown (ib) protocol ± MMC for 3 weeks and qPCR was carried out to assess brown adipogenesis. Raw Ct values of the respective genes are reported below the graphs. BAT selective genes: *UCP1* = uncoupling protein 1, *PRDM16* = PRD1-BF1-RIZ1 homologous domain containing 16, Data are mean ± SEM. n.s. = not significant; *p<0.05; **p<0.01; ***p<0.001.

On the basis of this observation, I set out to optimize a MMC-enhanced brown differentiation protocol for bmMSCs using the three key factors BMP7, T3 and rosiglitazone in various combinations with the existing white (iw) protocol ±MMC (Fig. 3.2). BMP-7 pre-treatment followed by a 3-week induction with T3 and rosiglitazone in a standard iw protocol (dexamethasone, IBMX, insulin and indomethacin) with MMC was most effective in upregulating *UCP1* mRNA

expression, and thus was selected as the brown protocol (ib) for the rest of the study (Fig. 3.2B).

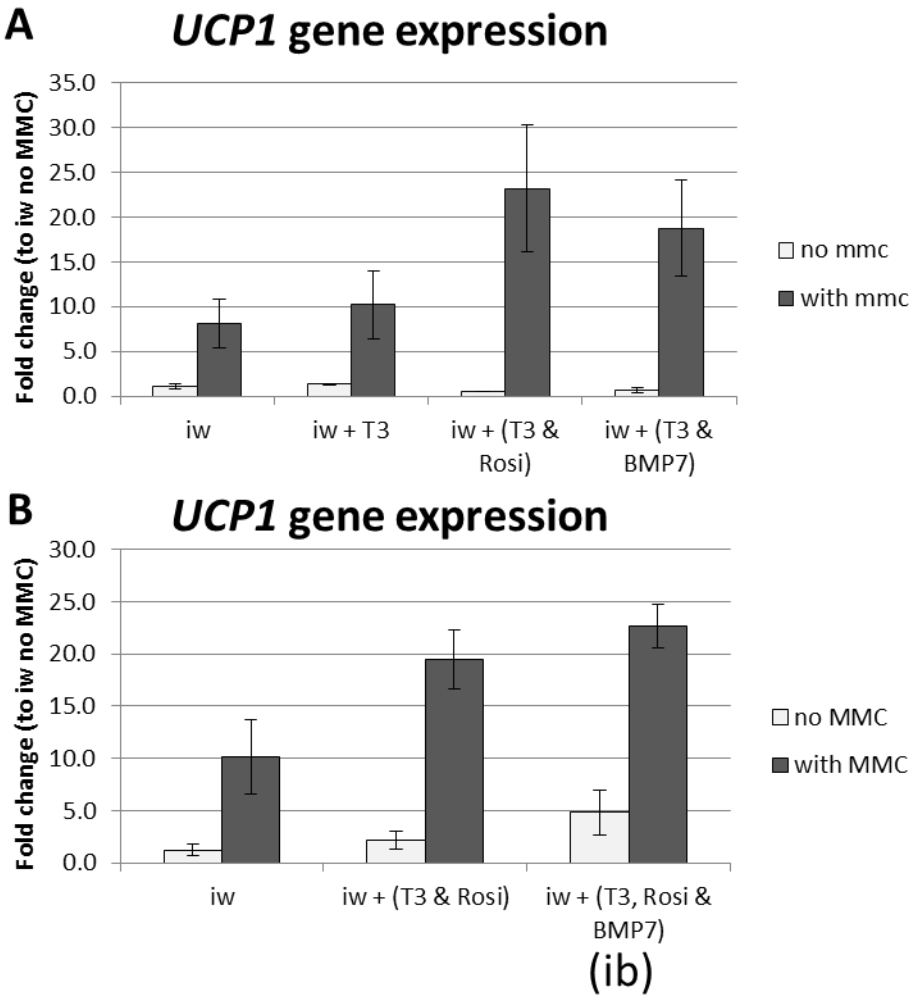


**Figure 3.2. Comparison of various brown induction (ib) protocols.** bmMSCs were chemically induced with various combinations of browning factors in addition to the base white (iw) protocol in the presence or absence of MMC and *UCP1* expression was measured using qPCR to assess the efficiency of brown adipocyte differentiation. (A) *UCP1* expression of various conditions compared to the standard white (iw) protocol: iw + T3 = T3 was added during the induction, iw + (T3 & BMP7) = cells were pre-treated with BMP7 3 days before induction and T3 was added during the induction, iw + (T3 and Rosi) = T3 and rosiglitazone were added during the induction. (B) *UCP1* expression of various conditions compared to the standard white (iw) protocol: iw + (T3 and Rosi) = T3 and rosiglitazone were added during the induction, iw + (T3, Rosi and BMP7) (the current ib protocol) = cells were pre-treated with BMP7 3 days before induction and T3 + rosiglitazone were added during the induction. Data are mean ± SEM.

I next characterized the bmMSC-derived adipocytes generated under the various conditions. The differentiated adipocytes assumed a rounded morphology, compared to undifferentiated controls which were spindle-shaped (Fig. 3.3A). It was observed that the cultures with MMC appeared to have a slightly higher cell density than the non-MMC cultures (Fig. 3.3B). bmMSC-derived adipocytes accumulated massive amounts of lipid droplets (Fig. 3.4A-B) which were morphologically multilocular, forming grape-like structures (Fig. 3.4C).

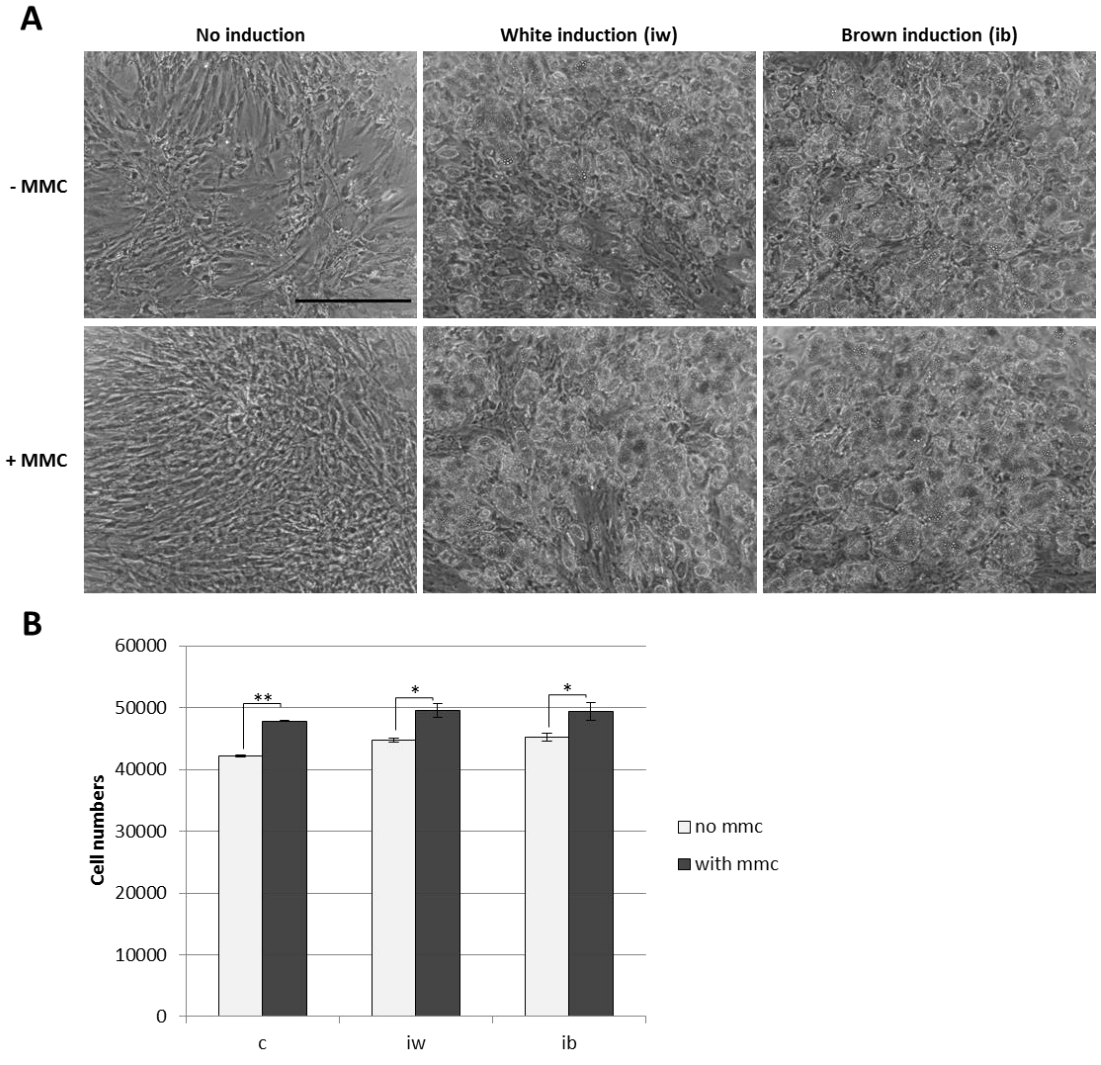


**Figure 3.3. bmMSC-derived adipocytes after a 3-week induction with a white (iw) or brown (ib) induction protocol ± macromolecular crowding (MMC).** (A) Phase contrast images taken at 4X magnification showed the change in cell morphology from spindle-like to round and the accumulation of lipid droplets. Scale bar: 500µm. (B) Adherent cytometry of DAPI-stained nuclei count to obtain cell numbers in the various conditions. Data are mean ± SEM. *p<0.05; **p<0.01.

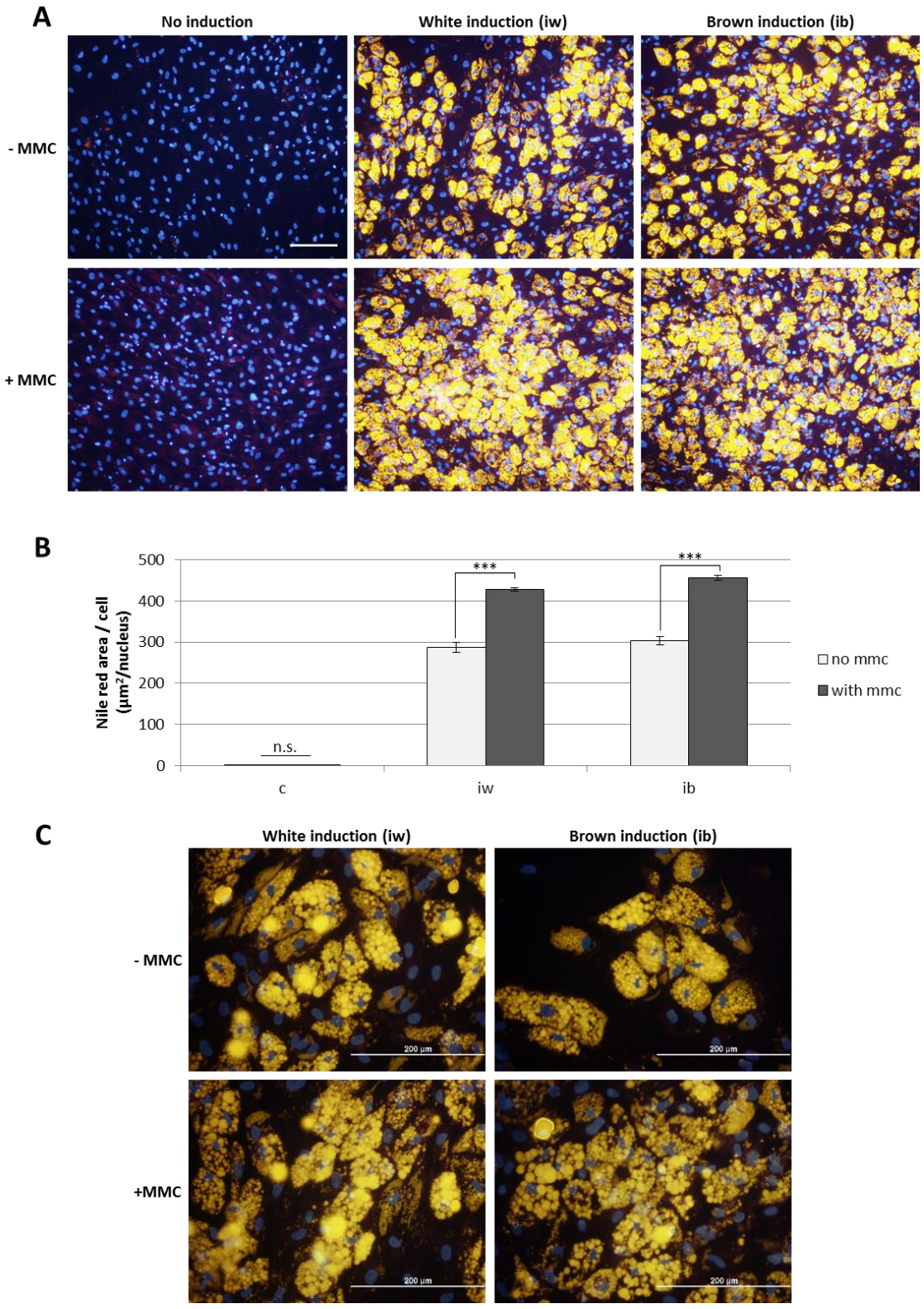


**Figure 3.4. Increased lipid droplet accumulation under MMC in bmMSC-derived adipocytes induced with white (iw) or brown (ib) induction protocols.** (A) Fluorescence images of Nile Red-stained lipid droplets (yellow) and DAPI-stained nuclei (blue) at 10X magnification. Scale bar: 200µm. (B) Adherent cytometry of fluorescent Nile Red area normalized to cell number (C) Fluorescence images at 40X magnification. Scale bar: 200µm. Data are mean ± SEM. n.s. = not significant; *p<0.05; **p<0.01; ***p<0.001.

MMC alone did not induce adipogenic differentiation, but yielded in both induction protocols a significantly greater lipid droplet accumulation per cell (Fig. 3.4B). Apparently the proportion of cells differentiating into adipocytes were lower in the MMC conditions, i.e. 11.3% decrease in the iw mmc group compared to iw group, and a significant 18.9% decrease in the ib mmc group compared to the ib group (Fig. 3.5). This could be attributed to the higher fragility of the cell membrane of the MMC-generated adipocytes due to the increased lipid load which rupture more easily by the shear force during the acquisition using flow cytometry, resulting in an underestimation of the true value, as hypothesized in (Aldridge et al., 2013).

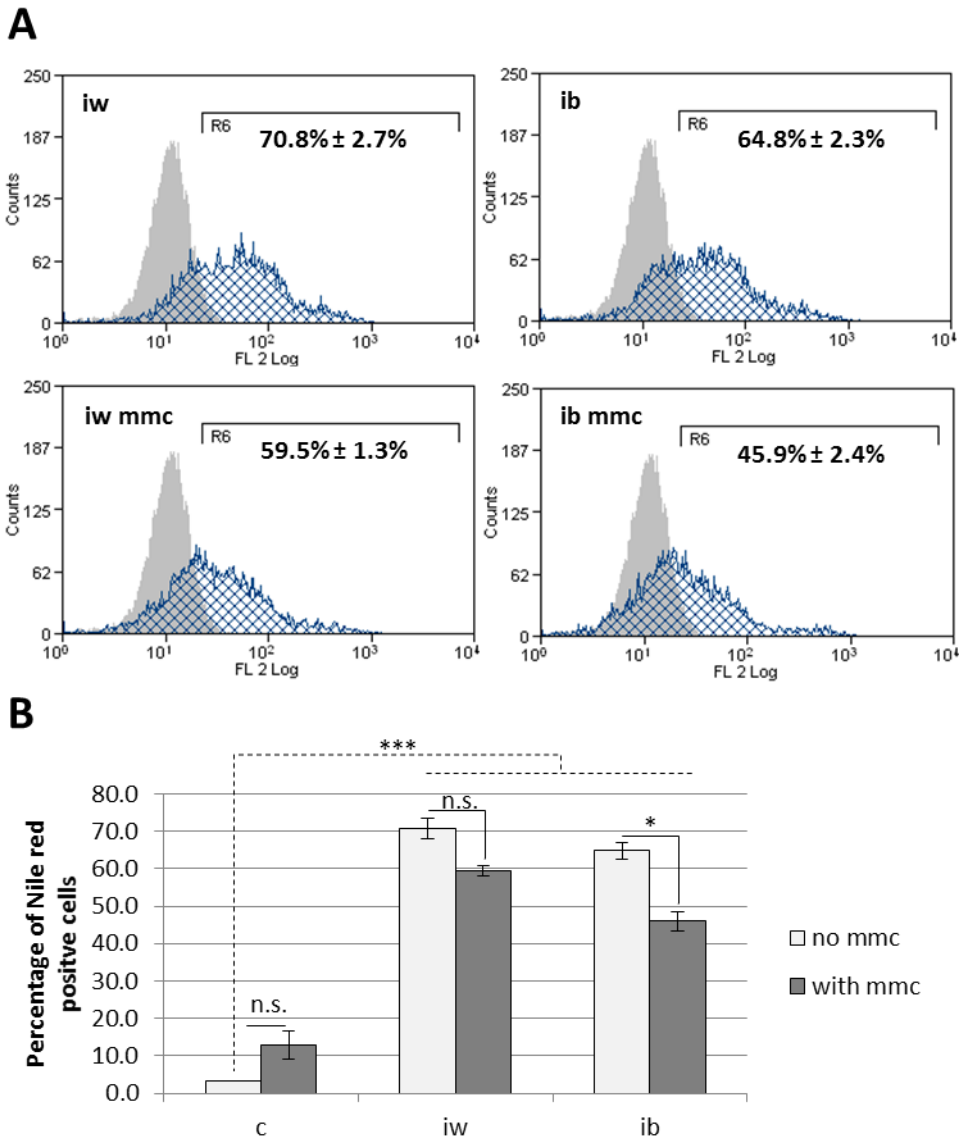


**Figure 3.5. Accelerated adipogenesis under MMC does not increase the percentage of differentiating cells.** (A) Representative flow cytometry graphs of Nile Red positive bmMSC-derived adipocytes induced with iw or ib protocol ±MMC as detected by the FL2 channel. (B) Flow cytometric count of Nile Red positive cells over total gated cell population, expressed as a percentage. Data are mean ± SEM. n.s. = not significant; *p<0.05; **p<0.01; ***p<0.001.

In addition, the bmMSC-derived adipocytes significantly upregulated the gene expression of key markers essential for adipocyte function such as glucose transporter type 4 (*GLUT4*), fatty acid binding protein 4 (*FABP4*), hormone sensitive lipase (*HSL*) and leptin (*LEP*) (Fig. 3.6). GLUT4 is an insulin-dependent glucose transporter, and facilitates glucose uptake into adipocytes in response to insulin stimulation (Funaki et al., 2004). FABP4 is involved in fatty acid trafficking within the adipocyte (Hertzel and Bernlohr, 2000), HSL catalyses the hydrolysis of tri- and di- acylglycerols during the lipolysis (Lampidonis et al., 2011), and leptin is an adipokine that regulates satiety (Klok et al., 2007).

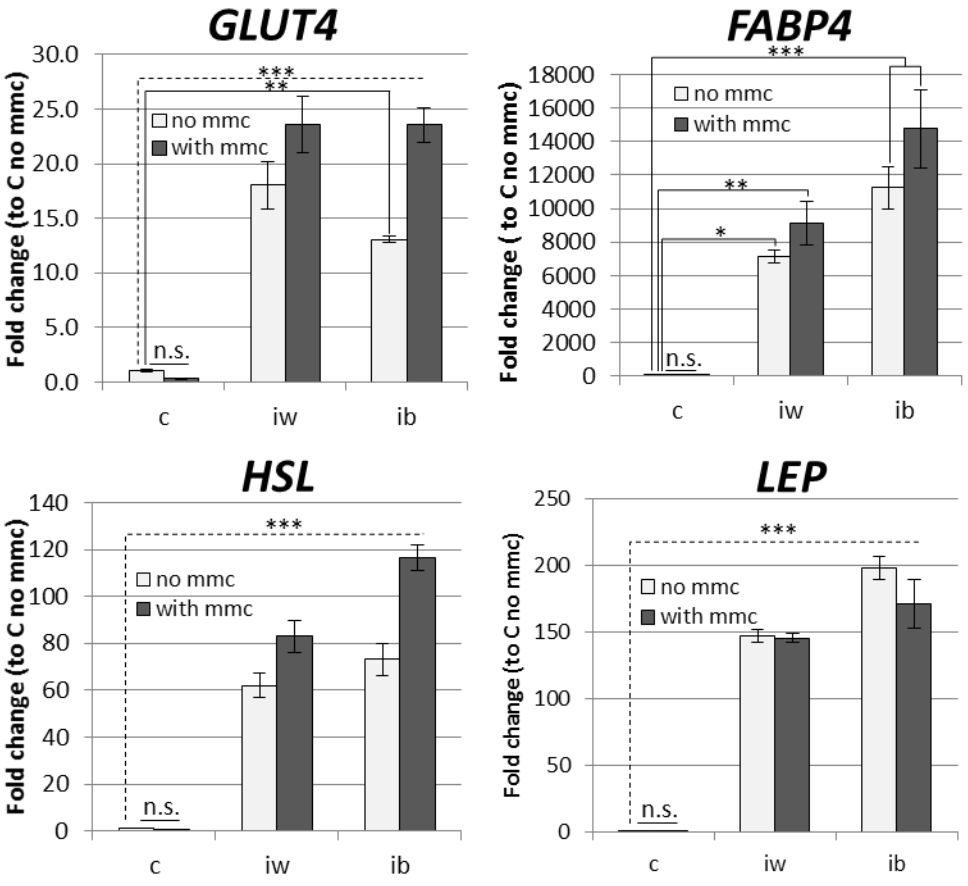


**Figure 3.6. Upregulation of key adipocyte genes in bmMSCs induced with the white (iw) or brown (ib) protocol ± MMC.** Expression of pan-adipocyte genes determined by qPCR, compared to non-induced controls (c no mmc group). *GLUT4* = glucose transporter type 4; *FABP4* = fatty acid binding protein 4; *HSL* = hormone sensitive lipase; *LEP* = leptin. Data are mean ± SEM. n.s. = not significant; *p<0.05; **p<0.01; ***p<0.001.

Based on the differential *UCP1* expression reported in figure 3.1, I investigated whether the *UCP1*-positive treatment groups correlated with the upregulation of classical brown (*ZIC1, LHX8*) or beige (*TBX1, CD137* and *TMEM26*) markers, and the down-regulation of a white (*HOXC9*) marker compared to iw-derived adipocytes and non-induced bmMSCs (refer to *Introduction section 1.6*). Classical brown marker *ZIC1* had the highest expression in the non-induced conditions (c no mmc, c with mmc). There was no difference in expression between the induced conditions (Fig. 3.7B). mRNA for *LHX8* (LIM homeobox protein 8) was not detected in the cultures after 35 cycles (Table 3.1). Beige markers *TBX1* and *TMEM26* were strongly downregulated in the bmMSC-derived adipocytes and there was no difference in expression between the induced conditions, while CD137 was downregulated in the MMC conditions (Fig. 3.7A). Moreover, the expression levels of the beige markers were low (Table 3.1), indicating that these markers may not be biologically relevant in bmMSC-derived adipocytes. Lastly, there was no difference in *HOXC9* expression between groups (Fig. 3.7C).

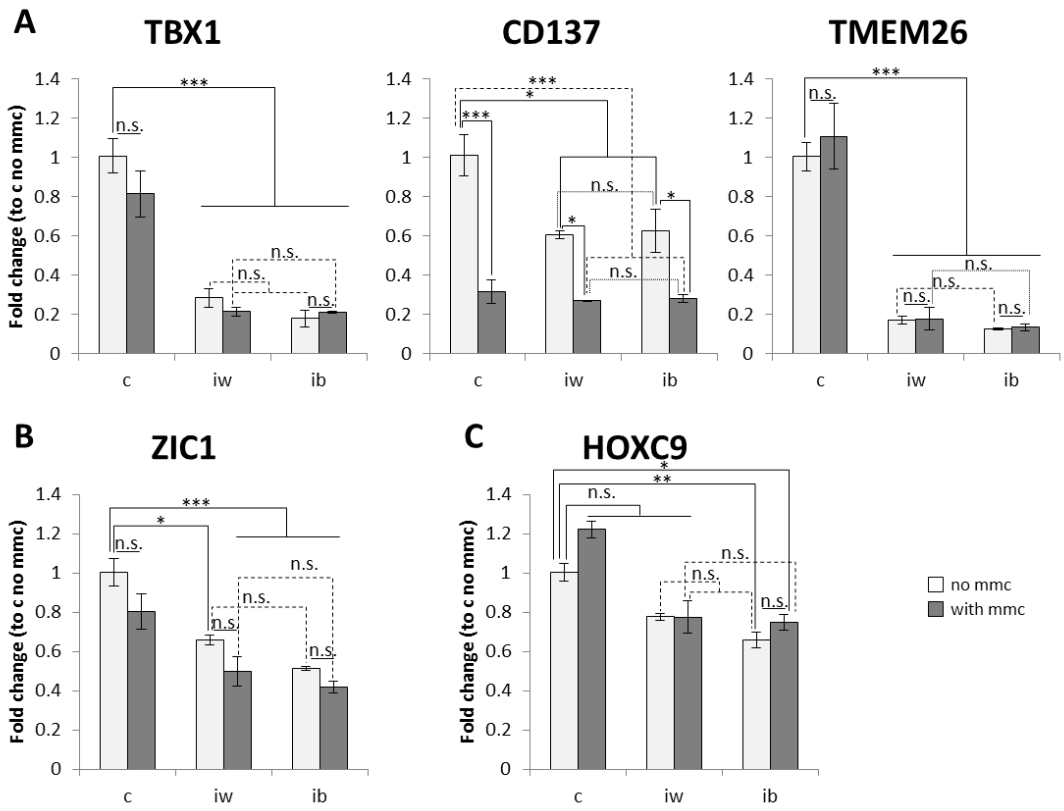


**Figure 3.7. Assessment of lineage markers expression for classical brown, beige and white adipocytes.** bmMSCs were chemically induced with a white (iw) or brown (ib) protocol ±MMC for 3 weeks and qPCR was carried out to assess lineage markers for the different populations of brown and white adipocytes in comparison with non-induced bmMSCs (c no mmc). (A) Beige selective genes: *TBX1* = T-box 1, *CD137* = tumor necrosis factor receptor superfamily, member 9 (*TNFRSF9*), *TMEM26* = transmembrane protein 26. (B) Classical-brown selective gene: *ZIC1* = Zic family member 1. (C) White selective gene: *HOXC9* = homeobox C9. Data are mean ± SEM. n.s. = not significant; *p<0.05; **p<0.01; ***p<0.001.

**Table 3.1. Raw Ct values of classical brown, beige and white markers.**

| Type | Marker | c | c mmc | iw | iw mmc | ib | ib mmc |
|---|---|---|---|---|---|---|---|
| Classical brown | *ZIC1* | 26.1 ± 0.1 | 26.3 ± 0.1 | 26.7 ± 0.1 | 26.9 ± 0.1 | 26.9 ± 0.1 | 27.0 ± 0.0 |
| | *LHX8* | no Ct | no Ct | no Ct | no Ct | no Ct | no Ct |
| Beige | *TBX1* | 30.4 ± 0.1 | 30.6 ± 0.1 | 32.3 ± 0.3 | 32.4 ± 0.1 | 32.8 ± 0.3 | 32.3 ± 0.1 |
| | *CD137* | 30.6 ± 0.2 | 32.2 ± 0.2 | 31.3 ± 0.0 | 32.2 ± 0.1 | 31.1 ± 0.2 | 32.0 ± 0.0 |
| | *TMEM26* | 30.4 ± 0.1 | 30.1 ± 0.2 | 32.9 ± 0.1 | 32.7 ± 0.3 | 33.1 ± 0.0 | 32.9 ± 0.1 |
| White | *HOXC9* | 24.9 ± 0.1 | 24.5 ± 0.1 | 25.3 ± 0.0 | 25.1 ± 0.1 | 25.3 ± 0.1 | 25.0 ± 0.0 |

Values are mean ± SEM.

### *3.2 MMC-generated brown adipocytes derived from adult human bone marrow MSCs are functional*

An important test for functional brown adipocytes is their thermogenic response to an adrenergic stimulus or the more generic downstream induction of cAMP by forskolin (refer to *Introduction section, figure 1.2*). I first investigated whether the bmMSC-derived adipocytes responded to a forskolin-dependent increase in cAMP by measuring their lipolytic response as both white and brown adipocytes undergo lipolysis upon a β-adrenergic stimulus (Robidoux et al., 2004; Souza et al., 2007). After a 16h forskolin stimulus, both iw- and ib- generated adipocytes ±MMC responded to this stimulus by emptying their lipid stores by 50-60% (Fig. 3.8A). Fluorescence images of the Nile Red-stained adipocytes showed that the forskolin-treated cells (Fig. 3.8D-E) had a significant decrease in intracellular lipid stores compared to vehicle controls (Fig. 3.8B-C), a clear indication of lipolysis.

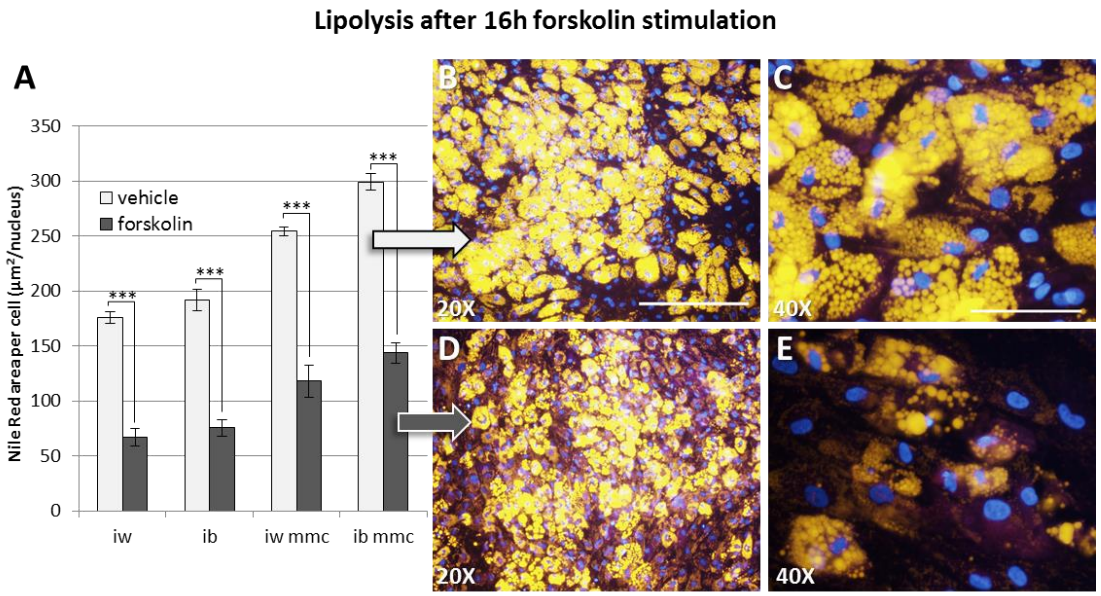


**Figure 3.8. bmMSC-derived adipocytes undergo lipolysis upon forskolin stimulation.** Adipocytes that were differentiated from bmMSCs were subjected to a forskolin (10µM) stimulus, and lipolysis was assessed by quantifying the loss of lipid stores. (A) Extent of lipolysis after a 16h forskolin treatment as captured by adherent cytometry quantifying Nile Red-positive area normalized to nuclei count. (B and C) vehicle treatment only, (D and E) 16h forskolin of ib mmc adipocytes. c = non-induced control; iw = white cocktail; ib = brown cocktail. Scale bar for 20X: 200µm. Scale bar for 40X: 100µm.

Next, to specifically assess the thermogenic response to a forskolin stimulus, I treated the cells with forskolin and measured the expression of thermogenic genes compared to vehicle controls. After a 4.5h forskolin stimulus, all MMC-generated adipocytes showed a greater upregulation of thermogenic genes *PGC1α* and *DIO2* compared to induction with cocktail alone. In addition, *UCP1* upregulation was significant only in the bmMSC-derived adipocytes induced with MMC (430-fold for iw mmc and 800-fold ib mmc in comparison to iw unstimulated) (Fig. 3.9).

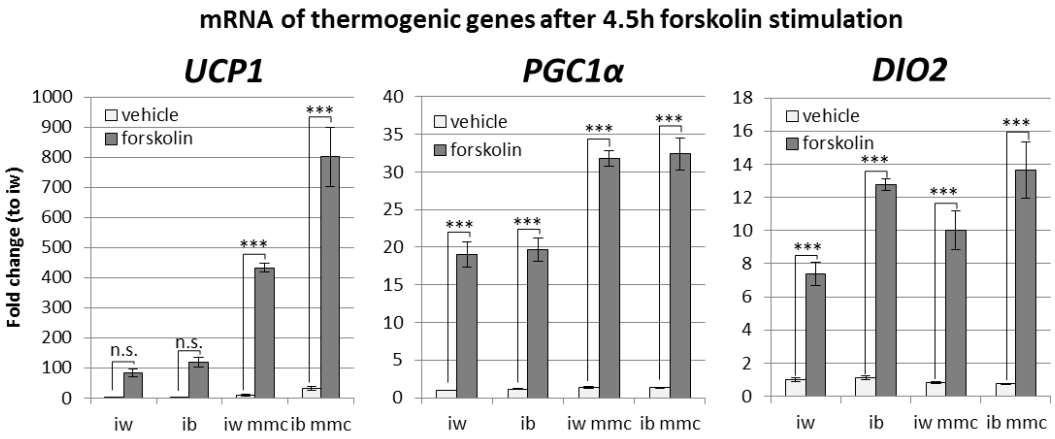


**Figure 3.9. Brown adipocytes generated under MMC significantly upregulate thermogenic genes upon forskolin stimlulation.** Adipocytes that were differentiated from bmMSCs were subjected to a forskolin (10μM) stimulus, and qPCR was performed to determine mRNA expression of thermogenic genes after a 4.5h forskolin treatment. *UCP1* = uncoupling protein 1; *PGC1α* = PPARγ co-activator 1α; *DIO2* = deiodinase, iodothyronine, type II. Data are mean ± SEM. ns. = not significant; *p<0.05; **p<0.01; ***p<0.001.

To further investigate the effect of UCP1 activation in mitochondrial membrane depolarisation due to the dissipation of the proton gradient (refer to *Introduction section, figure 1.1*), I made use of a cyanine cationic dye JC-1 (5,5′,6,6′-tetrachloro-1,1′,3,3′-tetraethylbenzimidazolocarbo-cyanine iodide). When accumulated preferentially in the interior-negative potential environment of the mitochondrial matrix the dye forms J-aggregates with emission at 585nm (orange-red) at high concentrations. When the mitochondrial membrane potential ($\Delta\psi_m$) decreases, there is an increased dissociation of J-aggregates to the monomer form with emission at 520nm (green) (Mathur et al., 2000; Smiley et al., 1991). Thus the spectral shift from orange-red to green indicates mitochondrial membrane depolarisation, which can be caused by uncoupled respiration due to the increased activity of UCP1. After a 4h forskolin stimulus, mitochondrial membrane depolarisation was observed to a greater extent in MMC-generated adipocytes when compared to vehicle controls (Fig. 3.10), which predicted an increased uncoupling

activity in the mitochondria caused by the increase of UCP1 activity in these adipocytes.

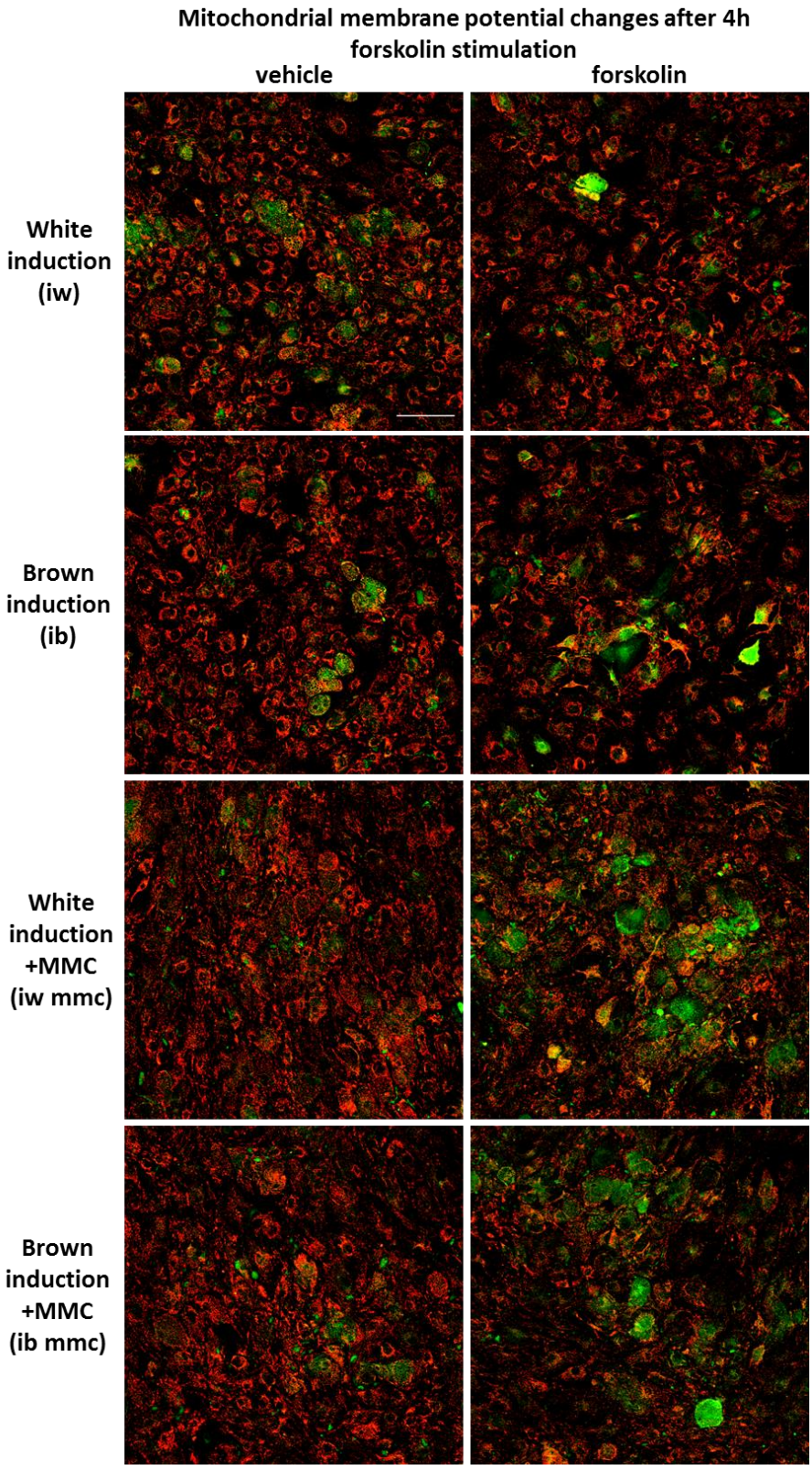


**Figure 3.10. Brown adipocytes generated under MMC show increased mitochondrial membrane depolarization after a forskolin stimulus.** Adipocytes differentiated from bmMSCs were subjected to a forskolin (10µM) stimulus, and mitochondrial membrane depolarization was assessed. (G) JC-1 staining of MSC-derived adipocytes after a 4h forskolin treatment (f) compared to vehicle (v) controls. Depolarised mitochondrial membranes appear in green. Scale bar: 200µm.

Finally, as a functional marker confirming a thermogenic response, the oxygen consumption rate (OCR) was determined in real time using the Seahorse XF analyser following a forskolin stimulus, and the mitochondrial function (mitochondrial respiration, uncoupled respiration and respiratory capacity) after forskolin stimulation was determined with the addition of the various metabolic compounds oligomycin, FCCP, rotenone and antimycin A in the sequence shown (Fig. 3.11A) (refer to *Materials and Methods section 2.7*). Brown-induced ib mmc adipocytes from an early passage showed an enhanced oxygen consumption rate (OCR) and uncoupled respiration over and above white (iw) adipocytes. In a 100min time window OCR increased in ib mmc by 40% compared to a 17% decrease in white adipocytes (iw) (Fig. 3.11B). Brown (ib mmc) adipocytes also showed a significant 80% increase in mitochondrial (Fig. 3.11C) and a 260% increase in uncoupled respiration (Fig. 3.11D), while white (iw) adipocytes did not respond significantly to the forskolin stimulus. The overall respiratory capacity of ib mmc adipocytes, although not significant, was about 40% higher than in iw adipocytes (Fig. 3.11E).

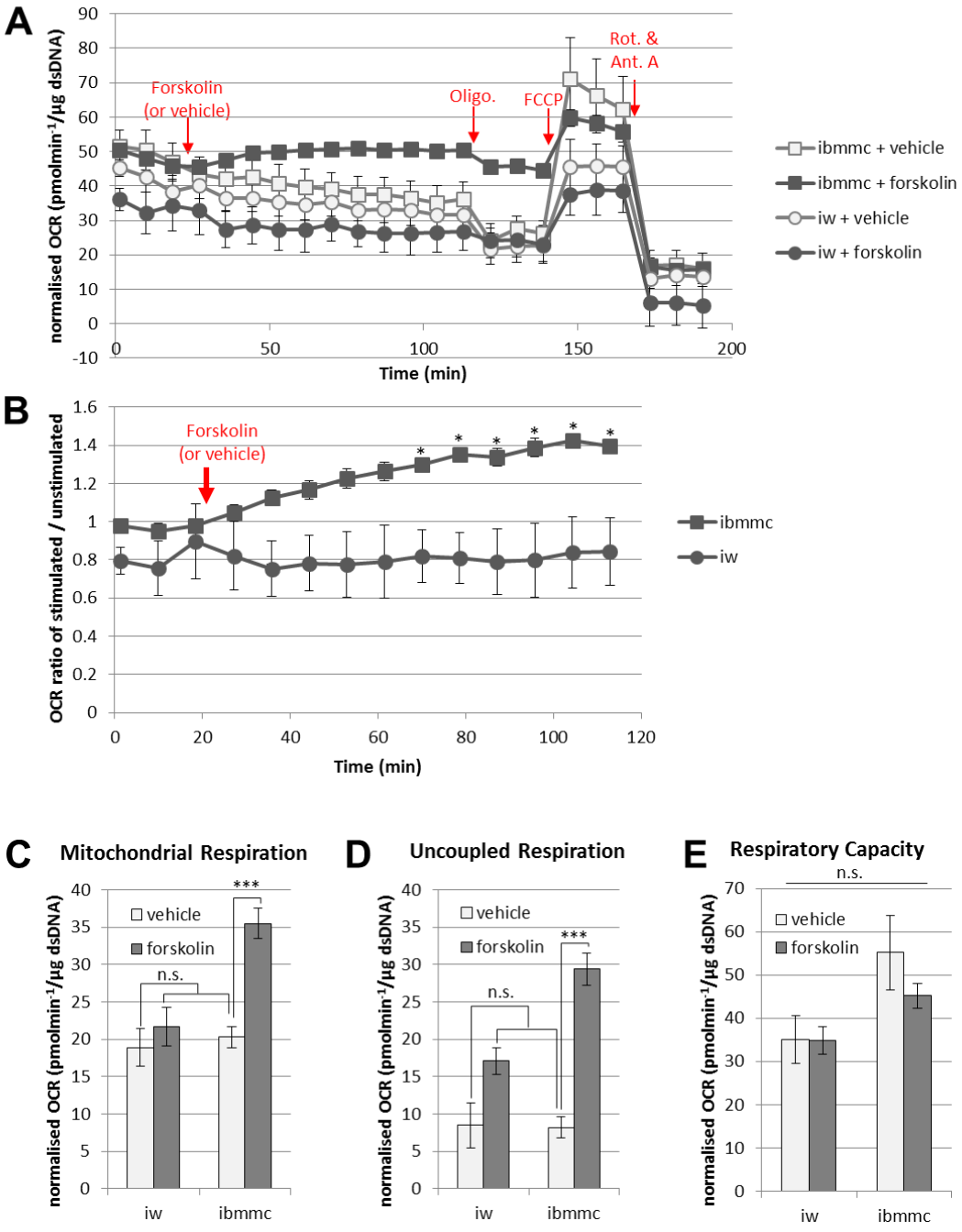


**Figure 3.11. bmMSC-derived brown adipocytes generated under MMC show an enhanced forskolin response compared to white induced (iw) adipocytes.** Cell cultures were monitored real-time for respiratory changes in the Seahorse FX analyser and afterwards analysed for DNA content. (A) Averaged oxidative respiratory capacity (OCR) of each group was normalised to DNA content with the various compounds added during the time course of the experiment to assess the mitochondrial respiratory function. (B) OCR ratio of forskolin-stimulated ib mmc and iw adipocytes normalized to vehicle controls. (C) mitochondrial respiration, (D) uncoupled respiration and (E) respiratory capacity of iw and ib mmc adipocytes. Data are mean ± SEM. ns. = not significant; *p<0.05; **p<0.01; ***p<0.001. Experiment performed together with Dr. Ying Li, Duke-NUS.

### *3.3 MMC-enhanced ECM provides signaling cues to enhance brown adipocyte differentiation*

To elucidate the mechanism of the sucrose co-polymer Ficoll in inducing the brown phenotype in bmMSC-derived adipocytes, my colleagues and I looked at the MMC effects of Ficoll in influencing adipocyte microenvironment formation by investigating collagen IV, a major adipocyte extracellular matrix (ECM) component (Lilla et al., 2002), and heparin sulphate proteoglycans (HSPG), which play an important role in growth factor sequestration (Taipale and Keski-Oja, 1997). bmMSC-derived adipocytes generated under MMC produced an enriched ECM characterised by a substantially increased deposition of collagen IV (3.4-fold for iw mmc and 4.7-fold for ib mmc, respectively) and perlecan, a heparan sulphate proteoglycan (2.5-fold and 3.0-fold, respectively) (Fig. 3.12B), consistent with what was reported previously (Ang et al., 2014). An in-depth analysis of the Col IV deposition using confocal microscopy revealed that the arrangement of Col IV in the MMC conditions had finer fibres which enveloped the adipocytes, whereas the non-MMC conditions had Col IV arranged in thick bundles and generally do not envelope the adipocytes (Fig. 3.13A). It is interesting to note that the (ib) induction protocol alone also promoted the fine fibre formation in some of the samples (Supp. Fig. 1). When the Z-stack images were assessed quantitatively, there was no significant difference in the thickness of Col IV deposited between MMC and non-MMC conditions, (Fig. 3.13B) although adipocytes induced with the ib protocol seemed to have a slightly thicker Col IV matrix. However, the density of Col IV was significantly higher in the MMC conditions with a 3.5-fold and 2.1-fold increase for the iw and ib groups respectively (Fig. 3.13C), correlating with what was observed in the images.

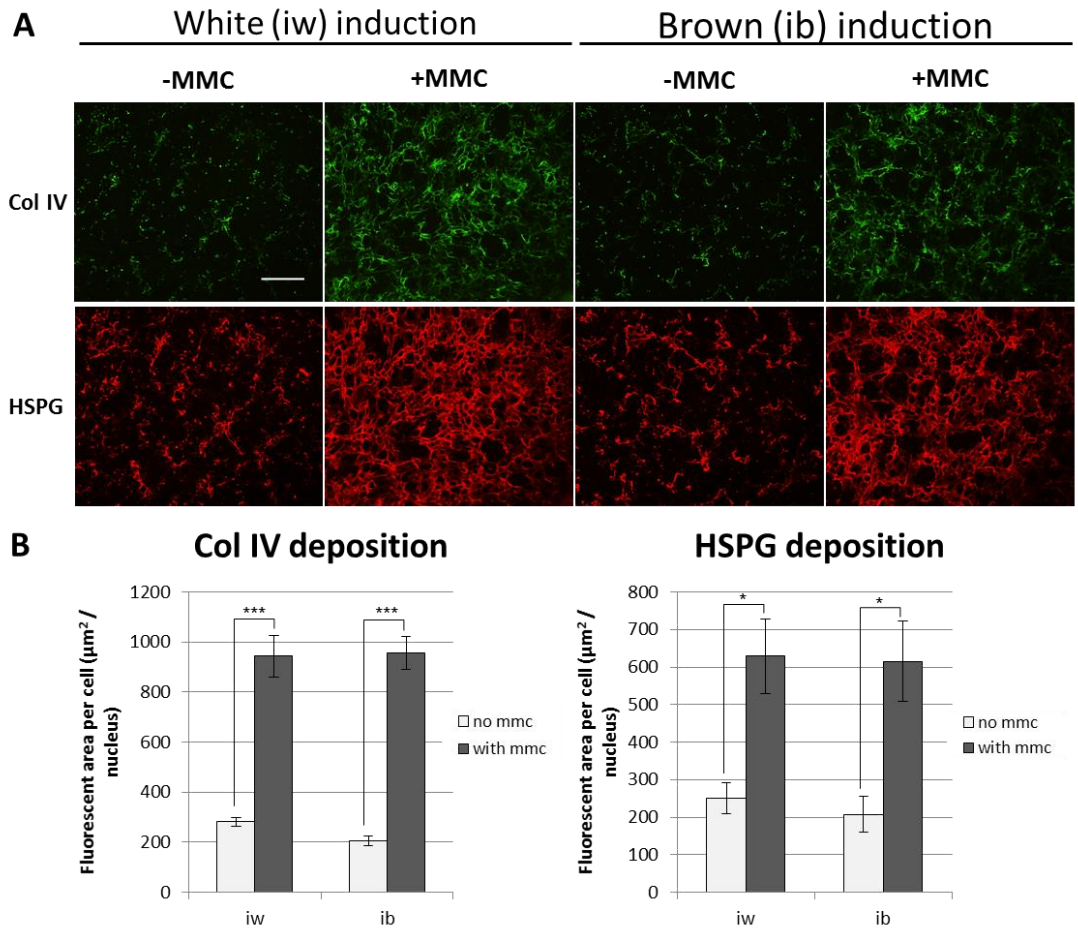


**Figure 3.12. MMC enhances microenvironment formation during adipogenic differentiation.** bmMSCs were chemically induced with a white (iw) or brown (ib) cocktail ± MMC for 3 weeks and ECM deposition was assessed immunocytochemically. (A) Immunocytochemistry images of deposited collagen IV (Col IV) and heparan sulphate proteoglycan II (perlecan/HSPG). Scale bar: 500µm. (B) Quantitative bioimaging analysis of fluorescent area normalized to cell number. Data are mean ± SEM. *$p<0.05$; ***$p<0.001$. Experiment performed together with Xiu Min Ang and Rókus Kriszt, NUS.

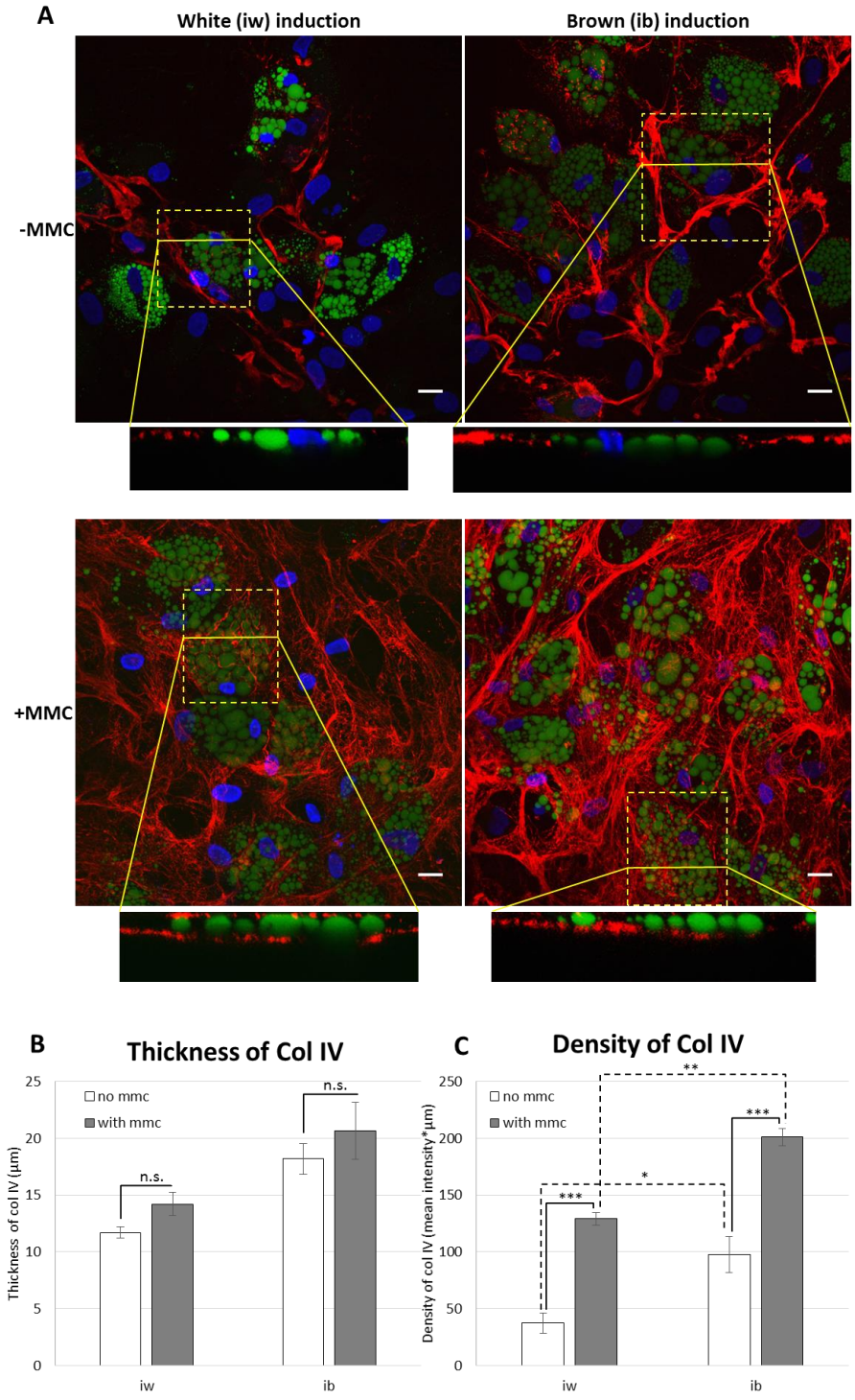


**Figure 3.13. MMC increases the density but not the thickness of Col IV during adipogenic differentiation.** bmMSCs were chemically induced with a white (iw) or brown (ib) induction protocol ± MMC for 3 weeks and Z-stack images was obtained for each condition through confocal microscopy. (A) Z-project images of DAPI (blue), Col IV (red) and BODIPY (green). The inserts are taken from the cross-section views of the Z-stack marked by the horizontal solid yellow line in each image. Scale bar: 20µm. (B & C) Bio-imaging analysis was performed on 3 Z-stacks per condition to assess the thickness (B) and the density (C) of Col IV deposited. Data are mean ± SEM. n.s. not significant; *p<0.05; **p<0.01; ***p<0.001. Experiment performed together with Anna Goralczyk, Rókus Kriszt, Jean-Yves Dewavrin, NUS; and Dr. Cedric Badowski, IMB A*STAR.

HSPG is known to sequester FGFs (Turner and Grose, 2010), so I assessed whether the enhanced brown adipogenesis in MMC-induced cultures was due to the increased sequestration of fibroblast growth factors (FGFs). As there was evidence for an autocrine production of both FGF1 and FGF2 at mRNA level (Fig. 3.14A), I proceeded to quantify these FGFs sequestered to the ECM. Whole cell layers of ib mmc (after three weeks) were treated with 2M NaCl at pH 7.4 to elute low binding affinity FGF2 that sequester to HSPG in the ECM as previously described (Moscatelli, 1992). This salt wash technique was applied to elute FGF1 as well. Both growth factors were recovered from matrices in substantial amounts (60-160 pg/ml), with no significant differences between iw and ib but with a tendency to a reduction of FGF content across all crowded cultures induced with MMC (Fig. 3.14B). mRNA for *FGF21* was not detected in bmMSC-derived adipocytes after 35 cycles (data not shown).

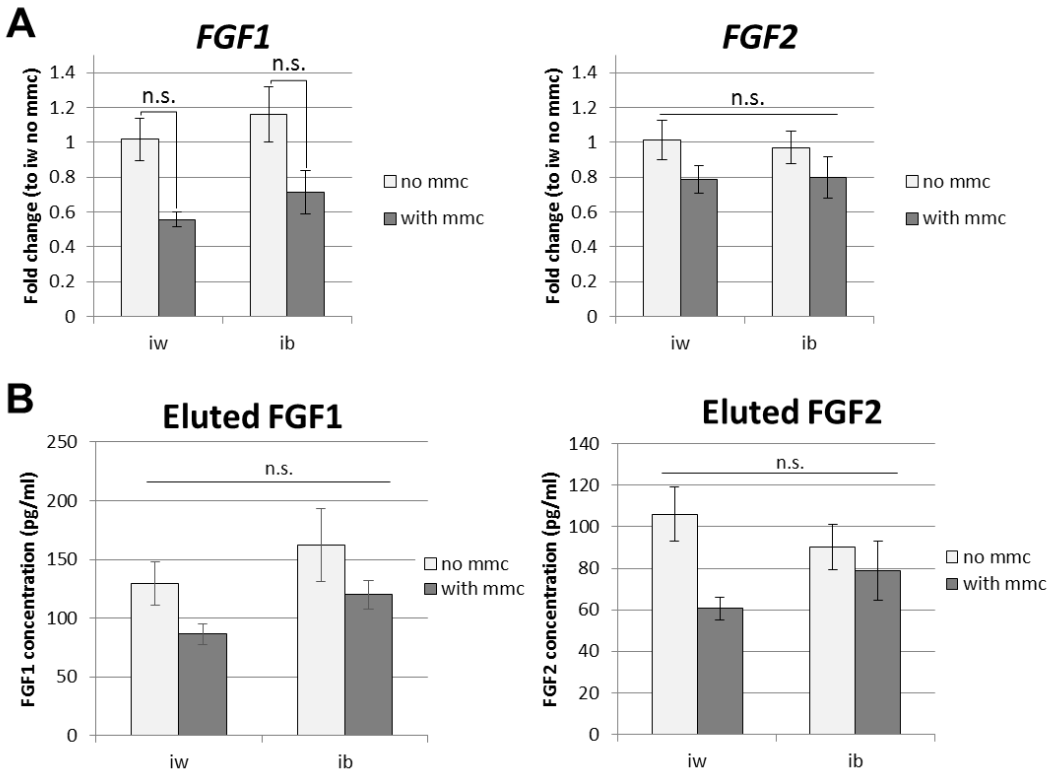


**Figure 3.14. MMC-enhanced ECM does not contain more FGFs.** bmMSCs were chemically induced with a white (iw) or brown (ib) cocktail ±MMC for 3 weeks. qPCR was carried out (on a separate experimental set) to determine the expression of *FGF1* and *FGF2*. To assess the amount of sequestered FGFs in the matrix, whole cell layers were treated with 2M NaCl to elute HSPG bound ligands and eluates were analysed by ELISA for presence of FGF 1 and 2. (A) Gene expression of *FGF1* and *FGF2*. (B) Salt eluates analysed for presence of FGF 1 and 2 by ELISA after completed 3 week adipogenic differentiation. Data are mean ± SEM. n.s. = not significant.

I reported in (Ang et al., 2014) that MMC-induced adipocytes produce an ECM that more closely mimics a native adipocyte matrix in terms of composition and structure, which could mediate pro-adipogenic signals to differentiating cells. With the increased deposition of col IV I next assessed the expression of integrins that are known to bind to collagens, namely α1β1 and α2β1 (Gullberg and Lundgren-Akerlund, 2002). While the expression levels of *ITGA1* and *ITGB1* did not differ significantly between conditions, the expression of *ITGA2* (the gene encoding integrin α2) was significantly lower by 30-40% in MMC-generated adipocytes (Fig.

3.15), indicative of a more adipogenic phenotype, in accordance with published literature (Ullah et al., 2013).

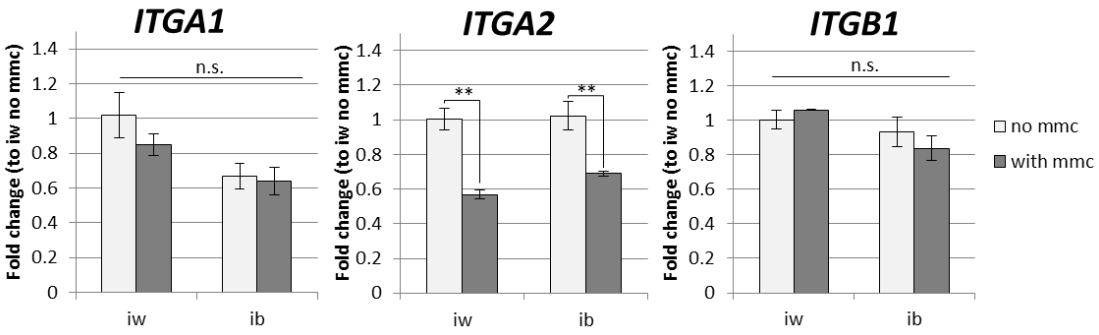


**Figure 3.15. MMC modulates *ITGA2* expression during adipogenic differentiation.** bmMSCs were chemically induced with a white (iw) or brown (ib) cocktail ±MMC for 3 weeks and expression of collagen-binding integrins by qPCR was assessed. *ITGA1* = integrin alpha 1, *ITGA2* = integrin alpha 2, *ITGB1* = integrin beta 1. Data are mean ± SEM. ns. = not significant; **p<0.01.

### *3.4 "Browning" of bmMSC-derived white adipocytes with MMC*

In the preceding sections, I have shown that sucrose co-polymer Ficoll when used as macromolecular crowder could enhance brown adipogenic differentiation of bmMSCs. In this section, I probed the system further and questioned whether the addition of MMC together with factors which promote brown adipocyte differentiation could enhance "browning" on already committed white adipocytes. The recruitment of beige adipocytes in a white adipose depot is known as "browning" (Bartelt and Heeren, 2014), and this term will be used in this section to describe the appearance of *UCP1*-positive adipocytes in the bmMSC-derived adipocyte cultures that previously had no *UCP1* mRNA expression. To achieve this aim, bmMSCs were first subjected to a standard white (iw) protocol for 3 weeks to generate mature bmMSC-derived white adipocytes. Then, for the next three weeks, these bmMSC-derived white adipocytes were exposed to a white (iw) or brown (ib) induction cocktail in the absence or presence of MMC (Fig. 3.16, (W and W/B) no MMC and

(W and W/B) MMC after 3 weeks). Other conditions comprising various combinations of iw and ib cocktails and the absence or presence of MMC were also carried out as controls to assess the browning effect of the cocktail alone and the browning effect of MMC alone, generating a total of 8 conditions. At the end of 6 weeks, qPCR analysis was carried out (Fig. 3.16).

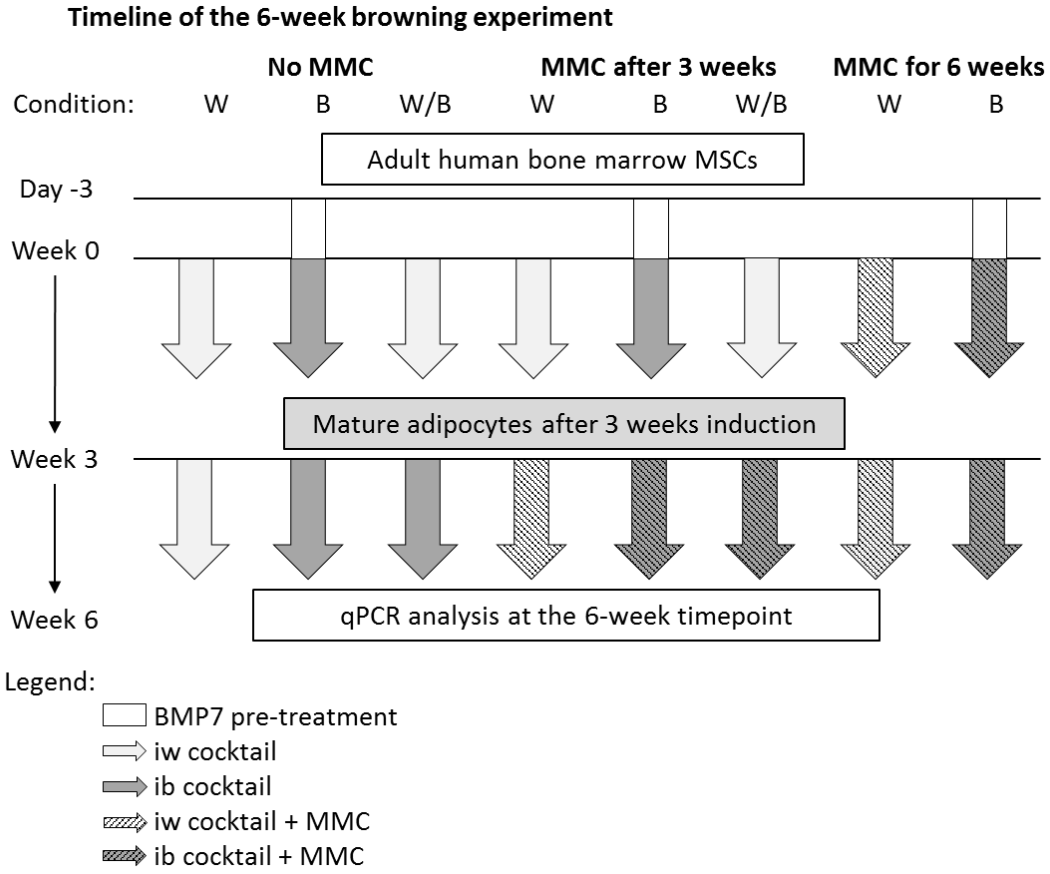


**Figure 3.16. 6-week adipogenic induction protocol to assess browning of WAT-differentiated bmMSCs ±MMC.** bmMSCs were subjected for 6 weeks to either a white or brown protocol in the presence or absence of MMC. A third group of cultures was subject to a white or brown protocol for 3 weeks and then switched to MMC or a brown protocol with MMC. The diagram shows the timeline and conditions used for the 6-week experiment.

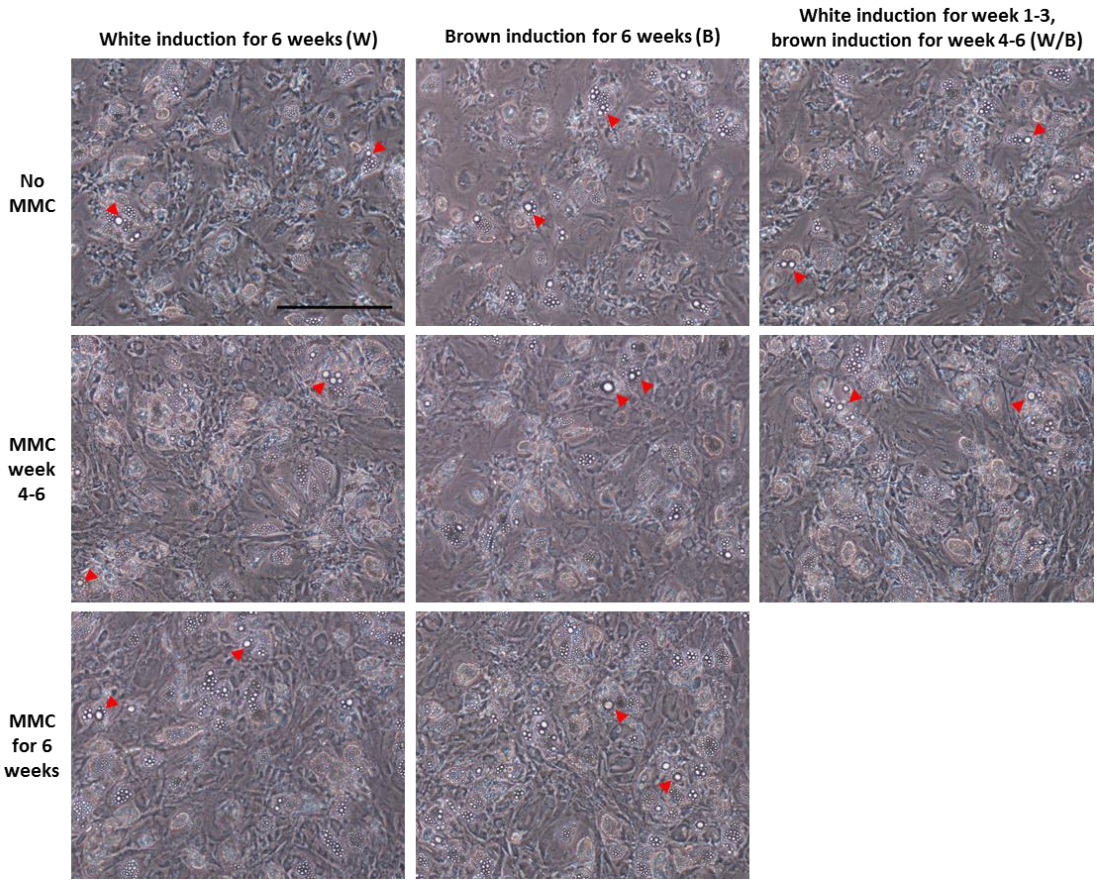


**Figure 3.17. bmMSCs differentiated under a 6-week adipogenic induction protocol accumulate larger lipid droplets than in a 3-week induction protocol.** bmMSCs were subjected for 6 weeks to either a white or brown protocol in the presence or absence of MMC. A third group of cultures was subject to a white or brown protocol for 3 weeks and then switched to MMC or a brown protocol with MMC. Phase contrast images at 4X magnification show accumulation of large lipid droplets (red arrows) in bmMSC-differentiated adipocytes under a 6-week induction protocol. Scale bar: 500µm.

Morphologically, the bmMSC-derived adipocytes cultured for 6 weeks accumulated large lipid droplets (Fig. 3.17, red arrows), which were absent in adipocytes at 3 weeks (refer to Fig. 3.3). In the initial experiments, after differentiating the bmMSCs using the iw protocol, I treated the cultures with browning factors (T3 and rosiglitazone) ± MMC from week 4-6 to investigate their potential to induce browning in the 3-week generated bmMSC-derived iw-adipocytes. However when the iw cocktail, comprising of dexamethasone, indomethacin, insulin and IBMX, was removed from week 4-6, the cultures showed a reversion of cell shape from rounded to spindle-like, accompanied by a loss of lipid droplets (Fig.

3.18, right panel). Thus I kept the 4 basic differentiation factors of the iw cocktail throughout the 6 weeks of differentiation.

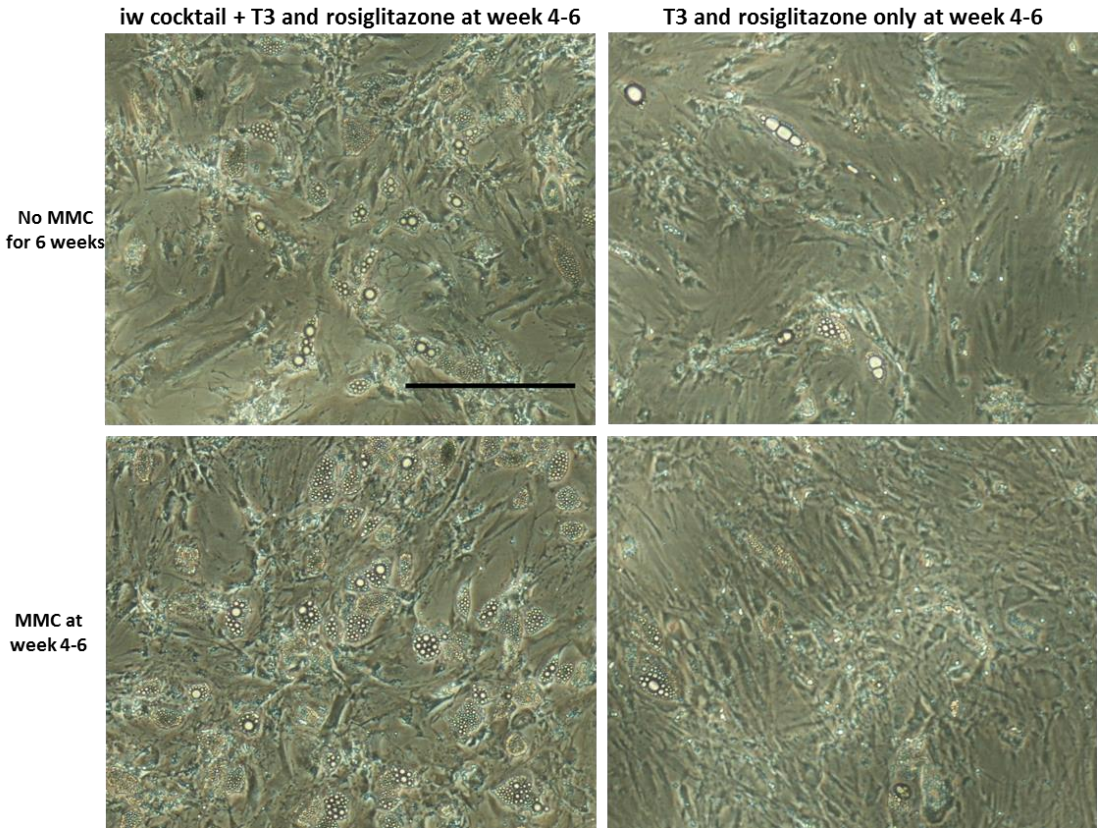


**Figure 3.18. The standard iw cocktail is needed to maintain the round morphology and the accumulation of lipid droplets in bmMSC-derived adipocytes.** Phase contrast images at 4X magnification of adipocyte cultures at the end of 6 weeks showing the reversion of cell shape from round to spindle-like and the loss of lipid droplets when the iw cocktail (dexamethasone, indomethacin, insulin and IBMX) was removed during week 4-6 of culture. Cells were seeded in 12 well plates at 25k/well (6.4k/cm$^2$) and grown to confluence before induction. Scale bar: 500µm.

The cultures differentiated according to the designed protocol in figure 3.16 were then harvested for RNA and qPCR analysis was carried out. bmMSC-derived adipocytes differentiated in either iw protocol and the ib mmc protocol for 6 weeks served as reference for baseline (1-fold) and maximal *UCP1* induction (16-fold), respectively (Fig. 3.19). In the absence of MMC, neither the switch to an ib induction cocktail after 3 weeks nor a full 6 weeks ib protocol induction led to a significant *UCP1* expression (1.2-fold, and 1.9-fold, respectively) (Fig 3.19, left column group).

In contrast, the addition of MMC to respective induction protocols in week 4-6 increased *UCP1* expression 4.8-fold in iw mmc, 6.1-fold (ib mmc) and 8.6-fold when the iw induction cocktail was switched to the ib induction cocktail (Fig. 3.19, middle column group). Of note, 6 weeks of iw mmc induced cultures achieved 14-fold *UCP1*, *closely approaching* maximal *UCP1* induction values (16-fold) obtained for 6 weeks of ib mmc induction (Fig. 3.19, right column group). In contrast, pan-adipocyte genes *FABP4* and *LEP* did not show a significant upregulation from the iw-generated adipocytes as a baseline (Fig. 3.20), indicating that the upregulation of *UCP1* was unique.

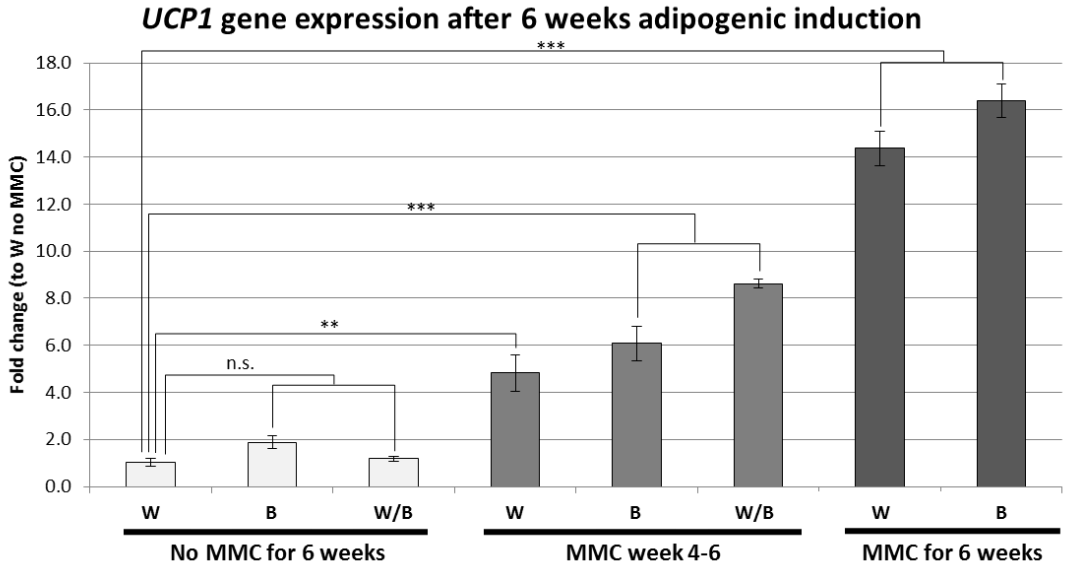


**Figure 3.19. Browning of WAT-differentiated bmMSCs with MMC.** bmMSCs were subjected for 6 weeks to either a white or brown protocol in the presence or absence of MMC. A third group of cultures was subjected to a white or brown protocol for 3 weeks and then switched to MMC or a brown protocol with MMC. Conversion of white to brown was monitored by *UCP1* mRNA expression. Data are mean ± SEM. n.s. = not significant; *p<0.05; **p<0.01; ***p<0.001.

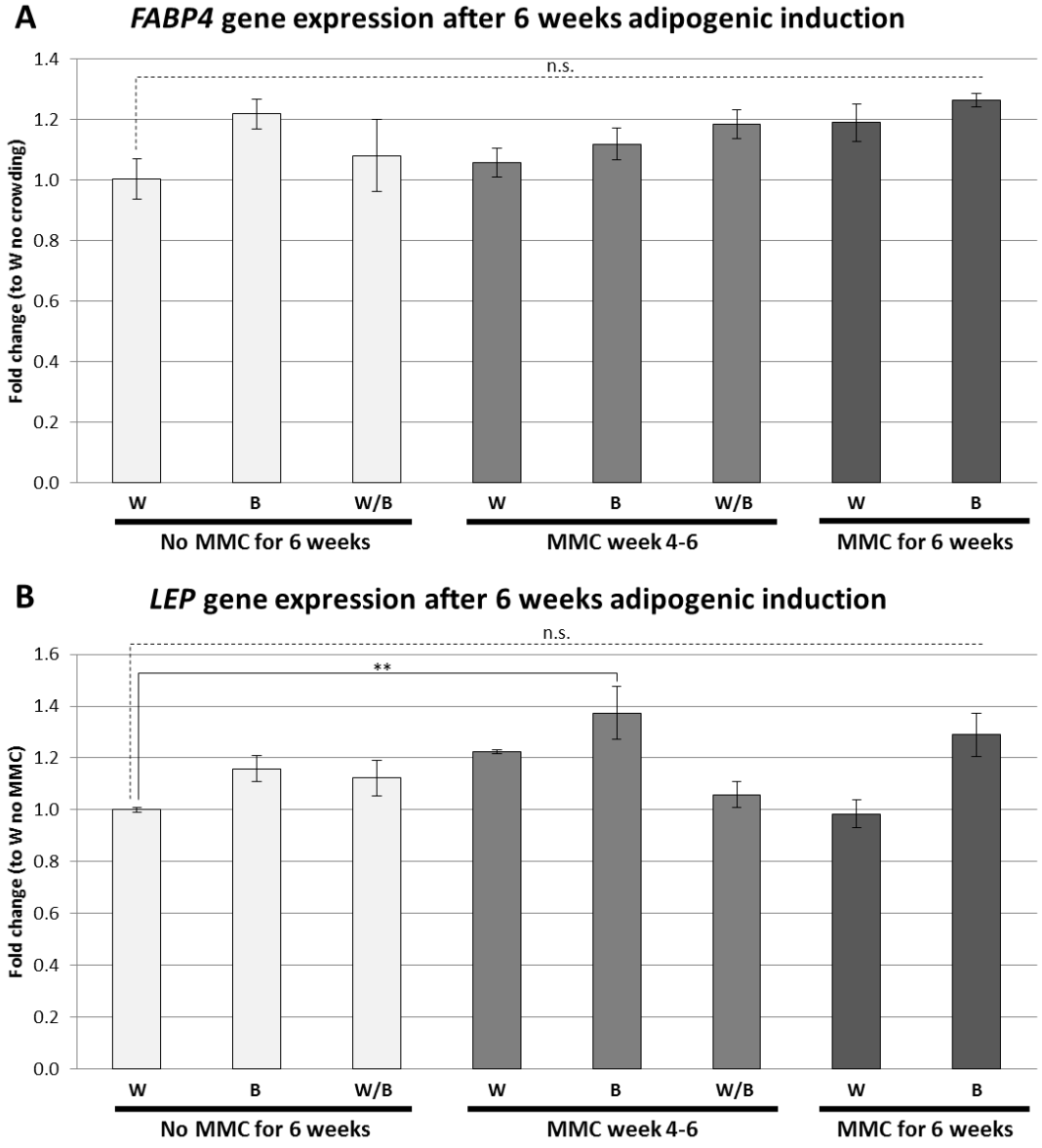


**Figure 3.20. Similar expression of pan-adipocyte genes after 6 weeks adipogenic induction with different induction protocols.** bmMSCs were subjected for 6 weeks to either a white or brown protocol in the presence or absence of MMC. A third group of cultures was subjected to a white or brown protocol for 3 weeks and then switched to MMC or a brown protocol with MMC. *LEP* and *FABP4* mRNA expression were measured. Data are mean ± SEM. n.s. = not significant; *p<0.05; **p<0.01; ***p<0.001.

### *3.5 MMC enhances adipogenic differentiation towards a brown adipocyte phenotype of progenitor cells isolated from the stromal vascular fraction (SVF) of abdominal subcutaneous fat*

So far I have shown that MMC enhanced brown adipogenesis in bmMSCs. I wanted to investigate whether MMC using sucrose co-polymer Ficoll also enhanced brown adipogenesis of other renewable adult progenitor cell sources which have a brown adipogenic potential. Subcutaneous white adipose tissue has shown browning capabilities under certain induction conditions (Schulz et al., 2011). Hence I obtained progenitor cells from the SVF of human abdominal subcutaneous fat as a kind gift from Dr Sue-Anne Toh and subjected them to the 3-week induction protocols ±MMC and measured *UCP1* mRNA expression. The SVFs underwent adipogenesis at the end of the 3-week induction, with the appearance of intracellular lipid droplets in the induced conditions (Fig. 3.21). In terms of *UCP1* expression, a similar trend was observed for this cell type (Fig. 3.22) as in the case of bmMSCs (refer to Fig. 3.1), where regardless of induction protocol used, MMC enhanced *UCP1* expression. *UCP1* was increased significantly by 30-fold in the ib mmc protocol compared to the white induction protocol alone.

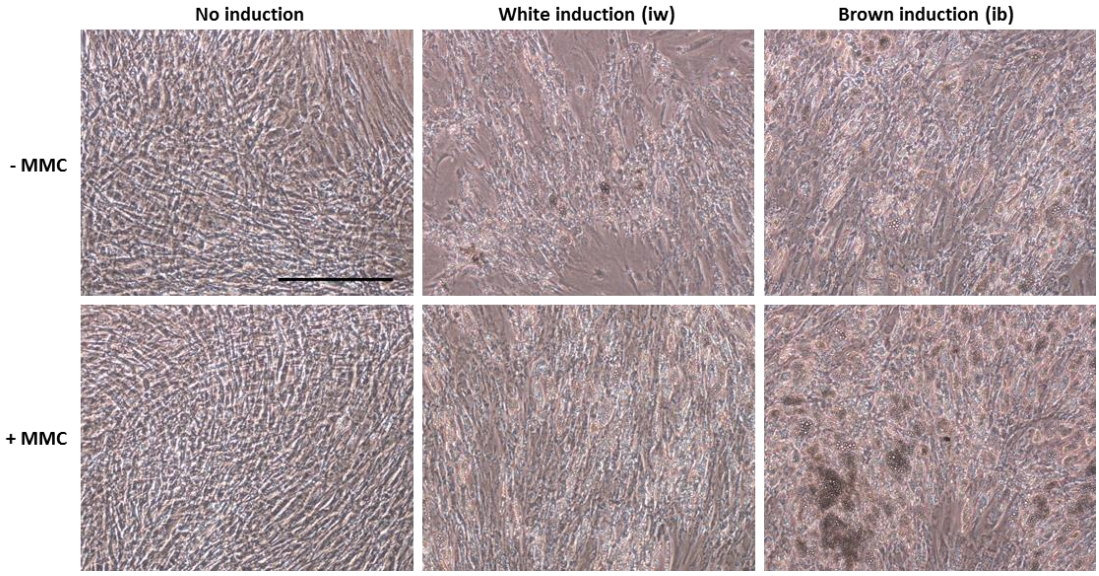


**Figure 3.21. SVF-derived adipocytes after a 3-week induction with a white (iw) or brown (ib) cocktail ± MMC.** Phase contrast images taken at 4X magnification showed the change in cell morphology from spindle-like to round and the accumulation of lipid droplets. Scale bar: 500µm.

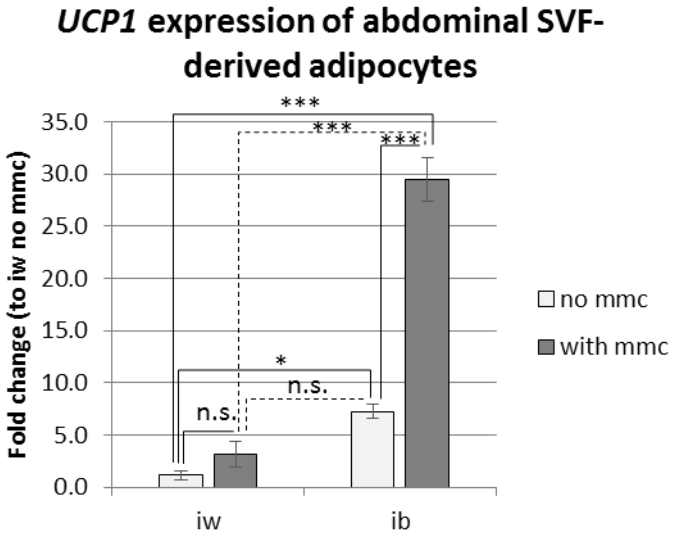


| Condition | Ct value |
|---|---|
| iw | 32.2 ± 0.4 |
| ib | 29.4 ± 0.1 |
| iw mmc | 30.7 ± 0.5 |
| ib mmc | 27.4 ± 0.1 |

**Figure 3.22. MMC enhances UCP1 expression in adipocytes differentiated from subcutaneous abdominal SVF-derived progenitors.** Progenitor cells isolated from the SVF of subcutaneous abdominal adipose tissue were chemically induced with a white (iw) or brown (ib) protocol ±MMC for 3 weeks and qPCR for UCP1 was carried out to assess brown adipogenesis. Raw Ct values of UCP1 are reported beside the graph. Data are mean ± SEM. n.s. = not significant; *p<0.05; **p<0.01; ***p<0.001.

### *3.6 Ficoll is taken up by bmMSC-derived ib mmc adipocytes, suggesting a MMC-independent mechanism of enhancing brown adipocyte differentiation*

So far I have assumed that the sucrose co-polymer Ficoll enhances brown adipogenic differentiation by MMC which leads to an increased matrix deposition and an enriched lineage-directing extracellular microenvironment. However, my laboratory has discovered recently that Ficoll can be taken up by undifferentiated bmMSCs and shows co-localisation with the mitochondria (Rashid et al., 2014a). Hence I sought to investigate whether both Ficoll species Fc70 and Fc400, are also taken up by bmMSC-derived adipocytes. iw and ib mmc- generated adipocytes were incubated with TRITC-labelled Fc70 or Fc400 for 1h and co-stained with mitotracker Green before confocal imaging. Compared to TRITC-alone controls, the uptake of Fc70 and Fc400 in iw-generated adipoyctes was not substantial, although Fc400 showed slightly more uptake into the cells (Fig. 3.23). For the ib mmc-generated adipocytes, uptake of Fc400 was substantially higher compared to Fc70 and TRITC alone (Fig. 3.24). Interestingly, Fc400 showed co-localisation with the mitotracker Green staining in the ib mmc-generated adipocytes, and also, to a lesser extent, in the iw-generated adipocytes (Fig. 3.24 and fig. 3.23, bottom right image, yellow staining).

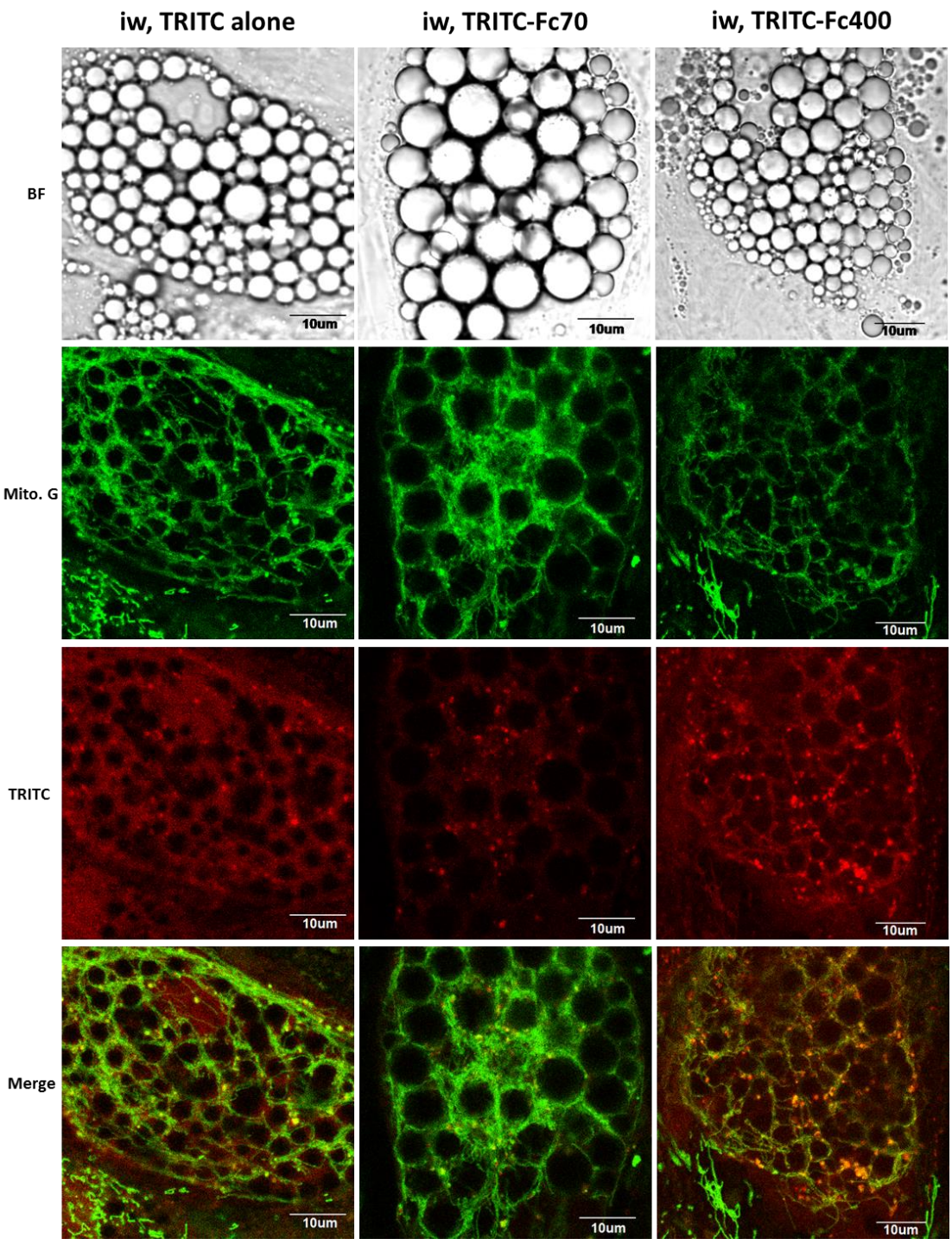


**Figure 3.23. Assessment of Ficoll uptake and mitochondrial co-localisation in bmMSC-derived white (iw) adipocytes.** Differentiated iw adipocytes were incubated with TRITC-labelled Ficoll70 or Ficoll400 and co-stained with mitotracker green. Confocal images of bright field (BF), mitochondria (mito. G), and TRITC-labelled Ficoll (TRITC) to assess its uptake into bmMSC-derived adipocytes. TRITC alone was used as a control. Scale bar: 10µm. Experiment performed together with Rafi Rashid, NUS.

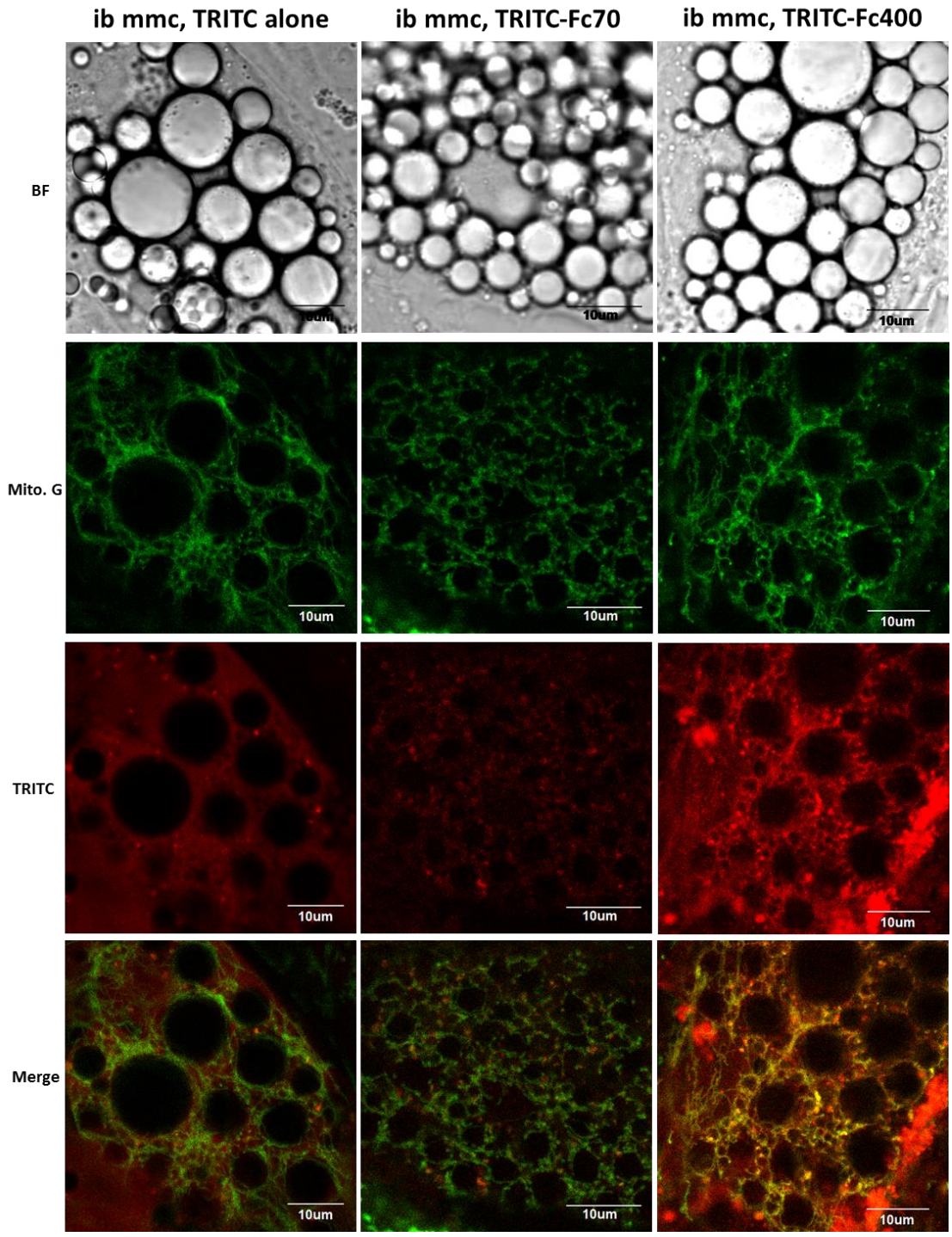


**Figure 3.24. Assessment of Ficoll uptake and mitochondrial co-localisation in bmMSC-derived brown adipocytes generated under MMC (ib mmc).** Differentiated ib mmc adipocytes were incubated with TRITC-labelled Ficoll70 or Ficoll400 and co-stained with mitotracker green. Confocal images of bright field (BF), mitochondria (mito. G), and TRITC-labelled Ficoll (TRITC) to assess Ficoll uptake into bmMSC-derived adipocytes. TRITC alone was used as a control. Scale bar: 10µm. Experiment performed together with Dr. Rafi Rashid, NUS.

# CHAPTER 4: DISCUSSION

## *4.1 Validation of hypotheses and their implications*

In this study, I have confirmed hypotheses 1 & 2 that human adult bone marrow mesenchymal stem cells (bmMSCs) possess the intrinsic potential to differentiate into functional brown adipocytes, and this potential is greatly augmented with the addition of Ficoll during adipogenic induction (refer to *Introduction section 1.10*). This knowledge gained provides insight to a fundamental question in literature concerning the identity of adult human bone marrow fat and presents a functional human brown adipocyte progenitor cell source comparable with other human brown adipocyte differentiation models. While there is evidence to support hypothesis 3 that Ficoll enhances the native brown adipocyte phenotype of bmMSCs via the macromolecular crowding (MMC) effect of generating a richer lineage-directing microenvironment, the fact that Ficoll is taken up by the bmMSC-derived adipocytes suggests that Ficoll may also promote brown adipogenesis by other means besides MMC. Lastly, this novel adipogenic differentiation method also upregulates *UCP1* expression of another sustainable progenitor cell type and thus opens up possibilities for therapeutic intervention and the development of a cell-based screening platforms to counteract obesity.

### *4.2 Yellow fat in bone marrow takes on a new meaning: presence of a population of brown fat in the bone marrow*

Bone marrow provides an environmental niche for haematopoiesis and bone. Fat is a major component of the bone marrow. In contrast to extramedullar fat depots, the type of fat and its function are largely unknown (Lecka-Czernik, 2012; Motyl and Rosen, 2011). Initially referred to as yellow adipose tissue, this depot was considered for a long time to occupy the space in bones no longer needed for hematopoiesis. However, research over the years have shown that marrow fat play a role in regulating haematopoiesis (Gimble et al., 2006; Naveiras et al., 2009) and possibly osteogenesis and systemic energy metabolism (Lecka-Czernik, 2012). Bone marrow fat has also been suspected to harbour a mixed white and brown fat phenotype (Calo et al., 2010; Gimble and Nuttall, 2004; Krings et al., 2012; Nishio et al., 2012; Olmsted-Davis et al., 2007). Although bone marrow mesenchymal stem cells (bmMSCs) give rise to bone, fat and supporting hematopoietic stroma (Minguell et al., 2001), whether they differentiate to both white and brown fat populations remains uncertain. Adult human bmMSCs have been shown to differentiate only into white adipocytes (Mackay et al., 2006). However, more recently some isolates of foetal bmMSCs have been found to differentiate into white adipocytes and others into brown albeit under identical induction conditions (Morganstein et al., 2010), showing an intrinsic potential in foetal bmMSCs to differentiate into brown adipocytes. Further, adenovirus-mediated overexpression of PGC1α in adult bmMSCs from a single donor yielded a modest 4-fold increase in UCP1 mRNA expression and a 2-fold increase in mitochondrial mass and oxygen consumption after subjecting the transduced cells to adipogenic induction for 6 days (Huang et al., 2011), although I

am sceptical that a late functional marker like UCP1 could be detected at such an early stage (6 days) of adipogenic differentiation for bmMSCs.

My findings reveal that there is an intrinsic potential in adult human bmMSCs to differentiate towards a brown fat phenotype without genetic manipulation, and it was made possible only through the addition of Ficoll during the adipogenic induction period. In our protocol, neither a standard white nor a brown induction protocol significantly induced expression of *UCP1* mRNA in bmMSCs. However, this changed dramatically when the sucrose co-polymer Ficoll was introduced into the cell cultures during adipogenic differentiation. *UCP1* expression levels showed a substantial boost in the brown induction protocol (including forskolin stimulation of up to 800-fold), as well as in the white induction protocol. I attempted to define the bmMSC-derived brown adipocyte population, in comparison with bmMSC-derived white adipocytes, using a gene marker panel that distinguishes white, beige and classical brown adipocytes which has been recently validated in humans (refer to *Introduction section 1.6*). The *UCP1*-positive adipocytes however did not show an upregulation of other classical brown or beige markers or a downregulation of white marker *HOXC9*. The only difference was for the beige marker *CD137*, which was markedly downregulated in the *UCP1*-positive adipocytes. Moreover, raw Ct values for the beige markers were low (Ct > 31) and may not be biologically relevant in bmMSC-derived adipocytes. However, as the markers for classical brown and beige adipocytes have been characterized using cells from various adipose tissue depots and not from bone marrow, it cannot be ruled out that bmMSC-derived white adipocytes that were used as the baseline for comparison have a molecular signature different from subcutaneous WAT that has been traditionally used as the benchmark of white

adipocytes. For future work the brown adipocyte population from bone marrow would need to be compared against this benchmark.

### *4.3 Comparability with other human brown adipocyte differentiation models*

This study shows that adult human bmMSCs can be differentiated into a functional brown adipocyte phenotype without genetic manipulation, as characterised by induction and high expression of *UCP1*, increased mitochondrial depolarisation, oxygen consumption and uncoupled respiration upon forskolin stimulation. I do have western blot data showing the presence of UCP1 protein in ib mmc-induced adipocytes, but there were issues with specificity of the antibodies used (Supp. Fig. 2). More importantly, I have shown that ib mmc-induced adipocytes are functional brown adipocytes, indicated by a substantial increase in thermogenic genes, oxygen consumption and uncoupled respiration when thermogenesis was stimulated in these cells.

The efficacy of differentiation (defined as the level of *UCP1* expression benchmarked against a white differentiation protocol) in this cell model is superior to adult human bmMSC-derived adipocytes overexpressing PGC1α (4-fold) (Huang et al., 2011), and is comparable to other human cell models aiming at brown adipocyte differentiation that were discussed in *Introduction section 1.8* (Table 1.5) including induced pluripotent cells (iPS) cells (20-fold) (Ahfeldt et al., 2012; Nishio et al., 2012), human multipotent adipose-derived stem cells (hMADS) isolated from young donors (13-39 fold) (Elabd et al., 2009; Pisani et al., 2011) and even to those seen in preadipocytes from the subclavicular region in human adults (20-40 fold) (Lee et al., 2011b). I am unable to compare our efficacy of differentiation with the recent publication on using brown adipose tissue derived stem cells from the mediastinum as

the authors did not report a fold change for *UCP1* mRNA (Silva et al., 2014). From the cell models discussed here, there are currently only 3 sources (hMADS, supraclavicular fat, mediastinal fat) of human brown fat progenitors that do not utilise genetic manipulation and hence are good candidates for cellular therapy and research. In comparison to these 3 sources, our method of generating adult human brown adipocytes is more advantageous as our cell source is autologous (unlike the hMADS), easily obtainable in sustainable numbers (unlike supraclavicular and mediastinal fat) and yet allows for a robust differentiation response (Fig. 4.1). I, together with my lab members have in fact used 3 different lots of bmMSCs with predictable and stable results of at least 20 differentiation rounds (verified together with Anna Goralczyk, Xiu Min Ang, Rókus Kriszt and Jarrod Sim, NUS).

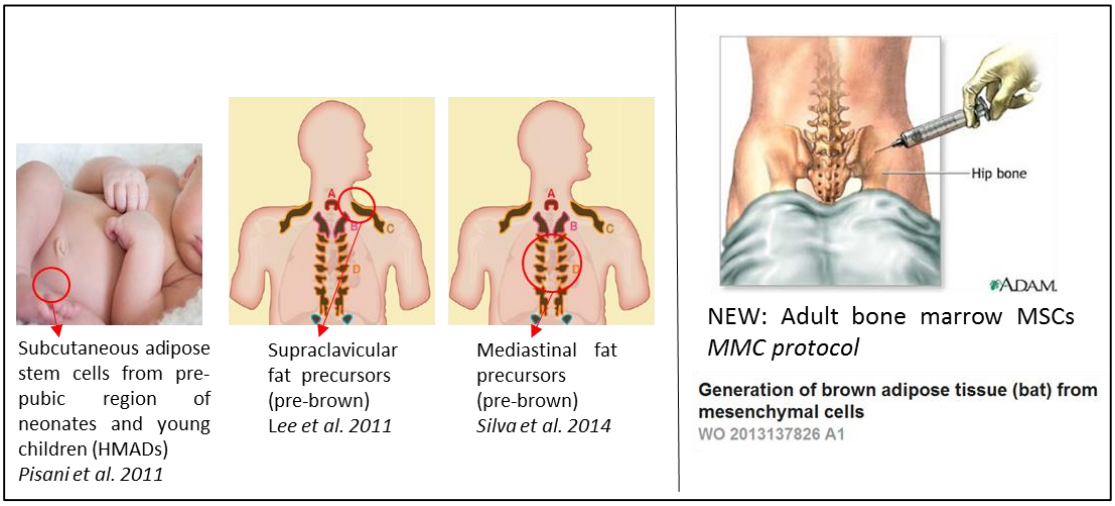


**Figure 4.1. Sources of human brown fat progenitors.** Of the 3 current sources for human BAT progenitor cells that do not require genetic manipulation (left panel) all are exhaustible, and 2 require involved surgery for harvest. On the other hand, our proposed bone marrow source (right panel) is autologous and easily obtainable in sustainable numbers.
[Image showing the supraclavicular and mediastinal fat locations was reprinted from Cell Metabolism, vol.11, Enerbäck S., "Human Brown Adipose Tissue", p248-252, Copyright (2010), with permission from Elsevier.]

### *4.4 Browning of bmMSC-derived white adipocytes with Ficoll*

One of the most significant findings in this study is that Ficoll also encourages the conversion of bmMSC-derived white adipocytes into a brown phenotype (16-fold increase in *UCP1* expression without genetic manipulation) which is comparable to the only other white-to-brown conversion model in humans using hMADS-derived adipocytes using a PPARγ agonist (15-28 fold) (Elabd et al., 2009; Pisani et al., 2011). This suggests that the bmMSC-derived adipocytes either retain the plasticity to transdifferentiate from white adipocytes to a population of *UCP1*-expressing brown adipocytes, or the bmMSCs comprise a mixed population of white and brown progenitors where under conditions emulated by Ficoll, favour the differentiation of the brown progenitors (*de novo* recruitment) (Fig. 4.2).

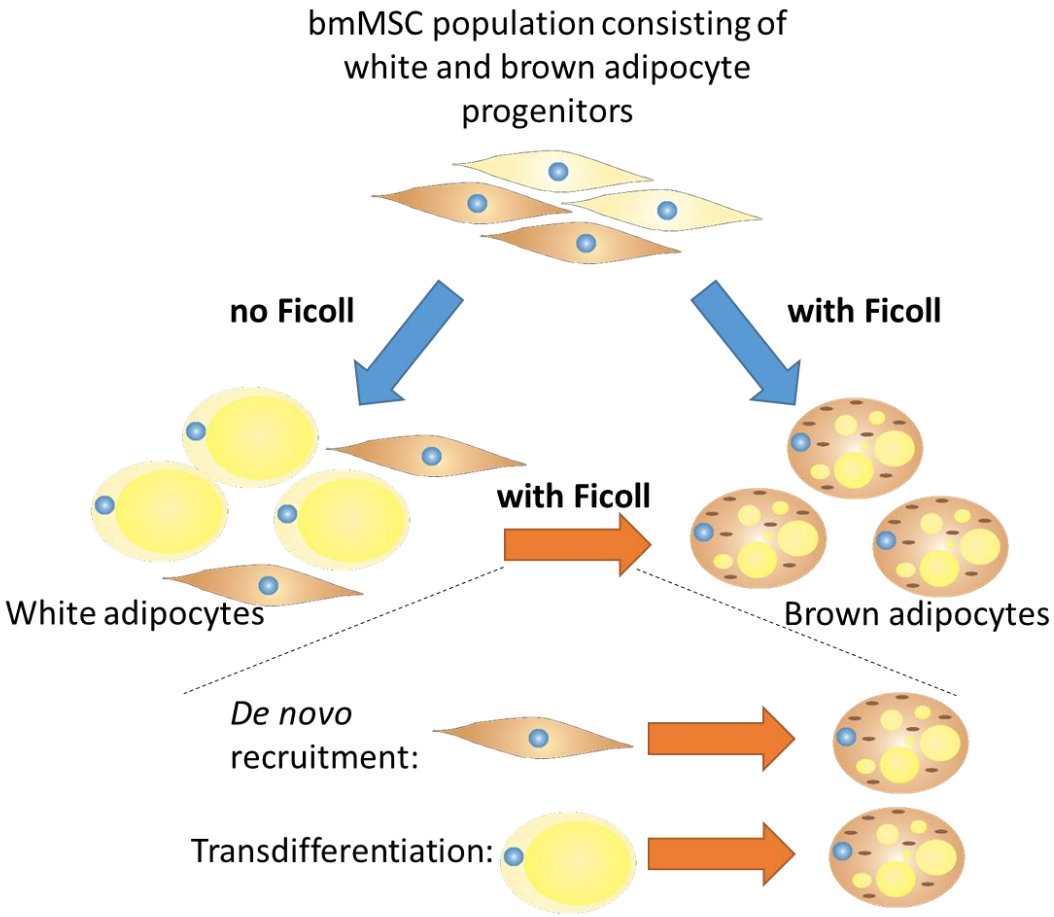


**Figure 4.2. Browning of bmMSC-derived white adipocytes with Ficoll.** Ficoll causes the browning of bmMSC-derived white adipocytes either by *de novo* recruitment of brown adipocyte stem cell progenitors, or a transdifferentiation of white adipocytes into *UCP1*-expressing brown adipocytes. Figure idea based on Bartelt and Heeren (2014).

### *4.5 MMC effects of Ficoll in enhancing brown adipocyte differentiation via the matrix*

Ficoll has been identified as an ideal candidate for macromolecular crowding (MMC) (Ellis, 2001) due to its comparable size (50-500kDa) with native macromolecules (e.g. albumin at 69kDa) in biological systems, neutral charge and low viscosity when dissolved in culture medium. In this study, I have used a crowding protocol using a mixture of Ficoll70 (Fc70) and Ficoll400 (Fc400) to create fraction volume occupancy of ~17% in the culture medium, thereby emulating the crowdedness of the perfused bone marrow compartment (Chen et al., 2011). Through the principle of excluded volume effect (EVE), MMC increases extracellular enzymatic reaction rates (refer to *Introduction section 1.9*), which result in increased ECM deposition and remodelling.

In support of the hypothesis that Ficoll augments brown adipogenesis in adult human bmMSCs via the macromolecular crowding (MMC) effect of generating a richer lineage-directing microenvironment and driving bmMSC-derived adipocytes towards a mature adipocyte phenotype, my data show that along with an enriched ECM, there was a greater accumulation of lipid droplets, indicative of a more mature phenotype. It has been reported that under MMC, bmMSCs also increase in proliferation presumably due to a richer microenvironment deposited (Chen et al., 2011). Thus, it is not unexpected that MMC increased cell density of our cultures observed in the phase contrast images after 3 weeks. This increased cell density due to the proliferation of non-differentiated cells residing in the adipocyte cultures generated under MMC might also contribute to a more efficient differentiation and attainment of a more mature phenotype as a high cell density favours adipogenic differentiation (McBeath et al., 2004).

To account for the enhanced 'browning' effect of MMC I initially considered that enhanced sequestration of fibroblast growth factors (FGFs) (Turner and Grose, 2010) previously implicated in brown adipogenesis, might be promoted by the richer heparin sulphate proteoglycans (HSPG) deposited under MMC (my data, (Ang et al., 2014)). While I found no evidence of *FGF21* expression, a notable browning factor (Fisher et al., 2012), I retrieved both FGF1 and 2 protein from salt-washed cell layers of bmMSC-derived adipocyte cultures at levels exceeding human serum concentrations by two orders of magnitude (Larsson et al., 2002). However, the amount of FGF eluted did not differ significantly between MMC and non-MMC cultured adipocytes. This is in contrast with a several fold increase in deposition of perlecan (HSPG2) in our cultures, a proteoglycan known for its ability to store FGF1 (Melrose et al., 2006) and FGF2 (Jiang and Couchman, 2003). It could be possible that although the MMC-generated matrices have a higher capacity to sequester FGFs, there may have been an increased ECM depletion of FGF, given that FGF2 bound to perlecan HS-chains can be released very efficiently by matrix metalloproteinases (Whitelock et al., 1996). As MMC-driven adipogenesis features extensive matrix remodelling and associated MMP activity (Ang et al., 2014), such a scenario is plausible. Besides FGFs, HSPG binds other growth factors including members of the epidermal growth factor (EGF) family (Taipale and Keski-Oja, 1997). It has been reported recently that several members of the EGF family such as betacellulin, heparin-binding EGF-like growth factor, epiregulin and parathyroid-hormone-related protein induced Ucp1 mRNA levels in murine primary adipocytes (Kir et al., 2014), hence it would be worthwhile to investigate the amount of these growth factors sequestered in the ECM generated by MMC.

It is possible that collagen IV, whose deposition is enhanced by MMC, is responsible for the increased sequestration of other growth factors which promote brown adipocyte differentiation. BMP7, a strong inductor of BAT, has recently been predicted to be sequestered into the ECM (Gregory et al., 2005). Furthermore, as collagen IV is known to bind BMPs such as BMP4 (Wang et al., 2008b), it is tempting to speculate that a higher amount of BMP7 is sequestered in the ECM generated under MMC and thus would explain the strong browning effects of MMC in the absence of exogenous BMP7. Another BMP candidate to investigate would be BMP4, which has been found to induce browning in murine beige but not classical brown adipocytes (Qian et al., 2013).

Besides sequestration of growth factors, the niche-specific composition and structure of the ECM influence the behaviour of bmMSCs through focal adhesions where integrin receptors interact with various ECM proteins and initiate a signalling cascade to regulate differentiation towards a particular cell fate (Docheva et al., 2007). In our study I found *ITGA2* significantly downregulated in adipocytes induced with MMC, indicative of a more adipogenic phenotype (Frith et al., 2012; Ullah et al., 2013). While there are no detailed reports of downstream integrin signalling effects in brown adipogenesis, our finding with *ITGA2* suggests that the ECM composition and structure generated under MMC enable bmMSCs to undergo adipogenic differentiation to a greater extent and exhibit its intrinsic brown potential. Other integrins involved in adipogenesis include integrins α6 (Frith et al., 2012) and α5 (Liu et al., 2005) which should also be investigated to strengthen this claim.

### *4.6 Possible non-MMC effect of Ficoll in enhancing brown adipocyte differentiation*

Mechanical stress due to osmotic challenge in cells have a profound effect on cell proliferation and differentiation. The forces produced are sensed by mechanosensitive channels which will translate these signals into biochemical signaling cascades to effect a cellular response (Blount et al., 2008; Niisato and Marunaka, 2008). Ficoll is a high molecular weight sucrose co-polymer formed by the co-polymerisation of sucrose with epichlorohydrin (Fig. 4.3). (Blount et al., 2008; Niisato and Marunaka, 2008). Ficoll is taken up by bmMSCs via pinocytosis and is broken down into smaller fragments at intralysosomal acidic pH 4.8 (Dr. Rafi Rashid's thesis; (Rashid et al., 2014a)). A possible scenario upon Ficoll uptake in the cells via endocytosis is that Ficoll is broken down into sucrose upon the decrease in luminal pH when endosomes mature into lysosomes, which in turn increases the luminal concentration leading to an influx of water into the lysosomes. Hypo-osmotic pressure stretches membranes and activate transient receptor potential (TRP) channels, a type of mechanosensitive channel (Gomis et al., 2008). TRP channels such as transient receptor potential vanilloid-4 (TRPV4) and transient receptor potential melastin 8 (TRPM8) regulate brown adipogenesis (Villarroya and Vidal-Puig, 2013). TRP channels are present in endosomes and lysosomes, and are involved in endosomal pathway signalling by regulating the release of $Ca^{2+}$ from endosomes and lysosomes (Abe and Puertollano, 2011). There is increasing evidence for endosomes serving as a signalling entities for crosstalk between cellular pathways (Palfy et al., 2012). In the *Results section 3.6*, I have shown that Ficoll was taken up by bmMSC-derived adipocytes, which may lead to intra-lysosomal hypotonic stress and the activation of lysosomal TRPs that enhance brown adipogenesis.

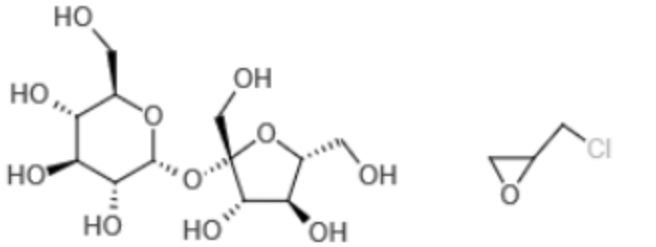


Sucrose Epichlorohydrin

**Figure 4.3. Components of Ficoll.** Ficoll is manufactured by the co-polymerisation of sucrose monomers with epichlorohydrin linkages. (Chemical structure drawings were made using a web-based software: http://web.chemdoodle.com/demos/sketcher)

### *4.7 Ficoll enhances brown adipogenesis of another adult cell source from subcutaneous white adipose tissue*

Preliminary data show that Ficoll enhanced the expression of *UCP1* significantly by 30-fold in adipocytes differentiated using a brown induction protocol from progenitors isolated from the stromal vascular fraction of the subcutaneous abdominal white adipose tissue as compared to a white induction protocol alone. This is an exciting finding as subcutaneous abdominal fat would pose as an ideal autologous cell source for obesity therapy as obese patients would be more willing to have their subcutaneous abdominal fat extracted as compared to aspirating their bone marrow.

# CHAPTER 5: CONCLUSION AND FUTURE OUTLOOK

I report for the first time of the generation of functional brown adipocytes from adult human bone marrow mesenchymal stem cells (bmMSCs) without the need for genetic manipulation, using Ficoll as a cell culture additive to unlock the intrinsic browning potential of bmMSCs. Ficoll enhances brown adipogenesis probably through the MMC effect of increasing matrix deposition and generating a richer lineage-directing matrix which promotes adipogenic differentiation to a more mature phenotype; but a non-MMC effect whereby upon uptake by the cells could increase intra-luminal hypo-osmotic stress and activate mechanosensitive channels which promotes brown adipogenesis in the cells is also plausible.

I believe that our data support exciting new opportunities for isolating and manipulating bmMSCs as a robust, autologous and sustainable source of human brown adipocytes. Moreover, I have preliminary data to show that subcutaneous adipose tissue is another potential renewable adult cell source of which Ficoll also enhances the intrinsic browning potential. Investing time and resources to further elucidate the mechanism of Ficoll in enhancing brown adipogenesis would be useful to better understand our system, which has promising translational applications in the fields of obesity and metabolic disorders. I hope to use these cells to develop an *in vitro* screening platform to identify agents that promote brown adipogenesis, as well as agents that stimulate the thermogenic programme in functional brown adipocytes. I would also like to conduct *in vivo* transplantation studies of our generated brown adipocytes into an animal model as a pre-clinical study of efficacy to explore the possibility of using these cells as a cell therapy to treat obesity in the future.

## BIBLIOGRAPHY


Abbott, A. (2003). Cell culture: biology's new dimension. Nature *424*, 870-872.

Abdallah, B.M., Jensen, C.H., Gutierrez, G., Leslie, R.G., Jensen, T.G., and Kassem, M. (2004). Regulation of human skeletal stem cells differentiation by Dlk1/Pref-1. J Bone Miner Res *19*, 841-852.

Abe, K., and Puertollano, R. (2011). Role of TRP channels in the regulation of the endosomal pathway. Physiology (Bethesda) *26*, 14-22.

Ahfeldt, T., Schinzel, R.T., Lee, Y.K., Hendrickson, D., Kaplan, A., Lum, D.H., Camahort, R., Xia, F., Shay, J., Rhee, E.P., et al. (2012). Programming human pluripotent stem cells into white and brown adipocytes. Nat Cell Biol *14*, 209-219.

Aldridge, A., Kouroupis, D., Churchman, S., English, A., Ingham, E., and Jones, E. (2013). Assay validation for the assessment of adipogenesis of multipotential stromal cells--a direct comparison of four different methods. Cytotherapy *15*, 89-101.

Almind, K., Manieri, M., Sivitz, W.I., Cinti, S., and Kahn, C.R. (2007). Ectopic brown adipose tissue in muscle provides a mechanism for differences in risk of metabolic syndrome in mice. Proc Natl Acad Sci U S A *104*, 2366-2371.

Ang, X.M., Lee, M.H., Blocki, A., Chen, C., Ong, L.L., Asada, H.H., Sheppard, A., and Raghunath, M. (2014). Macromolecular crowding amplifies adipogenesis of human bone marrow-derived mesenchymal stem cells by enhancing the pro-adipogenic microenvironment. Tissue Eng Part A *20*, 966-981.

Arterburn, D.E., and Courcoulas, A.P. (2014). Bariatric surgery for obesity and metabolic conditions in adults. BMJ *349*, g3961.

Atit, R., Sgaier, S.K., Mohamed, O.A., Taketo, M.M., Dufort, D., Joyner, A.L., Niswander, L., and Conlon, R.A. (2006). Beta-catenin activation is necessary and sufficient to specify the dorsal dermal fate in the mouse. Dev Biol *296*, 164-176.

Barbatelli, G., Murano, I., Madsen, L., Hao, Q., Jimenez, M., Kristiansen, K., Giacobino, J.P., De Matteis, R., and Cinti, S. (2010). The emergence of cold-induced brown adipocytes in mouse white fat depots is determined predominantly by white to brown adipocyte transdifferentiation. Am J Physiol Endocrinol Metab *298*, E1244-1253.

Bartelt, A., Bruns, O.T., Reimer, R., Hohenberg, H., Ittrich, H., Peldschus, K., Kaul, M.G., Tromsdorf, U.I., Weller, H., Waurisch, C., et al. (2011). Brown adipose tissue activity controls triglyceride clearance. Nat Med *17*, 200-205.

Bartelt, A., and Heeren, J. (2014). Adipose tissue browning and metabolic health. Nat Rev Endocrinol *10*, 24-36.

Bates, D.O., Levick, J.R., and Mortimer, P.S. (1993). Change in macromolecular composition of interstitial fluid from swollen arms after breast cancer treatment, and its implications. Clin Sci (Lond) *85*, 737-746.

Bell, C.G., Walley, A.J., and Froguel, P. (2005). The genetics of human obesity. Nat Rev Genet *6*, 221-234.

Bellisari, A. (2008). Evolutionary origins of obesity. Obes Rev *9*, 165-180.

Beranger, G.E., Karbiener, M., Barquissau, V., Pisani, D.F., Scheideler, M., Langin, D., and Amri, E.Z. (2013). In vitro brown and "brite"/"beige" adipogenesis: human cellular models and molecular aspects. Biochim Biophys Acta *1831*, 905-914.

Billon, N., and Dani, C. (2012). Developmental origins of the adipocyte lineage: new insights from genetics and genomics studies. Stem Cell Rev *8*, 55-66.

Blount, P., Li, Y., Moe, P.C., and Iscla, I. (2008). Mechanosensitive Channels Gated by Membrane Tension. In Mechanosensitive Ion Channels (Springer), pp. 71-101.

Bonet, M.L., Oliver, P., and Palou, A. (2013). Pharmacological and nutritional agents promoting browning of white adipose tissue. Biochim Biophys Acta *1831*, 969-985.

Calo, E., Quintero-Estades, J.A., Danielian, P.S., Nedelcu, S., Berman, S.D., and Lees, J.A. (2010). Rb regulates fate choice and lineage commitment in vivo. Nature *466*, 1110-1114.

Cannon, B., and Nedergaard, J. (2004). Brown adipose tissue: function and physiological significance. Physiol Rev *84*, 277-359.

Chen, C., Loe, F., Blocki, A., Peng, Y., and Raghunath, M. (2011). Applying macromolecular crowding to enhance extracellular matrix deposition and its remodeling in vitro for tissue engineering and cell-based therapies. Adv Drug Deliv Rev *63*, 277-290.

Chen, C.Z., Peng, Y.X., Wang, Z.B., Fish, P.V., Kaar, J.L., Koepsel, R.R., Russell, A.J., Lareu, R.R., and Raghunath, M. (2009). The Scar-in-a-Jar: studying potential antifibrotic compounds from the epigenetic to extracellular level in a single well. Br J Pharmacol *158*, 1196-1209.

Cinti, S. (2009). Transdifferentiation properties of adipocytes in the adipose organ. Am J Physiol Endocrinol Metab *297*, E977-986.

Cinti, S. (2011). Between brown and white: novel aspects of adipocyte differentiation. Ann Med *43*, 104-115.

Cohade, C., Osman, M., Pannu, H.K., and Wahl, R.L. (2003). Uptake in supraclavicular area fat ("USA-Fat"): description on 18F-FDG PET/CT. J Nucl Med *44*, 170-176.

Crisan, M., Casteilla, L., Lehr, L., Carmona, M., Paoloni-Giacobino, A., Yap, S., Sun, B., Leger, B., Logar, A., Penicaud, L., et al. (2008). A reservoir of brown adipocyte progenitors in human skeletal muscle. Stem Cells *26*, 2425-2433.

Cypess, A.M., and Kahn, C.R. (2010). Brown fat as a therapy for obesity and diabetes. Curr Opin Endocrinol Diabetes Obes *17*, 143-149.

Cypess, A.M., Lehman, S., Williams, G., Tal, I., Rodman, D., Goldfine, A.B., Kuo, F.C., Palmer, E.L., Tseng, Y.H., Doria, A., et al. (2009). Identification and importance of brown adipose tissue in adult humans. N Engl J Med *360*, 1509-1517.

Cypess, A.M., White, A.P., Vernochet, C., Schulz, T.J., Xue, R., Sass, C.A., Huang, T.L., Roberts-Toler, C., Weiner, L.S., Sze, C., et al. (2013). Anatomical localization, gene expression profiling and functional characterization of adult human neck brown fat. Nat Med *19*, 635-639.

Da Poian, A.T., El-Bacha, T., and Luz, M.R.M.P. (2010). Nutrient Utilization in Humans: Metabolism Pathways. Nature Education *3*, 1.

Degawa-Yamauchi, M., Moss, K.A., Bovenkerk, J.E., Shankar, S.S., Morrison, C.L., Lelliott, C.J., Vidal-Puig, A., Jones, R., and Considine, R.V. (2005). Regulation of adiponectin expression in human adipocytes: effects of adiposity, glucocorticoids, and tumor necrosis factor alpha. Obes Res *13*, 662-669.

Digby, J.E., Montague, C.T., Sewter, C.P., Sanders, L., Wilkison, W.O., O'Rahilly, S., and Prins, J.B. (1998). Thiazolidinedione exposure increases the expression of uncoupling protein 1 in cultured human preadipocytes. Diabetes *47*, 138-141.

Discher, D.E., Mooney, D.J., and Zandstra, P.W. (2009). Growth factors, matrices, and forces combine and control stem cells. Science *324*, 1673-1677.

Docheva, D., Popov, C., Mutschler, W., and Schieker, M. (2007). Human mesenchymal stem cells in contact with their environment: surface characteristics and the integrin system. J Cell Mol Med *11*, 21-38.

Du, F., Zhou, Z., Mo, Z.Y., Shi, J.Z., Chen, J., and Liang, Y. (2006). Mixed macromolecular crowding accelerates the refolding of rabbit muscle creatine kinase: implications for protein folding in physiological environments. J Mol Biol *364*, 469-482.

Dulloo, A.G. (2011). The search for compounds that stimulate thermogenesis in obesity management: from pharmaceuticals to functional food ingredients. Obes Rev *12*, 866-883.

Dushay, J., Chui, P.C., Gopalakrishnan, G.S., Varela-Rey, M., Crawley, M., Fisher, F.M., Badman, M.K., Martinez-Chantar, M.L., and Maratos-Flier, E. (2010). Increased fibroblast growth factor 21 in obesity and nonalcoholic fatty liver disease. Gastroenterology *139*, 456-463.

Ebert, A.D., and Svendsen, C.N. (2010). Human stem cells and drug screening: opportunities and challenges. Nat Rev Drug Discov *9*, 367-372.

Elabd, C., Basillais, A., Beaupied, H., Breuil, V., Wagner, N., Scheideler, M., Zaragosi, L.E., Massiera, F., Lemichez, E., Trajanoski, Z., et al. (2008). Oxytocin controls differentiation of human mesenchymal stem cells and reverses osteoporosis. Stem Cells *26*, 2399-2407.

Elabd, C., Chiellini, C., Carmona, M., Galitzky, J., Cochet, O., Petersen, R., Penicaud, L., Kristiansen, K., Bouloumie, A., Casteilla, L., et al. (2009). Human multipotent adipose-derived stem cells differentiate into functional brown adipocytes. Stem Cells *27*, 2753-2760.

Ellis, R.J. (2001). Macromolecular crowding: obvious but underappreciated. Trends Biochem Sci *26*, 597-604.

Enerback, S., Jacobsson, A., Simpson, E.M., Guerra, C., Yamashita, H., Harper, M.E., and Kozak, L.P. (1997). Mice lacking mitochondrial uncoupling protein are cold-sensitive but not obese. Nature *387*, 90-94.

Feldmann, H.M., Golozoubova, V., Cannon, B., and Nedergaard, J. (2009). UCP1 ablation induces obesity and abolishes diet-induced thermogenesis in mice exempt from thermal stress by living at thermoneutrality. Cell Metab *9*, 203-209.

Fisher, F.M., Kleiner, S., Douris, N., Fox, E.C., Mepani, R.J., Verdeguer, F., Wu, J., Kharitonenkov, A., Flier, J.S., Maratos-Flier, E., et al. (2012). FGF21 regulates PGC-1alpha and browning of white adipose tissues in adaptive thermogenesis. Genes Dev *26*, 271-281.

Frith, J.E., Mills, R.J., Hudson, J.E., and Cooper-White, J.J. (2012). Tailored integrin-extracellular matrix interactions to direct human mesenchymal stem cell differentiation. Stem Cells Dev *21*, 2442-2456.

Funaki, M., Randhawa, P., and Janmey, P.A. (2004). Separation of insulin signaling into distinct GLUT4 translocation and activation steps. Mol Cell Biol *24*, 7567-7577.

Gimble, J.M., and Nuttall, M.E. (2004). Bone and fat: old questions, new insights. Endocrine *23*, 183-188.

Gimble, J.M., Zvonic, S., Floyd, Z.E., Kassem, M., and Nuttall, M.E. (2006). Playing with bone and fat. J Cell Biochem *98*, 251-266.

Gomis, A., Soriano, S., Belmonte, C., and Viana, F. (2008). Hypoosmotic- and pressure-induced membrane stretch activate TRPC5 channels. J Physiol *586*, 5633-5649.

Greenspan, P., Mayer, E.P., and Fowler, S.D. (1985). Nile red: a selective fluorescent stain for intracellular lipid droplets. J Cell Biol *100*, 965-973.

Gregory, K.E., Ono, R.N., Charbonneau, N.L., Kuo, C.L., Keene, D.R., Bachinger, H.P., and Sakai, L.Y. (2005). The prodomain of BMP-7 targets the BMP-7 complex to the extracellular matrix. J Biol Chem *280*, 27970-27980.

Guerra, C., Koza, R.A., Yamashita, H., Walsh, K., and Kozak, L.P. (1998). Emergence of brown adipocytes in white fat in mice is under genetic control. Effects on body weight and adiposity. J Clin Invest *102*, 412-420.

Guilherme, A., Virbasius, J.V., Puri, V., and Czech, M.P. (2008). Adipocyte dysfunctions linking obesity to insulin resistance and type 2 diabetes. Nat Rev Mol Cell Biol *9*, 367-377.

Gullberg, D.E., and Lundgren-Akerlund, E. (2002). Collagen-binding I domain integrins--what do they do? Prog Histochem Cytochem *37*, 3-54.

Gupta, R.K., Mepani, R.J., Kleiner, S., Lo, J.C., Khandekar, M.J., Cohen, P., Frontini, A., Bhowmick, D.C., Ye, L., Cinti, S., et al. (2012). Zfp423 expression identifies committed preadipocytes and localizes to adipose endothelial and perivascular cells. Cell Metab *15*, 230-239.

Hany, T.F., Gharehpapagh, E., Kamel, E.M., Buck, A., Himms-Hagen, J., and von Schulthess, G.K. (2002). Brown adipose tissue: a factor to consider in symmetrical tracer uptake in the neck and upper chest region. Eur J Nucl Med Mol Imaging *29*, 1393-1398.

Harms, M., and Seale, P. (2013). Brown and beige fat: development, function and therapeutic potential. Nat Med *19*, 1252-1263.

Haslam, D.W., and James, W.P. (2005). Obesity. Lancet *366*, 1197-1209.

Hertzel, A.V., and Bernlohr, D.A. (2000). The mammalian fatty acid-binding protein multigene family: molecular and genetic insights into function. Trends Endocrinol Metab *11*, 175-180.

Huang, P.I., Chen, Y.C., Chen, L.H., Juan, C.C., Ku, H.H., Wang, S.T., Chiou, S.H., Chiou, G.Y., Chi, C.W., Hsu, C.C., et al. (2011). PGC-1alpha mediates differentiation of mesenchymal stem cells to brown adipose cells. J Atheroscler Thromb *18*, 966-980.

Jansen, P.A., Kamsteeg, M., Rodijk-Olthuis, D., van Vlijmen-Willems, I.M., de Jongh, G.J., Bergers, M., Tjabringa, G.S., Zeeuwen, P.L., and Schalkwijk, J. (2009). Expression of the vanin gene family in normal and inflamed human skin: induction by proinflammatory cytokines. J Invest Dermatol *129*, 2167-2174.

Jespersen, N.Z., Larsen, T.J., Peijs, L., Daugaard, S., Homoe, P., Loft, A., de Jong, J., Mathur, N., Cannon, B., Nedergaard, J., et al. (2013). A classical brown adipose tissue mRNA signature partly overlaps with brite in the supraclavicular region of adult humans. Cell Metab *17*, 798-805.

Jiang, X., and Couchman, J.R. (2003). Perlecan and tumor angiogenesis. J Histochem Cytochem *51*, 1393-1410.

Kajimura, S., Seale, P., Kubota, K., Lunsford, E., Frangioni, J.V., Gygi, S.P., and Spiegelman, B.M. (2009). Initiation of myoblast to brown fat switch by a PRDM16-C/EBP-beta transcriptional complex. Nature *460*, 1154-1158.

Kazantzis, M., Takahashi, V., Hinkle, J., Kota, S., Zilberfarb, V., Issad, T., Abdelkarim, M., Chouchane, L., and Strosberg, A.D. (2012). PAZ6 cells constitute a representative model for human brown pre-adipocytes. Front Endocrinol (Lausanne) *3*, 13.

Kim, G.W., Lin, J.E., Blomain, E.S., and Waldman, S.A. (2014). Antiobesity pharmacotherapy: new drugs and emerging targets. Clin Pharmacol Ther *95*, 53-66.

Kir, S., White, J.P., Kleiner, S., Kazak, L., Cohen, P., Baracos, V.E., and Spiegelman, B.M. (2014). Tumour-derived PTH-related protein triggers adipose tissue browning and cancer cachexia. Nature.

Klaus, S., Ely, M., Encke, D., and Heldmaier, G. (1995). Functional assessment of white and brown adipocyte development and energy metabolism in cell culture. Dissociation of terminal differentiation and thermogenesis in brown adipocytes. J Cell Sci *108 ( Pt 10)*, 3171-3180.

Klok, M.D., Jakobsdottir, S., and Drent, M.L. (2007). The role of leptin and ghrelin in the regulation of food intake and body weight in humans: a review. Obes Rev *8*, 21-34.

Kopecky, J., Clarke, G., Enerback, S., Spiegelman, B., and Kozak, L.P. (1995). Expression of the mitochondrial uncoupling protein gene from the aP2 gene promoter prevents genetic obesity. J Clin Invest *96*, 2914-2923.

Krings, A., Rahman, S., Huang, S., Lu, Y., Czernik, P.J., and Lecka-Czernik, B. (2012). Bone marrow fat has brown adipose tissue characteristics, which are attenuated with aging and diabetes. Bone *50*, 546-552.

Lampidonis, A.D., Rogdakis, E., Voutsinas, G.E., and Stravopodis, D.J. (2011). The resurgence of Hormone-Sensitive Lipase (HSL) in mammalian lipolysis. Gene *477*, 1-11.

Larsson, A., Skoldenberg, E., and Ericson, H. (2002). Serum and plasma levels of FGF-2 and VEGF in healthy blood donors. Angiogenesis *5*, 107-110.

Lean, M.E. (2010). Childhood obesity: time to shrink a parent. Int J Obes (Lond) *34*, 1-3.

Lecka-Czernik, B. (2012). Marrow fat metabolism is linked to the systemic energy metabolism. Bone *50*, 534-539.

Lee, E.K., Lee, M.J., Abdelmohsen, K., Kim, W., Kim, M.M., Srikantan, S., Martindale, J.L., Hutchison, E.R., Kim, H.H., Marasa, B.S., et al. (2011a). miR-130 suppresses adipogenesis by inhibiting peroxisome proliferator-activated receptor gamma expression. Mol Cell Biol *31*, 626-638.

Lee, P., Swarbrick, M.M., Zhao, J.T., and Ho, K.K. (2011b). Inducible brown adipogenesis of supraclavicular fat in adult humans. Endocrinology *152*, 3597-3602.

Lee, Y.H., Petkova, A.P., Mottillo, E.P., and Granneman, J.G. (2012). In vivo identification of bipotential adipocyte progenitors recruited by beta3-adrenoceptor activation and high-fat feeding. Cell Metab *15*, 480-491.

Lepper, C., and Fan, C.M. (2010). Inducible lineage tracing of Pax7-descendant cells reveals embryonic origin of adult satellite cells. Genesis *48*, 424-436.

Lidell, M.E., Betz, M.J., Dahlqvist Leinhard, O., Heglind, M., Elander, L., Slawik, M., Mussack, T., Nilsson, D., Romu, T., Nuutila, P., et al. (2013). Evidence for two types of brown adipose tissue in humans. Nat Med *19*, 631-634.

Lilla, J., Stickens, D., and Werb, Z. (2002). Metalloproteases and adipogenesis: a weighty subject. Am J Pathol *160*, 1551-1554.

Lin, S.C., and Li, P. (2004). CIDE-A, a novel link between brown adipose tissue and obesity. Trends Mol Med *10*, 434-439.

Liu, J., DeYoung, S.M., Zhang, M., Zhang, M., Cheng, A., and Saltiel, A.R. (2005). Changes in integrin expression during adipocyte differentiation. Cell Metab *2*, 165-177.

Liu, X., Rossmeisl, M., McClaine, J., Riachi, M., Harper, M.E., and Kozak, L.P. (2003). Paradoxical resistance to diet-induced obesity in UCP1-deficient mice. J Clin Invest *111*, 399-407.

Lowell, B.B., V, S.S., Hamann, A., Lawitts, J.A., Himms-Hagen, J., Boyer, B.B., Kozak, L.P., and Flier, J.S. (1993). Development of obesity in transgenic mice after genetic ablation of brown adipose tissue. Nature *366*, 740-742.

Mackay, D.L., Tesar, P.J., Liang, L.N., and Haynesworth, S.E. (2006). Characterizing medullary and human mesenchymal stem cell-derived adipocytes. J Cell Physiol *207*, 722-728.

Mairal, A., Langin, D., Arner, P., and Hoffstedt, J. (2006). Human adipose triglyceride lipase (PNPLA2) is not regulated by obesity and exhibits low in vitro triglyceride hydrolase activity. Diabetologia *49*, 1629-1636.

Mathur, A., Hong, Y., Kemp, B.K., Barrientos, A.A., and Erusalimsky, J.D. (2000). Evaluation of fluorescent dyes for the detection of mitochondrial membrane potential changes in cultured cardiomyocytes. Cardiovasc Res *46*, 126-138.

Mayanagi, T., Morita, T., Hayashi, K., Fukumoto, K., and Sobue, K. (2008). Glucocorticoid receptor-mediated expression of caldesmon regulates cell migration via the reorganization of the actin cytoskeleton. J Biol Chem *283*, 31183-31196.

Mazzoleni, G., Di Lorenzo, D., and Steimberg, N. (2009). Modelling tissues in 3D: the next future of pharmaco-toxicology and food research? Genes Nutr *4*, 13-22.

McBeath, R., Pirone, D.M., Nelson, C.M., Bhadriraju, K., and Chen, C.S. (2004). Cell shape, cytoskeletal tension, and RhoA regulate stem cell lineage commitment. Dev Cell *6*, 483-495.

Melrose, J., Roughley, P., Knox, S., Smith, S., Lord, M., and Whitelock, J. (2006). The structure, location, and function of perlecan, a prominent pericellular proteoglycan of fetal, postnatal, and mature hyaline cartilages. J Biol Chem *281*, 36905-36914.

Minguell, J.J., Erices, A., and Conget, P. (2001). Mesenchymal stem cells. Exp Biol Med (Maywood) *226*, 507-520.

Minton, A.P. (2001). The influence of macromolecular crowding and macromolecular confinement on biochemical reactions in physiological media. J Biol Chem *276*, 10577-10580.

MOH (2010). Ministry of Health - National Health Survey 2010. E.D.C. Division, ed.

Moore, K.A., and Lemischka, I.R. (2006). Stem cells and their niches. Science *311*, 1880-1885.

Morganstein, D.L., Wu, P., Mane, M.R., Fisk, N.M., White, R., and Parker, M.G. (2010). Human fetal mesenchymal stem cells differentiate into brown and white adipocytes: a role for ERRalpha in human UCP1 expression. Cell Res *20*, 434-444.

Moscatelli, D. (1992). Basic fibroblast growth factor (bFGF) dissociates rapidly from heparan sulfates but slowly from receptors. Implications for mechanisms of bFGF release from pericellular matrix. J Biol Chem *267*, 25803-25809.

Motyl, K.J., and Rosen, C.J. (2011). Temperatures rising: brown fat and bone. Discov Med *11*, 179-185.

Naveiras, O., Nardi, V., Wenzel, P.L., Hauschka, P.V., Fahey, F., and Daley, G.Q. (2009). Bone-marrow adipocytes as negative regulators of the haematopoietic microenvironment. Nature *460*, 259-263.

Nedergaard, J., Bengtsson, T., and Cannon, B. (2007). Unexpected evidence for active brown adipose tissue in adult humans. Am J Physiol Endocrinol Metab *293*, E444-452.

Nedergaard, J., Bengtsson, T., and Cannon, B. (2011). New powers of brown fat: fighting the metabolic syndrome. Cell Metab *13*, 238-240.

Nelson, T.L., Vogler, G.P., Pedersen, N.L., Hong, Y., and Miles, T.P. (2000). Genetic and environmental influences on body fat distribution, fasting insulin levels and CVD: are the influences shared? Twin Res *3*, 43-50.

Niisato, N., and Marunaka, Y. (2008). Osmotransduction Through Volume-Sensitive Cl-Channels. In Mechanosensitive Ion Channels (Springer), pp. 179-202.

Nishio, M., Yoneshiro, T., Nakahara, M., Suzuki, S., Saeki, K., Hasegawa, M., Kawai, Y., Akutsu, H., Umezawa, A., Yasuda, K., et al. (2012). Production of functional classical brown adipocytes from human pluripotent stem cells using specific hemopoietin cocktail without gene transfer. Cell Metab *16*, 394-406.

Olmsted-Davis, E., Gannon, F.H., Ozen, M., Ittmann, M.M., Gugala, Z., Hipp, J.A., Moran, K.M., Fouletier-Dilling, C.M., Schumara-Martin, S., Lindsey, R.W., et al. (2007). Hypoxic adipocytes pattern early heterotopic bone formation. Am J Pathol *170*, 620-632.

Orava, J., Nuutila, P., Noponen, T., Parkkola, R., Viljanen, T., Enerback, S., Rissanen, A., Pietilainen, K.H., and Virtanen, K.A. (2013). Blunted Metabolic Responses to Cold and Insulin Stimulation in Brown Adipose Tissue of Obese Humans. Obesity (Silver Spring) *21*, 2279–2287.

Osborn, M., Franke, W.W., and Weber, K. (1977). Visualization of a system of filaments 7-10 nm thick in cultured cells of an epithelioid line (Pt K2) by immunofluorescence microscopy. Proc Natl Acad Sci U S A *74*, 2490-2494.

Ouellet, V., Labbe, S.M., Blondin, D.P., Phoenix, S., Guerin, B., Haman, F., Turcotte, E.E., Richard, D., and Carpentier, A.C. (2012). Brown adipose tissue oxidative metabolism contributes to energy expenditure during acute cold exposure in humans. J Clin Invest *122*, 545-552.

Ouellet, V., Routhier-Labadie, A., Bellemare, W., Lakhal-Chaieb, L., Turcotte, E., Carpentier, A.C., and Richard, D. (2011). Outdoor temperature, age, sex, body mass index, and diabetic status determine the prevalence, mass, and glucose-uptake activity of 18F-FDG-detected BAT in humans. J Clin Endocrinol Metab *96*, 192-199.

Palfy, M., Remenyi, A., and Korcsmaros, T. (2012). Endosomal crosstalk: meeting points for signaling pathways. Trends Cell Biol *22*, 447-456.

Petrovic, N., Walden, T.B., Shabalina, I.G., Timmons, J.A., Cannon, B., and Nedergaard, J. (2010). Chronic peroxisome proliferator-activated receptor gamma (PPARgamma) activation of epididymally derived white adipocyte cultures reveals a population of thermogenically competent, UCP1-containing adipocytes molecularly distinct from classic brown adipocytes. J Biol Chem *285*, 7153-7164.

Pisani, D.F., Djedaini, M., Beranger, G.E., Elabd, C., Scheideler, M., Ailhaud, G., and Amri, E.Z. (2011). Differentiation of Human Adipose-Derived Stem Cells into "Brite" (Brown-in-White) Adipocytes. Front Endocrinol (Lausanne) *2*, 87.

Pittenger, M.F., Mackay, A.M., Beck, S.C., Jaiswal, R.K., Douglas, R., Mosca, J.D., Moorman, M.A., Simonetti, D.W., Craig, S., and Marshak, D.R. (1999). Multilineage potential of adult human mesenchymal stem cells. Science *284*, 143-147.

Qian, S.W., Tang, Y., Li, X., Liu, Y., Zhang, Y.Y., Huang, H.Y., Xue, R.D., Yu, H.Y., Guo, L., Gao, H.D., et al. (2013). BMP4-mediated brown fat-like changes in white adipose tissue alter glucose and energy homeostasis. Proc Natl Acad Sci U S A *110*, E798-807.

Rashid, R., Beyer, S., Blocki, A., Le Visage, C., Trau, D., Wohland, T., and Raghunath, M. (2014a). Mitochondrial routing of glucose and sucrose polymers after pinocytotic uptake: avenues for drug delivery. Biomacromolecules *15*, 2119-2127.

Rashid, R., Lim, N.S., Chee, S.M., Png, S.N., Wohland, T., and Raghunath, M. (2014b). Novel Use for Polyvinylpyrrolidone as a Macromolecular Crowder for Enhanced Extracellular Matrix Deposition and Cell Proliferation. Tissue Eng Part C Methods.

Robidoux, J., Martin, T.L., and Collins, S. (2004). Beta-adrenergic receptors and regulation of energy expenditure: a family affair. Annu Rev Pharmacol Toxicol *44*, 297-323.

Rosenwald, M., Perdikari, A., Rulicke, T., and Wolfrum, C. (2013). Bi-directional interconversion of brite and white adipocytes. Nat Cell Biol *15*, 659-667.

Rosenwald, M., and Wolfrum, C. (2014). The origin and definition of brite versus white and classical brown adipocytes. Adipocyte *3*, 4-9.

Rothwell, N.J., and Stock, M.J. (1983). Luxuskonsumption, diet-induced thermogenesis and brown fat: the case in favour. Clin Sci (Lond) *64*, 19-23.

Saito, M., Okamatsu-Ogura, Y., Matsushita, M., Watanabe, K., Yoneshiro, T., Nio-Kobayashi, J., Iwanaga, T., Miyagawa, M., Kameya, T., Nakada, K., et al. (2009). High incidence of metabolically active brown adipose tissue in healthy adult humans: effects of cold exposure and adiposity. Diabetes *58*, 1526-1531.

Sanchez-Gurmaches, J., Hung, C.M., Sparks, C.A., Tang, Y., Li, H., and Guertin, D.A. (2012). PTEN loss in the Myf5 lineage redistributes body fat and reveals subsets of white adipocytes that arise from Myf5 precursors. Cell Metab *16*, 348-362.

Sato, T., Oshima, T., Yoshihara, K., Yamamoto, N., Yamada, R., Nagano, Y., Fujii, S., Kunisaki, C., Shiozawa, M., Akaike, M., et al. (2009). Overexpression of the fibroblast growth factor receptor-1 gene correlates with liver metastasis in colorectal cancer. Oncol Rep *21*, 211-216.

Schulz, T.J., Huang, T.L., Tran, T.T., Zhang, H., Townsend, K.L., Shadrach, J.L., Cerletti, M., McDougall, L.E., Giorgadze, N., Tchkonia, T., et al. (2011). Identification of inducible brown adipocyte progenitors residing in skeletal muscle and white fat. Proc Natl Acad Sci U S A *108*, 143-148.

Seale, P., Bjork, B., Yang, W., Kajimura, S., Chin, S., Kuang, S., Scime, A., Devarakonda, S., Conroe, H.M., Erdjument-Bromage, H., et al. (2008). PRDM16 controls a brown fat/skeletal muscle switch. Nature *454*, 961-967.

Sharp, L.Z., Shinoda, K., Ohno, H., Scheel, D.W., Tomoda, E., Ruiz, L., Hu, H., Wang, L., Pavlova, Z., Gilsanz, V., et al. (2012). Human BAT possesses molecular signatures that resemble beige/brite cells. PLoS One *7*, e49452.

Silva, F.J., Holt, D.J., Vargas, V., Yockman, J., Boudina, S., Atkinson, D., Grainger, D.W., Revelo, M.P., Sherman, W., Bull, D.A., et al. (2014). Metabolically active human brown adipose tissue derived stem cells. Stem Cells *32*, 572-581.

Smiley, S.T., Reers, M., Mottola-Hartshorn, C., Lin, M., Chen, A., Smith, T.W., Steele, G.D., Jr., and Chen, L.B. (1991). Intracellular heterogeneity in mitochondrial membrane potentials revealed by a J-aggregate-forming lipophilic cation JC-1. Proc Natl Acad Sci U S A *88*, 3671-3675.

Souza, S.C., Christoffolete, M.A., Ribeiro, M.O., Miyoshi, H., Strissel, K.J., Stancheva, Z.S., Rogers, N.H., D'Eon, T.M., Perfield, J.W., 2nd, Imachi, H., et al. (2007). Perilipin regulates the thermogenic actions of norepinephrine in brown adipose tissue. J Lipid Res *48*, 1273-1279.

Taipale, J., and Keski-Oja, J. (1997). Growth factors in the extracellular matrix. FASEB J *11*, 51-59.

Tan, A.B., Kress, S., Castro, L., Sheppard, A., and Raghunath, M. (2013). Cellular re- and de-programming by microenvironmental memory: why short TGF-beta1 pulses can have long effects. Fibrogenesis Tissue Repair *6*, 12.

Timmons, J.A., Wennmalm, K., Larsson, O., Walden, T.B., Lassmann, T., Petrovic, N., Hamilton, D.L., Gimeno, R.E., Wahlestedt, C., Baar, K., et al. (2007). Myogenic gene expression signature establishes that brown and white adipocytes originate from distinct cell lineages. Proc Natl Acad Sci U S A *104*, 4401-4406.

Tiraby, C., Tavernier, G., Lefort, C., Larrouy, D., Bouillaud, F., Ricquier, D., and Langin, D. (2003). Acquirement of brown fat cell features by human white adipocytes. J Biol Chem *278*, 33370-33376.

Tran, K.V., Gealekman, O., Frontini, A., Zingaretti, M.C., Morroni, M., Giordano, A., Smorlesi, A., Perugini, J., De Matteis, R., Sbarbati, A., et al. (2012). The vascular endothelium of the adipose tissue gives rise to both white and brown fat cells. Cell Metab *15*, 222-229.

Tseng, Y.H., Cypess, A.M., and Kahn, C.R. (2010). Cellular bioenergetics as a target for obesity therapy. Nat Rev Drug Discov *9*, 465-482.

Tseng, Y.H., Kokkotou, E., Schulz, T.J., Huang, T.L., Winnay, J.N., Taniguchi, C.M., Tran, T.T., Suzuki, R., Espinoza, D.O., Yamamoto, Y., et al. (2008). New role of bone morphogenetic protein 7 in brown adipogenesis and energy expenditure. Nature *454*, 1000-1004.

Turner, N., and Grose, R. (2010). Fibroblast growth factor signalling: from development to cancer. Nat Rev Cancer *10*, 116-129.

Tvrdik, P., Asadi, A., Kozak, L.P., Nedergaard, J., Cannon, B., and Jacobsson, A. (1997). Cig30, a mouse member of a novel membrane protein gene family, is involved in the recruitment of brown adipose tissue. J Biol Chem *272*, 31738-31746.

Uldry, M., Yang, W., St-Pierre, J., Lin, J., Seale, P., and Spiegelman, B.M. (2006). Complementary action of the PGC-1 coactivators in mitochondrial biogenesis and brown fat differentiation. Cell Metab *3*, 333-341.

Ullah, M., Sittinger, M., and Ringe, J. (2013). Extracellular matrix of adipogenically differentiated mesenchymal stem cells reveals a network of collagen filaments, mostly interwoven by hexagonal structural units. Matrix Biol *32*, 452-465.

van Marken Lichtenbelt, W.D., Vanhommerig, J.W., Smulders, N.M., Drossaerts, J.M., Kemerink, G.J., Bouvy, N.D., Schrauwen, P., and Teule, G.J. (2009). Cold-activated brown adipose tissue in healthy men. N Engl J Med *360*, 1500-1508.

Vernochet, C., Peres, S.B., Davis, K.E., McDonald, M.E., Qiang, L., Wang, H., Scherer, P.E., and Farmer, S.R. (2009). C/EBPalpha and the corepressors CtBP1 and CtBP2 regulate repression of select visceral white adipose genes during induction of the brown phenotype in white adipocytes by peroxisome proliferator-activated receptor gamma agonists. Mol Cell Biol *29*, 4714-4728.

Vijgen, G.H., Bouvy, N.D., Teule, G.J., Brans, B., Schrauwen, P., and van Marken Lichtenbelt, W.D. (2011). Brown adipose tissue in morbidly obese subjects. PLoS One *6*, e17247.

Villarroya, F., and Vidal-Puig, A. (2013). Beyond the sympathetic tone: the new brown fat activators. Cell Metab *17*, 638-643.

Virtanen, K.A., Lidell, M.E., Orava, J., Heglind, M., Westergren, R., Niemi, T., Taittonen, M., Laine, J., Savisto, N.J., Enerback, S., et al. (2009). Functional brown adipose tissue in healthy adults. N Engl J Med *360*, 1518-1525.

Wadsworth, G.R., and Oliveiro, C.J. (1953). Plasma protein concentration of normal adults living in Singapore. Br Med J *2*, 1138-1139.

Walden, T.B., Hansen, I.R., Timmons, J.A., Cannon, B., and Nedergaard, J. (2012). Recruited vs. nonrecruited molecular signatures of brown, "brite," and white adipose tissues. Am J Physiol Endocrinol Metab *302*, E19-31.

Wang, H., Zhang, Y., Yehuda-Shnaidman, E., Medvedev, A.V., Kumar, N., Daniel, K.W., Robidoux, J., Czech, M.P., Mangelsdorf, D.J., and Collins, S. (2008a). Liver X receptor alpha is a transcriptional repressor of the uncoupling protein 1 gene and the brown fat phenotype. Mol Cell Biol *28*, 2187-2200.

Wang, X., Harris, R.E., Bayston, L.J., and Ashe, H.L. (2008b). Type IV collagens regulate BMP signalling in Drosophila. Nature *455*, 72-77.

Westerberg, R., Mansson, J.E., Golozoubova, V., Shabalina, I.G., Backlund, E.C., Tvrdik, P., Retterstol, K., Capecchi, M.R., and Jacobsson, A. (2006). ELOVL3 is an important component for early onset of lipid recruitment in brown adipose tissue. J Biol Chem *281*, 4958-4968.

Whitelock, J.M., Murdoch, A.D., Iozzo, R.V., and Underwood, P.A. (1996). The degradation of human endothelial cell-derived perlecan and release of bound basic fibroblast growth factor by stromelysin, collagenase, plasmin, and heparanases. J Biol Chem *271*, 10079-10086.

WHO Obesity facts from the World Health Organisation. http://www.who.int/gho/ncd/risk_factors/obesity_text/en/index.html; http://www.who.int/mediacentre/factsheets/fs311/en/index.html.

WHO (2008). Global Health Observatory - Overweight and Obesity.

WHO (2014). World Health Organization: Obesity and Overweight.

Wu, J., Bostrom, P., Sparks, L.M., Ye, L., Choi, J.H., Giang, A.H., Khandekar, M., Virtanen, K.A., Nuutila, P., Schaart, G., et al. (2012). Beige adipocytes are a distinct type of thermogenic fat cell in mouse and human. Cell *150*, 366-376.

Yajnik, C. (2000). Interactions of perturbations in intrauterine growth and growth during childhood on the risk of adult-onset disease. Proc Nutr Soc *59*, 257-265.

Yoneshiro, T., Aita, S., Kawai, Y., Iwanaga, T., and Saito, M. (2012). Nonpungent capsaicin analogs (capsinoids) increase energy expenditure through the activation of brown adipose tissue in humans. Am J Clin Nutr *95*, 845-850.

Yoneshiro, T., Aita, S., Matsushita, M., Kameya, T., Nakada, K., Kawai, Y., and Saito, M. (2011). Brown adipose tissue, whole-body energy expenditure, and thermogenesis in healthy adult men. Obesity (Silver Spring) *19*, 13-16.

Zang, R., Li, D., Tang, I.C., Wang, J., and Yang, S.T. (2012). Cell-Based Assays in High-Throughput Screening for Drug Discovery. International Journal of Biotechnology for Wellness Industries *1*, 31-51.

Zeiger, A.S., Loe, F.C., Li, R., Raghunath, M., and Van Vliet, K.J. (2012). Macromolecular crowding directs extracellular matrix organization and mesenchymal stem cell behavior. PLoS One *7*, e37904.

Zhang, H., Guo, F., and Zhu, G. (2012). Involvement of host cell integrin alpha2 in Cryptosporidium parvum infection. Infect Immun *80*, 1753-1758.

Zilberfarb, V., Pietri-Rouxel, F., Jockers, R., Krief, S., Delouis, C., Issad, T., and Strosberg, A.D. (1997). Human immortalized brown adipocytes express functional beta3-adrenoceptor coupled to lipolysis. J Cell Sci *110 ( Pt 7)*, 801-807.

Zingaretti, M.C., Crosta, F., Vitali, A., Guerrieri, M., Frontini, A., Cannon, B., Nedergaard, J., and Cinti, S. (2009). The presence of UCP1 demonstrates that metabolically active adipose tissue in the neck of adult humans truly represents brown adipose tissue. FASEB J *23*, 3113-3120.

## APPENDIX

### *Supplementary Figures*

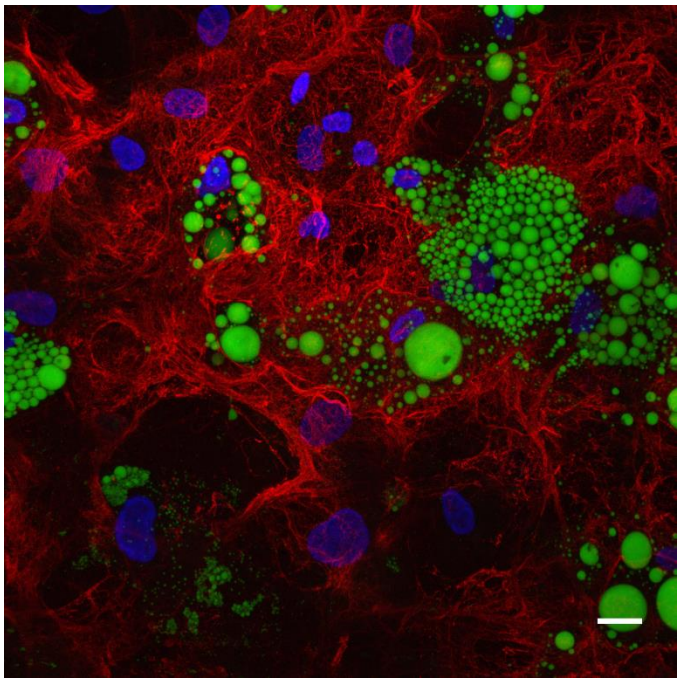

**Supplementary figure 1. hbmMSC-generated adipocytes also produced fine Col IV fibres under the brown induction (ib) protocol without MMC.** Z-project image of DAPI (blue), Col IV (red) and BODIPY (green). Scale bar: 20µm. Experiment performed together with Anna Goralczyk, Rókus Kriszt, Jean-Yves Dewavrin, NUS; and Dr. Cedric Badowski, IMB A*STAR.

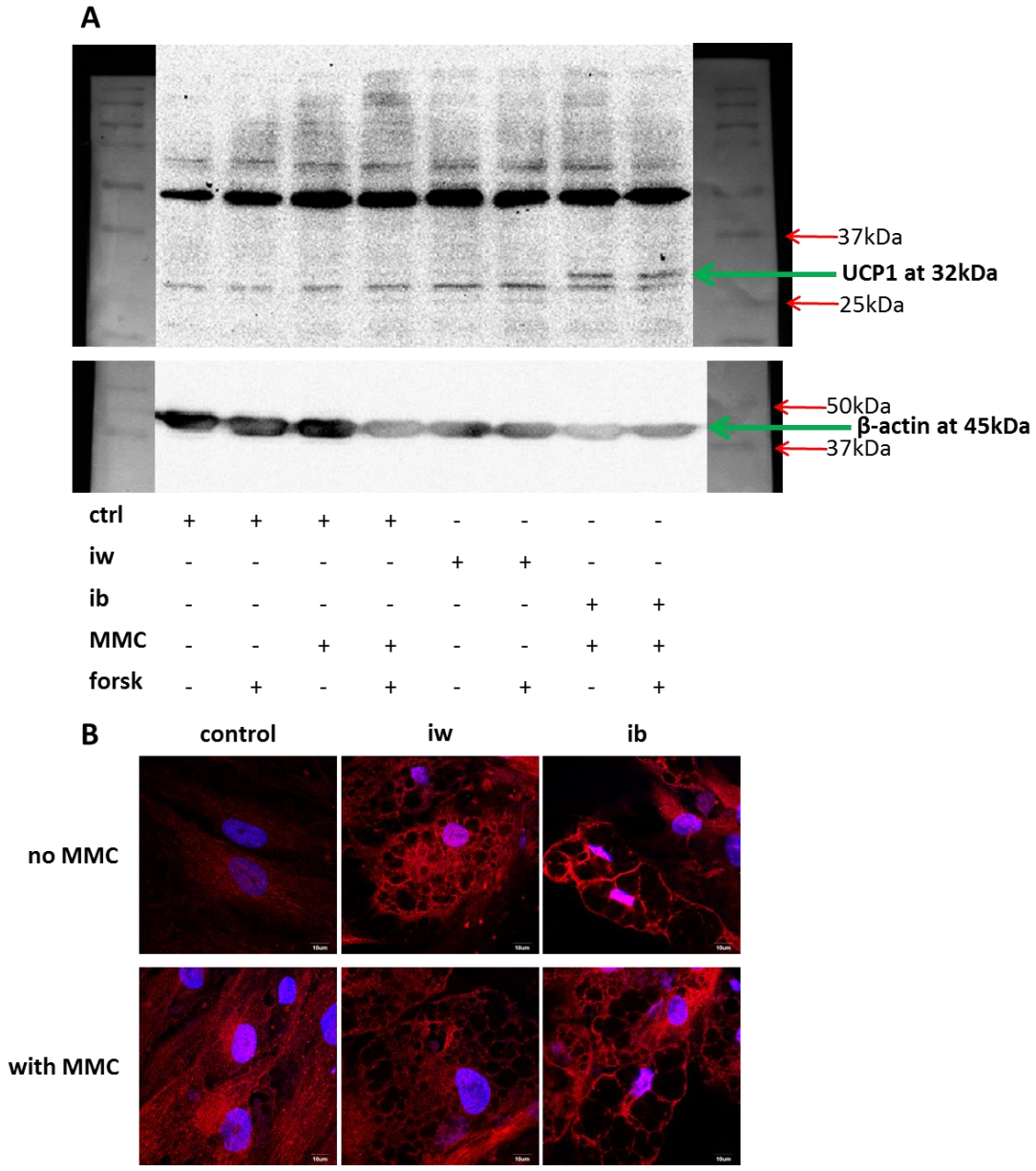


**Supplementary figure 2. Use of commercial antibodies to detect UCP1 protein in bmMSC-derived adipocytes.** (A) Western blot of bmMSC-derived adipocytes for UCP1 and β-actin. bmMSCs were differentiated into adipocytes with a white (iw) or brown +MMC (ib mmc) induction protocol for 3 weeks. Non-induced cells were cultured in maintenance medium ±MMC as a control. Cells were then treated with 4h 10µM forskolin (forsk) or vehicle (DMSO). UCP1 antibody used was ab10983 (Abcam). Despite the presence of a ~50kDa band throughout all samples, probably due to the naturally occurring antibodies to keratin in rabbit sera (Osborn et al., 1977), a ~32kDa band was detected only in the ib mmc samples. (B) bmMSCs were chemically induced into adipocytes with a white (iw) or brown (ib) induction protocol ±MMC for 3 weeks. Non-induced cells were cultured in maintenance medium ±MMC as a control. Presence of UCP1 was determined by immunocytochemistry. UCP1 (red) antibody used is U6382 (Sigma). Nuclei were stained with DAPI (blue).

### *Conference*

International Society for Stem Cell Research, Yokohama, Japan, 13-16 June, 2012: Poster Presentation

### *Patent Application*

Generation of brown adipose tissue (BAT) from mesenchymal cells. PCT/SG2013/000102 Date of filling: 12 March 2013
Patent application no.: 11201405257W

### *Manuscripts*

*Ang, X.M., *Lee, M.H., Blocki, A., Chen, C., Ong, L.L., Asada, H.H., Sheppard, A., and Raghunath, M. (2014). Macromolecular crowding amplifies adipogenesis of human bone marrow-derived mesenchymal stem cells by enhancing the pro-adipogenic microenvironment. Tissue Eng Part A 20, 966-981. **Both authors share first authorship.*

Lee, M.H. et al. Human Functional Brown Fat Phenotype derived from adult bmMSCs and browning of bmMSC-derived white adipocytes through macromolecular crowding. *Manuscript in preparation.*